

UCSF

UC San Francisco Electronic Theses and Dissertations

Title

Domain regulation and mutational dysregulation of the histone demethylase KDM5C

Permalink

<https://escholarship.org/uc/item/09h049dp>

Author

Ugur, Fatima Seyma

Publication Date

2022

Peer reviewed|Thesis/dissertation

Domain regulation and mutational dysregulation of the histone demethylase KDM5C

by
Fatima Seyma Ugur

DISSERTATION
Submitted in partial satisfaction of the requirements for degree of
DOCTOR OF PHILOSOPHY

in
Chemistry and Chemical Biology

in the
GRADUATE DIVISION
of the
UNIVERSITY OF CALIFORNIA, SAN FRANCISCO

Approved:

DocuSigned by:

Danica Galonic Fujimori

Danica Galonic Fujimori

82967A5AE18B4D6...

Chair

DocuSigned by:

Geeta Narlikar

Geeta Narlikar

DocuSigned by:

John Gross

John Gross

DocuSigned by:

Barbara Panning

Barbara Panning

7BD74D2E31C74B7...

Committee Members

Copyright 2022

by

Fatima Seyma Ugur

ACKNOWLEDGMENTS

I am immensely grateful for being able to obtain and experience my PhD at UCSF with the help and support from many people. It has been a privilege to do so in the CCB graduate program where I have been surrounded by talented colleagues and their interesting and inspiring work and willingness to help.

I would like to thank my advisor Danica Fujimori for all the support and assistance over the years and for allowing independent pursuits on my project. My thesis committee Geeta Narlikar, Barbara Panning, and John Gross contributed many critical insights and recommendations on my work, and I am thankful for their guidance and feedback. The training and guidance provided by Mark Kelly on protein NMR has been a highlight of my PhD and my work would not have advanced without it. I would also like to thank Daniele Canzio for great ideas and for providing thoughtful and interesting recommendations.

I am very appreciative of my time shared with past and present members of the Fujimori Lab. From them, I have received so much help, mentorship, and advice, in addition to sharing many fun times. I am forever indebted to my wonderful labmates Kaitlyn Tsai and Letitia Sarah for their constant support and for all the days in the lab together. Our shared PhDs have been full of laughter and full of help through all the struggles, and I am so grateful for their friendship. I would also like to thank friends and colleagues Cynthia Chio, Sasha Dickinson, and Ryan Tibble for their help on my work, brainstorming, and great discussions. Sharing and navigating the PhD experience with my CCB cohort Emily Kang, Ryan Tibble, Sergei Pourmal, and Nick Rettko has been very enjoyable and our endless lunch conversations will remain memorable.

This PhD would not have been possible without my friends and family. I am especially grateful for my parents for all their love and support and my brother for the adventures and inspiration.

CONTRIBUTIONS

Chapters from this thesis are adapted from unpublished work that has been submitted for publication:

Ugur, F. S.; Kelly, M. J. S.; Fujimori, D. G. Chromatin sensing by the auxiliary domains of KDM5C regulates its demethylase activity and is disrupted by X-linked intellectual disability mutations. *bioRxiv* doi: 10.1101/2022.01.13.476263.

This work was supported by the UCSF Discovery Fellows program and National Science Foundation Graduate Research Fellowship to F. S. U. and by the National Institutes of Health (R01 GM114044, R01 GM114044-03S1, and R01 CA250459) to D. G. F.

Domain regulation and mutational dysregulation of the histone demethylase KDM5C

Fatima Seyma Ugur

ABSTRACT

The H3K4me3 chromatin modification, a hallmark of promoters of actively transcribed genes, is dynamically removed by the KDM5 family of histone demethylases. The KDM5 demethylases have several accessory domains, two of which, ARID and PHD1, lie between the segments of the catalytic domain. KDM5C, which has a unique role in neural development, harbors a number of mutations adjacent to its accessory domains that cause X-linked intellectual disability (XLID). The roles of these accessory domains remain unknown, limiting an understanding of how XLID mutations affect KDM5C activity. Work in this thesis focuses on a mechanistic understanding of accessory domain functional roles within KDM5C and dysregulation by select XLID mutations. Through *in vitro* binding and kinetic studies using nucleosomes, we find that while the ARID domain is required for efficient nucleosome demethylation, the PHD1 domain alone has an inhibitory role in KDM5C catalysis. In addition, the unstructured linker region between the ARID and PHD1 domains is necessary for nucleosome binding. Our data suggests a model in which the PHD1 domain regulates DNA recognition by KDM5C based on available H3K4me3 substrate cues. Importantly, we find that XLID mutations adjacent to the ARID and PHD1 domains disrupt this regulation by enhancing DNA binding, resulting in the loss of specificity of substrate chromatin recognition and rendering demethylase activity sensitive to inhibition by linker DNA. Our findings suggest a unifying model by which XLID mutations could alter chromatin recognition and enable euchromatin-specific dysregulation of demethylation by KDM5C.

TABLE OF CONTENTS

| | |
|---|-----------|
| Chapter 1: Introduction | 1 |
| Chapter 2: Accessory domain regulation of chromatin sensing and demethylation by KDM5C | 6 |
| Results | 7 |
| Discussion..... | 19 |
| Supplemental Figures..... | 25 |
| Chapter 3: Dysregulation of KDM5C by X-linked intellectual disability mutations | 35 |
| Results | 36 |
| Discussion..... | 42 |
| Supplemental Figures..... | 45 |
| Chapter 4: Additional biochemical studies of KDM5C..... | 46 |
| Chapter 5: Materials and Methods | 59 |
| References | 68 |

LIST OF FIGURES

Chapter 1: Introduction

- Figure 1.1.** The protein architecture of the human KDM5 demethylase family. 2
- Figure 1.2.** H3 tail recognition by PHD domains with H3K4me specific binding pockets. 3
- Figure 1.3.** X-linked intellectual disability mutations in KDM5C. 4

Chapter 2: Accessory domain regulation of chromatin sensing and demethylation by KDM5C

- Figure 2.1.** The ARID & PHD1 region of KDM5C contributes to efficient nucleosome demethylation and has a modest contribution to nucleosome binding. 8
- Figure 2.2.** The PHD1 domain of KDM5C preferentially binds the unmodified H3 tail and has an inhibitory role towards nucleosome demethylation. 10
- Figure 2.3.** DNA recognition by the ARID domain is needed for nucleosome demethylation but not nucleosome binding by KDM5C. 13
- Figure 2.4.** KDM5C recognizes flanking DNA in the absence of H3K4me3 due to regulation by PHD1. 16
- Figure 2.5.** Model of KDM5C regulation by the ARID-linker-PHD1 region. 20
- Figure S2.1.** Substrate demethylation and nucleosome binding by KDM5C constructs. 26
- Figure S2.2.** H3 ligand recognition by PHD1 and substrate demethylation and binding by PHD1 mutant KDM5C. 28
- Figure S2.3.** DNA recognition by ARID and substrate demethylation by ARID mutant KDM5C. 29
- Figure S2.4.** KDM5 family sequence alignment. 30
- Figure S2.5.** Characterization of ARID-PHD1 linker region contribution to substrate demethylation and linker DNA recognition by KDM5C constructs. 32
- Figure S2.6.** Features of ligand recognition and histone tail binding by PHD1. 34

Chapter 3: Dysregulation of KDM5C by X-linked intellectual disability mutations

| | |
|--|----|
| Figure 3.1. X-linked intellectual disability mutations enhance nucleosome binding by KDM5C..... | 37 |
| Figure 3.2. X-linked intellectual disability mutations reduce demethylase activity in the presence of flanking DNA. | 39 |
| Figure 3.3. The A388P XLID mutation does not reduce H3 tail binding by PHD1 but alters the state of the linker region C-terminal to PHD1..... | 41 |
| Figure 3.4. Model of H3K4me3 surveillance by KDM5C and dysregulation by XLID mutations on chromatin..... | 43 |
| Figure S3.1. Effect of A388P mutation on the catalytic domains and nucleosome binding by XLID mutants..... | 45 |

Chapter 4: Additional biochemical studies of KDM5C

| | |
|--|----|
| Figure 4.1. Glutaraldehyde cross-linking of KDM5C and nucleosome bound KDM5C. | 48 |
| Figure 4.2. Binding kinetics of PHD1 domain and histone tail peptides. | 50 |
| Figure 4.3. Dynamic residues in PHD1 with broadened chemical shifts in the apo PHD1 HSQC spectrum. | 51 |
| Figure 4.4. Chemical shift changes of PHD1 binding to H3K4me0/1/2/3 tail peptides and perturbation differences due to H3K4 methylation states. | 53 |
| Figure 4.5. HSQC spectra of PHD1 binding to H3K4me0/1/2/3 tail peptides. | 56 |
| Figure 4.6. H3K4me3 substrate peptide demethylation by KDM5C..... | 58 |

CHAPTER 1

INTRODUCTION

The eukaryotic genome is packaged in the cell nucleus as chromatin, the complex of DNA and histone proteins. The nucleosome is the fundamental unit of chromatin wherein 147 bp of DNA is wrapped around an octamer of the histone proteins H2A, H2B, H3, and H4. The basic and unstructured histone tails protrude from the nucleosome core and are extensively post translationally modified¹. These histone modifications are catalyzed, removed, and recognized by extensive chromatin modifying enzymes and binding proteins through diverse catalytic and reader domain families². Regulation of chromatin binding proteins by various domains influences their chromatin recognition and enzymatic activities, often with involvement of multiple histone modifications and chromatin features³. This regulation enables the establishment and coordination of certain modifications together with a chromatin state at specific regions on the genome^{4,5}. These modification distribution patterns often correlate with specific biological processes and outcomes, such as gene transcription and cellular identity^{1,4}.

The methylation of lysine 4 on histone H3 is a chromatin modification found on euchromatin, where H3K4 trimethylation (H3K4me3) is present at gene promoter regions associated with active transcription, and where H3K4 monomethylation (H3K4me1) is found at active enhancer regions⁵. While H3K4me1/2 is demethylated by the KDM1/LSD family, H3K4me1/2/3 is dynamically regulated by the KDM5/JARID1 subfamily of Jumonji histone demethylases⁶⁻¹¹. This demethylase family harbors unique accessory domains in addition to its catalytic domain comprised of the JmjN and JmjC segments that form a composite active site for demethylation^{12,13}. KDM5A (RBP2, JARID1A), KDM5B (PLU-1, JARID1B), KDM5C (SMCX, JARID1C), and KDM5D (SMCY, JARID1D) all contain an AT-rich interaction domain (ARID),

C₅HC₂ zinc finger domain (ZnF), and 2-3 plant homeodomains (PHD1-3) (**Figure 1.1**). Despite sharing similar domain architecture, these KDM5 demethylases have a variety of seemingly irredundant biological functions in cellular development and differentiation.



Figure 1.1. The protein architecture of the human KDM5 demethylase family. The members of the KDM5 family of histone demethylases with indicated length and catalytic Jumonji (JmjN, JmjC), AT-rich interaction (ARID), plant homeodomain (PHD1-3), and zinc finger (Zf) domains.

The insertion of the ARID and PHD1 domains between the JmjN and JmjC segments of the catalytic domain is unique to the KDM5 family, and ARID and PHD1 are required for demethylase activity *in vivo*^{8,14–17}. ARID domains are DNA binding domains, and the ARID domains of KDM5A/B have been shown to bind to GC-rich DNA with differing sequence preferences^{17–19}. PHD domains are H3K4 methylation reader domains with varying specificity towards unmethylated and methylated H3K4 states^{20–26}. They typically recognize the N-terminal residues of the H3 tail with H3K4 methylation specificity established by residues found in the structurally conserved H3K4 binding pocket (**Figure 1.2**)^{2,26}. PHD1 of KDM5A/B preferentially binds the unmethylated H3 tail, and this recognition of the demethylation product allosterically stimulates demethylase activity of KDM5A *in vitro*^{27–32}.

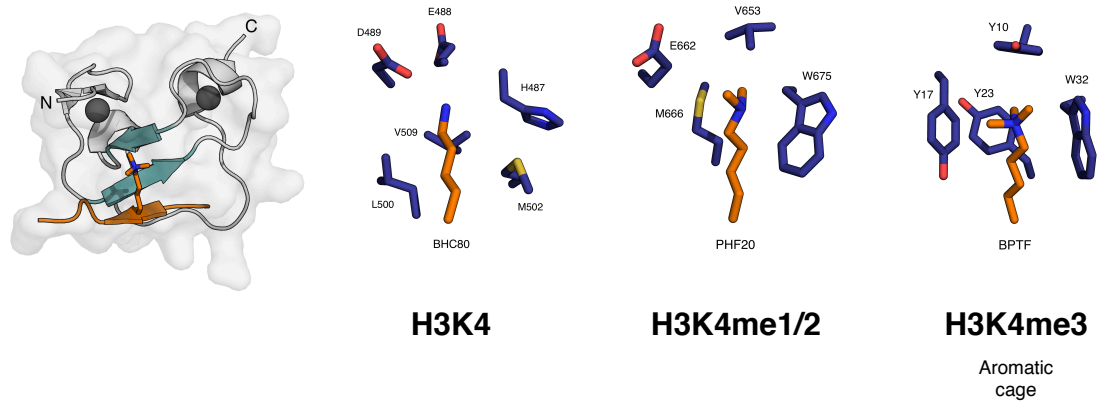


Figure 1.2. H3 tail recognition by PHD domains with H3K4me specific binding pockets.

Left: Structure of a representative PHD domain²³ in complex with H3K4me3 peptide (orange) and zinc (dark gray). *Right:* Representative PHD H3K4 binding pockets for indicated ligands^{20,21,23}.

An understanding of ligand recognition by these domains and their roles in the context of the physiologically relevant substrate, the nucleosome, is very limited. While the regulatory functions of ligand recognition by the ARID and PHD1 accessory domains on chromatin is also not entirely clear, the shared protein domain architecture within the KDM5 family suggests that their functions may be conserved. The ARID and PHD1 domains have not been extensively studied in KDM5C, which possesses a unique function in neural development and has nonredundant demethylase activity^{6,33}.

KDM5C is ubiquitously expressed but has highest expression levels in the brain^{34,35}. This demethylase is important for neural development and dendrite morphogenesis, and KDM5C knockout mice have abnormal dendritic branching and display memory defects, impaired social behavior, and aggression^{6,33}. KDM5C fine-tunes the expression of neurodevelopmental genes, as gene expression levels only change less than 2 fold upon knockout of KDM5C in mice^{33,36}. KDM5C localizes to enhancers in addition to promoter regions and has been shown to also fine tune enhancer function by demethylating spurious H3K4me3 at enhancers during neuronal maturation^{33,36-38}. In line with its neurodevelopmental function, several missense and nonsense

mutations that cause X-linked intellectual disability (XLID) are found throughout KDM5C^{35,39–43} (**Figure 1.3**). As KDM5C is located on the X-chromosome and the Y paralog KDM5D cannot compensate for its function, males with KDM5C XLID mutations are primarily affected with a range of mild to severe symptoms of limitations in cognition, memory, and adaptive behavior^{34,35,41,42,44}. Some functionally characterized mutations have been shown to reduce demethylase activity despite not occurring in the catalytic domains, and a select few mutations have been found to not affect demethylase activity, disrupting nonenzymatic functions instead^{6,15,43,45,46}. The consequences of these XLID mutations on KDM5C at its target regions within chromatin to affect gene expression during neural development is not fully understood. Interestingly, a number of XLID mutations are present throughout and in between the accessory domains of KDM5C, suggesting potential disruption of their regulatory functions. The impact of these mutations on demethylase regulation is hindered by the limited understanding of the accessory domain roles in KDM5C.

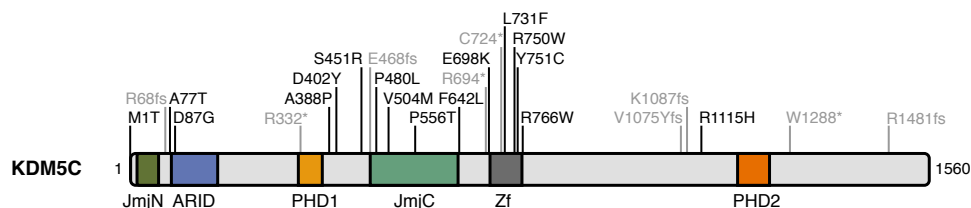


Figure 1.3. X-linked intellectual disability mutations in KDM5C. Missense and nonsense (indicated in light gray) XLID mutations found in KDM5C.

Here in this thesis, we sought to determine the functions of the ARID and PHD1 accessory domains in KDM5C (Chapter 2) and evaluate whether these functions might be disrupted by XLID mutations (Chapter 3). We approached these questions by interrogating the recognition and demethylation of nucleosomes by KDM5C, as nucleosome substrates enable extended interactions by multiple domains of the demethylase. Our findings reveal that the

ARID and PHD1 domains, as well as the linker between them, regulate nucleosome demethylation and chromatin recognition by KDM5C. We find that DNA recognition by ARID contributes to nucleosome demethylation but not nucleosome binding, which is instead driven by the unstructured linker between ARID and PHD1. In contrast, we find that PHD1 inhibits demethylation. Furthermore, we find that XLID mutations near these regulatory domains alter the conformational state of KDM5C to disrupt interdomain interactions and enhance affinity towards nucleosomes, resulting in nonproductive chromatin recognition and inhibition of demethylation in the presence of linker DNA. Our findings define functional roles of the ARID and PHD1 domains in the regulation of KDM5C and provide rationale for disruption of this regulation by XLID mutations. We demonstrate a unique regulation of KDM5C activity that allows for plasticity of H3K4me3 demethylation which is hindered by mutations in X-linked intellectual disability.

CHAPTER 2

**Accessory domain regulation of chromatin
sensing and demethylation by KDM5C**

RESULTS

ARID & PHD1 region contributes to productive nucleosome demethylation

Previous work has demonstrated that KDM5C is capable of demethylating H3K4me3 peptides and that the catalytic JmjN-JmjC domain and zinc finger domain are necessary for demethylase activity^{6,12,46}. To evaluate the contributions of the ARID and PHD1 domains, we sought to interrogate the recognition and demethylation of nucleosomes, given the expected interactions of these domains with DNA and histone tails, respectively. We utilized an N-terminal fragment of KDM5C containing the residues 1 to 839 necessary to monitor demethylation *in vitro* (KDM5C¹⁻⁸³⁹), as well as an analogous construct where the ARID and PHD1 region (residues 83 to 378) is replaced by a short linker (KDM5C¹⁻⁸³⁹ ΔAP) (**Figure 2.1A**)¹². We measured binding affinities of these constructs to both unmodified and substrate H3K4me3 core nucleosomes containing 147 bp DNA by electrophoretic mobility shift assay. KDM5C binds nucleosomes with weak affinity and with two-fold specificity towards substrate nucleosomes, with K_d^{app} of ~8 μM for the H3K4me3 nucleosome and ~15 μM for the unmodified nucleosome (**Figure 2.1B**). Surprisingly, the ARID and PHD1 domains have a modest contribution to nucleosome binding, as KDM5C¹⁻⁸³⁹ ΔAP displays only a 2-2.5 fold reduction in nucleosome affinity and retains the two fold preference towards the substrate nucleosome (**Figure 2.1B**). Thus, nucleosome affinity appears to be largely driven by H3K4me3 recognition. The absence of a significant enhancement of nucleosome binding through an ARID and PHD1 domain mediated multivalent interaction suggests a more complex role of these domains rather than simply facilitating chromatin recruitment.

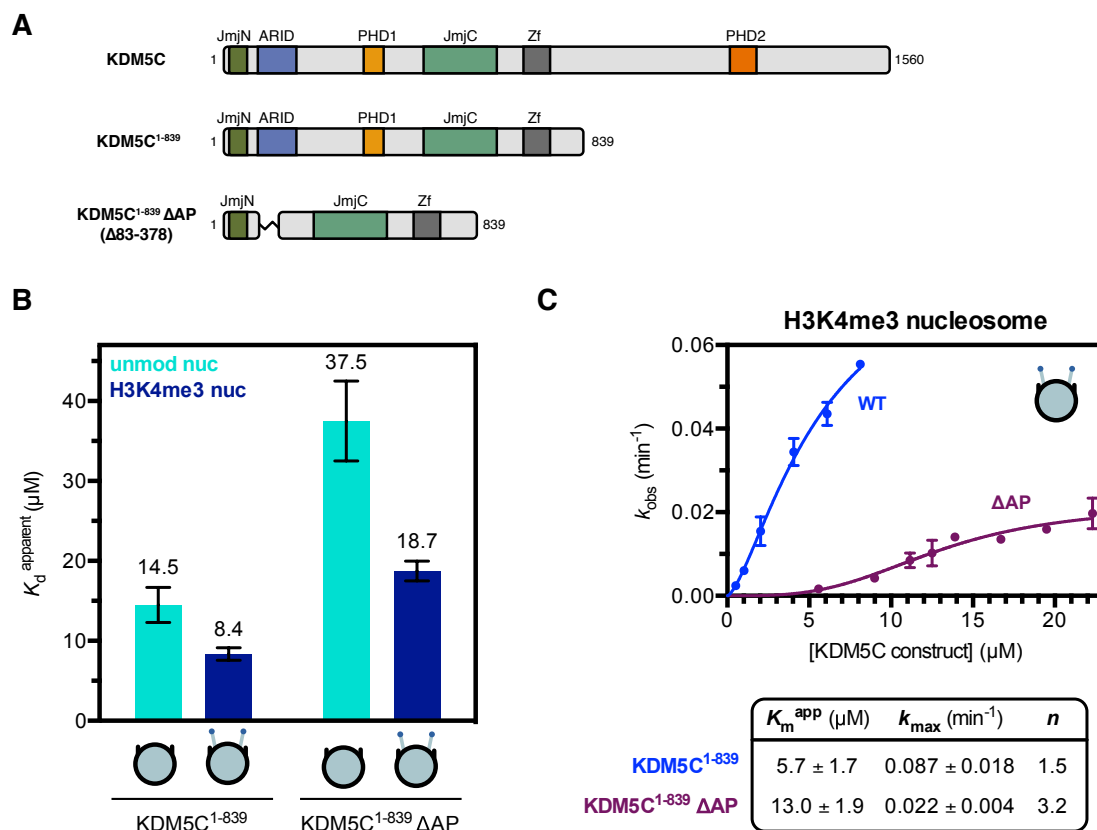


Figure 2.1. The ARID & PHD1 region of KDM5C contributes to efficient nucleosome demethylation and has a modest contribution to nucleosome binding.

(A) Domain architecture of KDM5C and KDM5C constructs used in this study. **(B)** Unmodified and substrate nucleosome binding by KDM5C constructs with apparent dissociation constants (K_d^{app}) measured by EMSA (binding curves in Figure S2.1B). Due to unattainable saturation of binding, a lower limit for the dissociation constant is presented for the unmodified nucleosome. **(C)** Demethylation kinetics of the H3K4me3 substrate nucleosome by KDM5C constructs under single turnover conditions. Observed rates are fit to a cooperative kinetic model, with n denoting the Hill coefficient. Representative kinetic traces used to determine observed demethylation rates are in Figure S2.1C. All error bars represent SEM of at least two independent experiments ($n \geq 2$).

We next interrogated the demethylase activity of KDM5C towards the H3K4me3 substrate nucleosome *in vitro* by utilizing a TR-FRET based kinetic assay that detects formation of the H3K4me1/2 product nucleosome. In order to measure true catalytic rates (k_{max}), demethylation was performed under single turnover conditions with enzyme in excess⁴⁷. We find that KDM5C¹⁻⁸³⁹ demethylates the substrate nucleosome with an observed catalytic rate of $\sim 0.09 \text{ min}^{-1}$ and KDM5C¹⁻⁸³⁹ ΔAP with a 4-fold lower catalytic rate of $\sim 0.02 \text{ min}^{-1}$ (**Figure 2.1C**), indicating that the ARID and PHD1 region contributes to productive catalysis on the

nucleosome. The contribution of the ARID and PHD1 domain region towards efficient demethylation appears to be through interactions of these domains with the nucleosome, as the catalytic efficiency (k_{max}/K_m^{app}) of KDM5C¹⁻⁸³⁹ Δ AP relative to wild type is only 3-fold lower on the substrate H3K4me3 peptide, as opposed to the 9 fold reduction in catalytic efficiency on the substrate nucleosome (**Figure S2.1A**). As the ARID and PHD1 domains are poorly functionally characterized in KDM5C, we sought to next investigate the features of the nucleosome that they recognize.

PHD1 domain inhibits KDM5C catalysis

The PHD1 domain of KDM5C has been previously shown to bind to H3K9me3 through peptide pull down⁶. To interrogate the histone binding and specificity of PHD1, we purified the PHD1 domain and quantified binding to histone peptides by nuclear magnetic resonance (NMR) spectroscopy and bio-layer interferometry. We observe near identical binding between the H3 and H3K9me3 tail peptide, indicating no specific binding of PHD1 towards the H3K9me3 modification (**Figure S2.2A**). Furthermore, we observe biphasic binding kinetics of PHD1 binding the H3 tail peptide, indicative of a two-step binding mechanism (**Figure S2.2B**). Large chemical shift changes of a majority of assigned residues in PHD1 occur upon titration of the H3 tail peptide in HSQC NMR spectra (**Figure 2.2A, Figure S2.2C**). The observed affinity of PHD1 towards the H3 tail is surprisingly weak with a dissociation constant of 130 μ M, about 100-fold weaker than the affinity of the homologous PHD1 of KDM5A towards the H3 tail (**Figure 2.2B**)^{29,32}. Despite this difference in affinity, PHD1 of KDM5C retains the same specificity towards the unmodified H3 tail over H3K4 methylated tail peptides as observed in the PHD1 domains of KDM5A/B (**Figure 2.2B**). Interestingly, the induced changes in PHD1 upon H3 tail binding is linked to its methylation specificity, as chemical shifts in PHD1 decrease upon binding as the methylation state of H3K4 is increased (**Figure 2.2B**). This suggests a conformational coupling of the PHD1 domain with ligand recognition may be present.

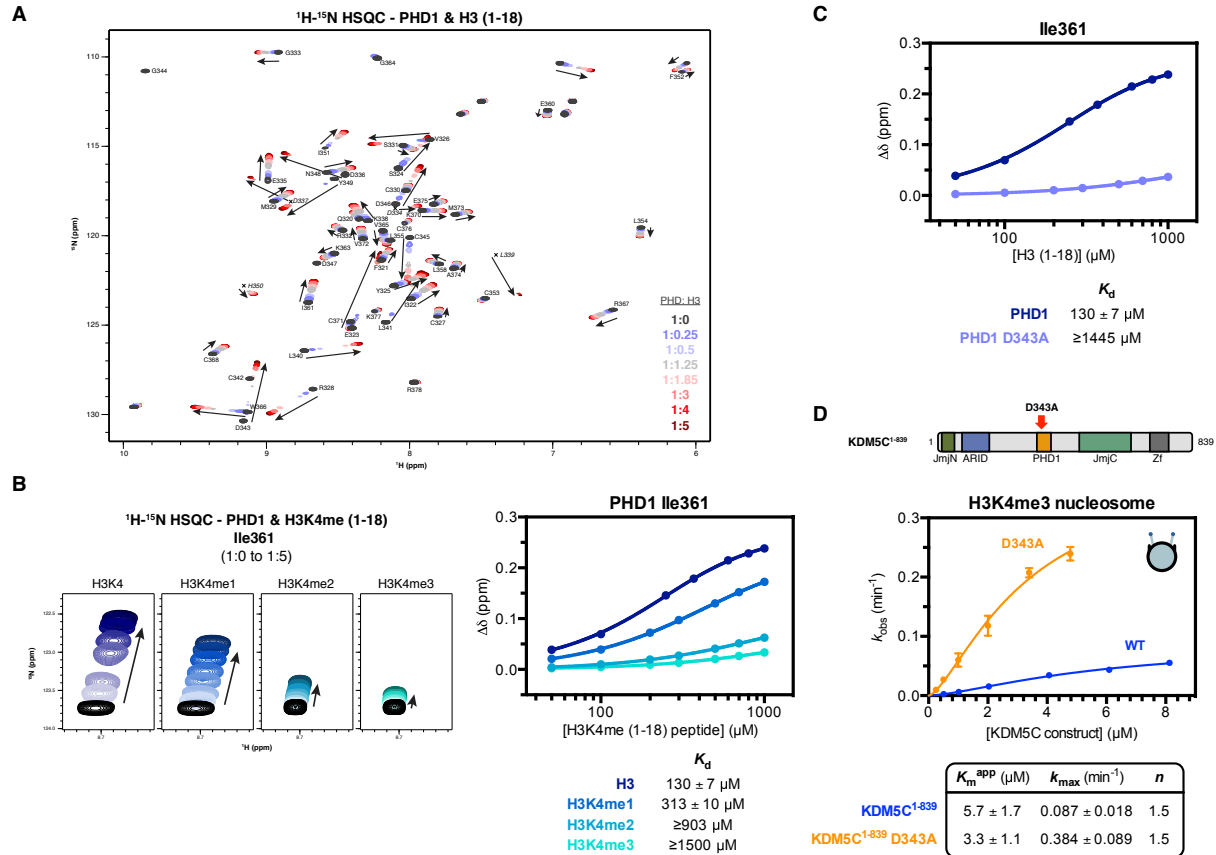


Figure 2.2. The PHD1 domain of KDM5C preferentially binds the unmodified H3 tail and has an inhibitory role towards nucleosome demethylation.

(A) 2D ¹H-¹⁵N HSQC spectra of PHD1 titrated with increasing amounts of H3 (1-18) peptide with indicated molar ratios. Backbone assignments of residues in PHD1 are labeled. (B) 2D ¹H-¹⁵N HSQC of I361 in PHD1 upon titration of H3K4me0/1/2/3 (1-18) peptides (*left*) with dissociation constants determined from the chemical shift change ($\Delta\delta$) of I361 with standard error (*right*). Due to incomplete saturation of binding, a lower limit for the dissociation constant is presented for the H3K4me2/3 peptides. (C) Binding of the H3 (1-18) tail peptide by PHD1 and PHD1 D343A mutant measured by NMR titration HSQC experiments. The chemical shift change ($\Delta\delta$) of I361 in PHD1 was fit to obtain dissociation constants with standard error. Due to incomplete saturation of binding by the D343A mutant, a lower limit for the dissociation constant is presented. (D) Demethylation kinetics of the H3K4me3 substrate nucleosome by wild type and PHD1 mutant KDM5C¹⁻⁸³⁹ under single turnover conditions. Observed rates are fit to a cooperative kinetic model, with n denoting the Hill coefficient. Wild type kinetic curve replotted from Figure 2.1C for comparison. Error bars represent SEM of at least two independent experiments ($n \geq 2$).

In order to investigate the function of PHD1 binding to the H3 tail in the context of the KDM5C enzyme, we sought to disrupt PHD1 binding through mutagenesis. One of the largest chemical shift perturbations that occurs in PHD1 upon H3 tail binding is at the D343 residue, a residue homologous to D312 in PHD1 of KDM5A where this residue is involved in H3R2 recognition (Figure S2.2D)⁴⁸. Similarly to PHD1 of KDM5A, we observe a dependence of

histone tail binding on recognition of the H3R2 residue by PHD1 of KDM5C (**Figure S2.2E**). Like the mutation of D312 in KDM5A, the D343A mutation decreases the affinity of KDM5C PHD1 to the H3 tail at least 10 fold (**Figure 2.2C**)²⁹. When introduced into the KDM5C¹⁻⁸³⁹ enzyme, the D343A mutation does not affect the catalytic rate of H3K4me3 peptide demethylation (**Figure S2.2F**). Surprisingly, the D343A PHD1 mutant enzyme demethylates the H3K4me3 nucleosome more rapidly than wild type KDM5C¹⁻⁸³⁹, with a ~4 fold increase of k_{max} (**Figure 2.2D**). No significant change in nucleosome binding due to the D343A mutation in KDM5C¹⁻⁸³⁹ was observed (**Figure S2.2G**). This data supports an inhibitory role of the PHD1 domain in nucleosome demethylation by KDM5C. This inhibitory role is in stark contrast to that observed for the PHD1 domain in KDM5A, where binding of the H3 tail to PHD1 is stimulatory towards *in vitro* demethylation, suggesting a unique regulation of KDM5C²⁹.

ARID domain contributes to nucleosome demethylation by KDM5C

In contrast to the inhibition of KDM5C demethylation by the PHD1 domain alone, together the ARID and PHD1 domains provide catalytic enhancement on nucleosomes (**Figure 2.1C**). We hypothesize that this effect may be due to the ability of the ARID domain to interact with DNA, similarly to the previously demonstrated DNA recognition by the ARID domains of KDM5A/B¹⁷⁻¹⁹. To test this hypothesis and to facilitate further DNA engagement, we interrogated binding of KDM5C¹⁻⁸³⁹ towards nucleosomes containing 20 bp flanking DNA on both ends (187 bp nucleosome). Strikingly, we observe at least a 3-fold gain in affinity towards the 187 bp nucleosome compared to the core 147 bp nucleosome (**Figure 2.3A**), demonstrating that KDM5C is capable of recognizing flanking DNA. KDM5C¹⁻⁸³⁹ Δ AP has similar affinity towards both the flanking DNA-containing and core nucleosome (**Figure 2.3B**), indicating that the ARID and PHD1 region is responsible for the recognition of flanking DNA.

To test whether the recognition of flanking DNA is mediated by the ARID domain and to further analyze DNA recognition, we purified the KDM5C ARID domain and interrogated its ability to bind the flanking DNA present in the 187 bp nucleosome used in this study. We find that the ARID domain binds the 5' flanking DNA fragment, with a dissociation constant of 10 μ M (**Figure S2.3A**). Minimal binding was observed for the 3' flanking DNA fragment (**Figure S2.3A**), suggesting that the ARID domain may possess sequence specificity in DNA binding. We utilized NMR spectroscopy to identify the residues of the ARID domain involved in DNA binding. Previously determined assignments for the ARID domain were reliably transferred to a majority of resonances observed in the ^1H - ^{15}N HSQC of ARID, and modest chemical shift changes of select ARID residues were observed upon titration of the 5' flanking DNA fragment (**Figure S2.3B**, **Figure S2.3C**)⁴⁹. The perturbed residues localize to a surface on the structure of KDM5C ARID (**Figure 2.3C**), with the most notable chemical shift changes at the K101, V105, E106, R107, and N148 residues⁴⁹.

We interrogated the contributions of several identified residues, K101, R107, and N148, towards DNA binding through mutagenesis, where we tested binding to the 147 bp 601 core nucleosome positioning sequence (**Figure 2.3D**). We find the N148A mutation does not significantly affect DNA binding by ARID, while the K101A and R107A mutations reduce DNA binding by 4-5 fold (**Figure 2.3D**). A further 24-fold reduction in DNA binding was observed upon the K101A/R107A double mutation in ARID (**Figure 2.3D**), indicating that the K101 and R107 residues are significantly involved in DNA recognition. These residues parallel those identified in the ARID domains of KDM5A/B where the homologous residues, R112 of KDM5A and K119 & R125 of KDM5B, contribute to DNA binding, suggesting conservation of DNA binding residues in the KDM5 family^{17,19}.

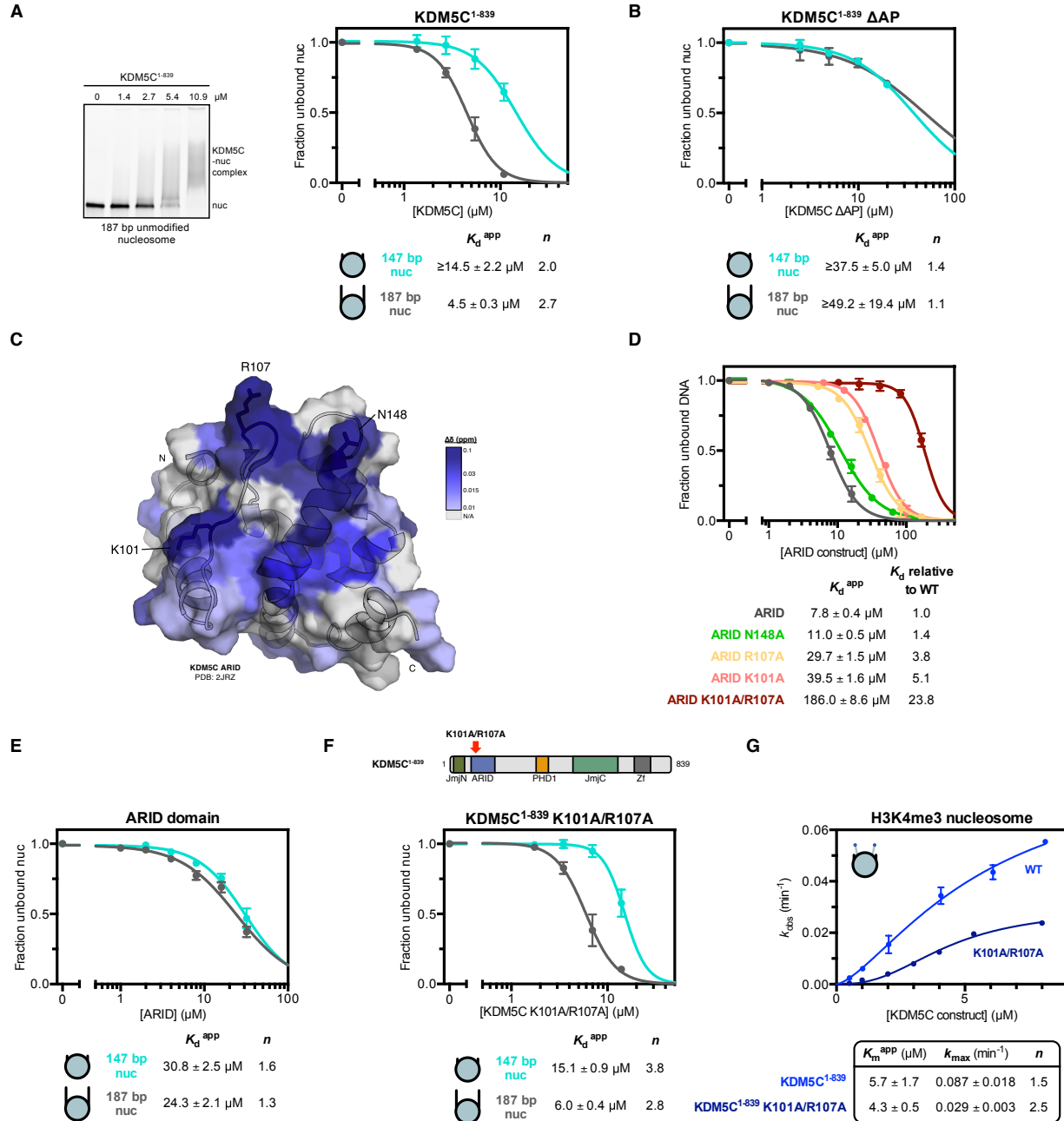


Figure 2.3. DNA recognition by the ARID domain is needed for nucleosome demethylation but not nucleosome binding by KDM5C.

(A) Binding of KDM5C¹⁻⁸³⁹ to unmodified nucleosomes with and without 20 bp flanking DNA. Representative gel shift of KDM5C binding to the 187 bp nucleosome (*left*). Nucleosome binding curves measured by EMSA fit to a cooperative binding model to determine apparent dissociation constants (K_d^{app}), with n denoting the Hill coefficient (*right*). Due to unattainable saturation of binding, a lower limit for the dissociation constant is presented for the unmodified core nucleosome. **(B)** Nucleosome binding curves of KDM5C¹⁻⁸³⁹ ΔAP binding to unmodified nucleosomes with and without 20 bp flanking DNA. Due to unattainable saturation of binding, a lower limit for the dissociation constant is presented. **(C)** Chemical shift changes of ARID binding to 20 bp 5' flanking DNA colored by the gradient and mapped to the KDM5C ARID structure (PDB: 2JRZ) of residues with backbone assignments in the ¹H-¹⁵N HSQC spectrum. Significantly perturbed residues are labeled. **(D)** DNA (147 bp 601 core nucleosome positioning sequence) binding by ARID and ARID mutants. Binding curves were measured by EMSA and fit to a cooperative binding model to determine apparent dissociation constants (K_d^{app}). **(E)** Nucleosome binding curves of

the ARID domain binding to unmodified nucleosomes with and without 20 bp flanking DNA. **(F)** Nucleosome binding curves of ARID mutant KDM5C¹⁻⁸³⁹ K101A/R107A binding to unmodified nucleosomes with and without 20 bp flanking DNA. **(G)** Demethylation kinetics of the H3K4me3 core substrate nucleosome by wild type and ARID mutant KDM5C¹⁻⁸³⁹ under single turnover conditions. Observed rates are fit to a cooperative kinetic model, with n denoting the Hill coefficient. Wild type kinetic curve replotted from Figure 2.1C for comparison. All error bars represent SEM of at least two independent experiments ($n \geq 2$).

We next interrogated DNA binding by the ARID domain in the context of the 147 bp and 187 bp nucleosome. We find the ARID domain does not display a strong binding preference for the flanking DNA-containing nucleosome and instead binds both nucleosomes with a similar weak affinity (**Figure 2.3E**). The observed nucleosome binding corresponds to a 3-4 fold reduction in affinity relative to the 147 bp non-nucleosomal DNA counterpart (**Figure 2.3D**, **Figure 2.3E**).

We then investigated the function of ARID in the context of the KDM5C enzyme towards nucleosome binding and demethylation by introducing the K101A/R107A double mutation into KDM5C¹⁻⁸³⁹. We find that ARID mutant KDM5C¹⁻⁸³⁹ retains a similar binding affinity as wild type KDM5C¹⁻⁸³⁹ towards both the flanking DNA-containing and core nucleosome (**Figure 2.3F**, **Figure 2.3A**). This indicates that the ARID domain does not contribute to nucleosome binding and to the recognition of flanking DNA by KDM5C, in contrast to our original hypothesis. However, ARID mutant KDM5C¹⁻⁸³⁹ has a reduced ability to demethylate the H3K4me3 nucleosome, with a 3-fold reduction in k_{\max} relative to wild type KDM5C¹⁻⁸³⁹ (**Figure 2.3G**). Reduced catalysis by the ARID mutant enzyme is only observed on the nucleosome, as the K101A/R107A double mutation does not reduce the catalytic rate of H3K4me3 peptide demethylation (**Figure S2.3D**). The similarity of catalytic rates of nucleosome demethylation between ARID mutant KDM5C¹⁻⁸³⁹ and KDM5C¹⁻⁸³⁹ Δ AP (0.029 min⁻¹ and 0.022 min⁻¹, respectively) implicates the ARID-DNA interaction as the significant contributor in the ARID and PHD1 region towards catalysis rather than nucleosome recognition (**Figure 2.3G**, **Figure 2.1C**).

PHD1 regulates recognition of flanking DNA on the nucleosome by KDM5C

Unlike wild type (**Figure 2.3A**) and ARID mutant KDM5C (**Figure 2.3F**), KDM5C¹⁻⁸³⁹ ΔAP has reduced nucleosome binding and a loss in the ability to discriminate between the 147 bp and 187 bp nucleosome (**Figure 2.3B**). This indicates that the ARID domain is not the contributing element of the ARID and PHD1 domain region that is responsible for the recognition of flanking DNA. Thus, we rationalized that the linker region between ARID and PHD1 might contribute to this recognition. The ARID-PHD1 linker region of KDM5C is the longest among KDM5 family members and contains many basic residues (**Figure S2.4**). This linker region also has low conservation in the KDM5 family and is predicted to be disordered in KDM5C (**Figure S2.4, Figure S2.5A**). We generated a construct where the linker region (residues 176 to 317) is replaced by a short (GGG)₅ linker sequence (KDM5C¹⁻⁸³⁹ Δlinker) (**Figure 2.4A**). KDM5C¹⁻⁸³⁹ Δlinker possesses similar catalytic efficiencies as wild type KDM5C¹⁻⁸³⁹ on both the H3K4me3 nucleosome and H3K4me3 substrate peptide (**Figure S2.5B, Figure S2.5C**), indicating that the enzyme without the ARID-PHD1 linker is functionally active. We then assessed binding of KDM5C¹⁻⁸³⁹ Δlinker to the 147 bp and 187 bp nucleosome and surprisingly did not detect any nucleosome binding (**Figure 2.4A**). Deletion of the linker region also diminishes DNA binding by KDM5C¹⁻⁸³⁹ to 147 bp non-nucleosomal DNA (**Figure S2.5D**). Thus, the ARID-PHD1 linker may drive nucleosome binding through DNA binding and appears to be the functional region that can affect flanking DNA recognition by KDM5C. These results indicate that, unlike the ARID domain, the ARID-PHD1 linker contributes to nucleosome binding but not demethylation.

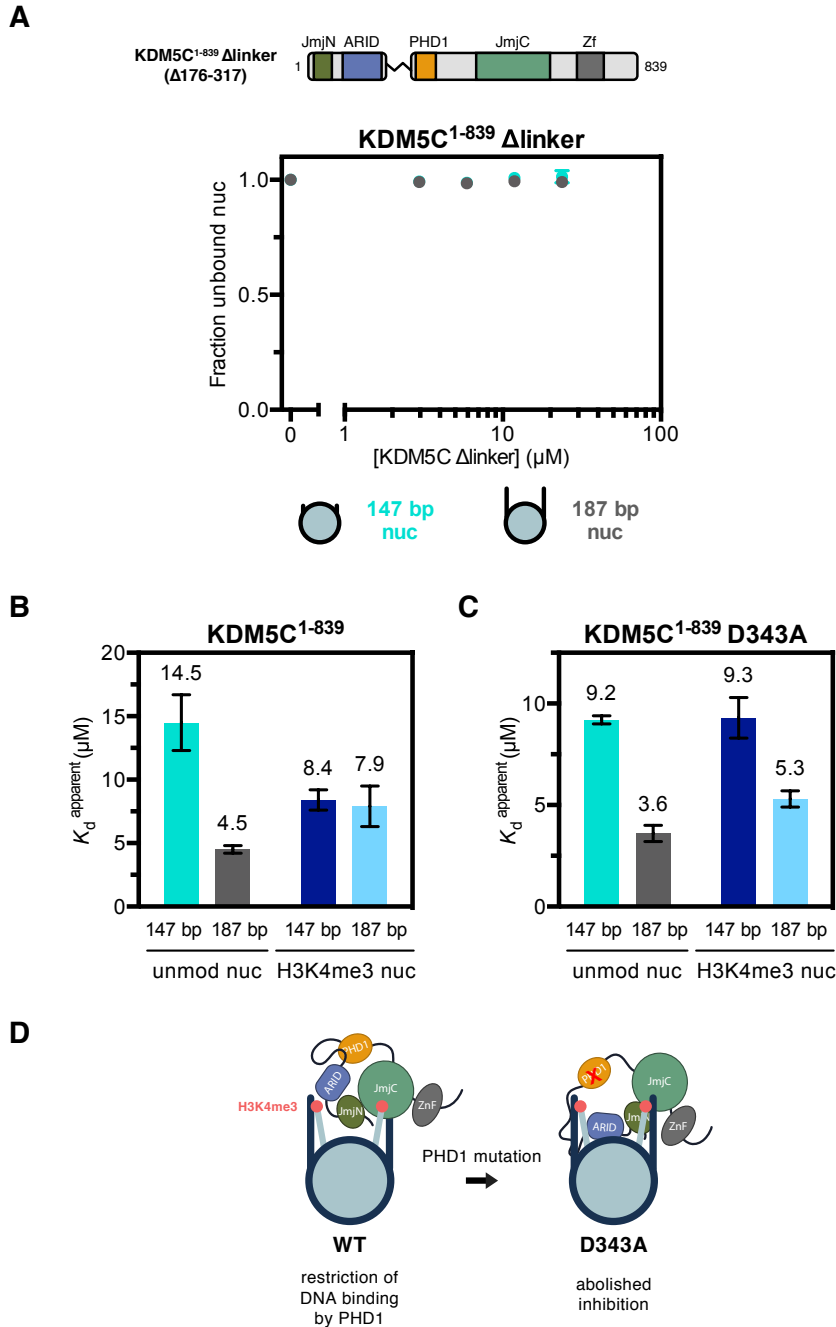


Figure 2.4. KDM5C recognizes flanking DNA in the absence of H3K4me3 due to regulation by PHD1.

(A) Binding of KDM5C¹⁻⁸³⁹ Δlinker to unmodified nucleosomes with and without 20 bp flanking DNA. Nucleosome binding curves were measured by EMSA. **(B)** Nucleosome binding by KDM5C¹⁻⁸³⁹ with apparent dissociation constants (K_d^{app}) measured by EMSA and fit to a cooperative binding model (substrate nucleosome binding curves in Figure S2.5E). Select dissociation constants replotted from Figure 2.1B and Figure 2.3A for comparison. **(C)** Nucleosome binding by PHD1 mutant KDM5C¹⁻⁸³⁹ D343A with apparent dissociation constants (K_d^{app}) measured by EMSA (binding curves in Figure S2.5F). **(D)** Model for KDM5C inhibition, where PHD1 prevents flanking DNA recognition in the presence of H3K4me3, and its relief by the PHD1 mutation that disrupts the inhibition. All error bars represent SEM of at least two independent experiments ($n \geq 2$).

We next interrogated recognition of flanking DNA on the nucleosome in the presence of the H3K4me3 substrate, as recognition of both could facilitate recruitment of KDM5C to its target sites in euchromatin³³. Intriguingly, KDM5C¹⁻⁸³⁹ has similar binding affinity for both the core and flanking DNA-containing H3K4me3 nucleosome, with K_d^{app} of $\sim 8 \mu\text{M}$, indicating no engagement of flanking DNA in the presence of the H3K4me3 substrate (**Figure 2.4B**). This contrasts with unmodified nucleosome binding, where KDM5C has a clear preference for nucleosomes with flanking DNA (**Figure 2.4B**).

Since KDM5C recognizes flanking DNA only in the context of the unmodified nucleosome, we considered the possibility that the ability to engage flanking DNA is coupled to binding of the H3 tail product to the PHD1 domain. To test this model, we interrogated the effect of the PHD1 D343A mutation, which abrogates H3 binding, on the recognition of flanking DNA by KDM5C. We find that PHD1 mutant KDM5C¹⁻⁸³⁹ D343A still retains the 3-fold affinity gain towards the unmodified 187 bp nucleosome ($K_d^{app} = 3.6 \mu\text{M}$) compared to the unmodified core nucleosome ($K_d^{app} = 9.2 \mu\text{M}$) (**Figure 2.4C**). In addition, PHD1 mutant KDM5C displays a ~ 2 fold affinity gain towards the 187 bp H3K4me3 nucleosome ($K_d^{app} = 5.3 \mu\text{M}$), relative to the H3K4me3 core nucleosome ($K_d^{app} = 9.3 \mu\text{M}$) (**Figure 2.4C**). Although modest, this improved binding demonstrates that, unlike wild type KDM5C, PHD1 mutant KDM5C can recognize flanking DNA in the presence of the H3K4me3 substrate. These findings suggest that flanking DNA recognition, likely mediated by the ARID-PHD1 linker region, is regulated by the PHD1 domain.

The observation that PHD1 mutant KDM5C can constantly recognize flanking DNA lead us to hypothesize that, beyond disruption of H3 tail binding, the D343A mutation may also disrupt intramolecular interactions within the demethylase which restrict the ability of the ARID-PHD1 linker and ARID to interact with DNA (**Figure 2.4D**). This PHD1-imposed inhibition model is consistent with the strong catalytic enhancement observed with the PHD1 mutant

demethylase under single turnover conditions (**Figure 2.2D**), as the ARID-DNA interaction beneficial for catalysis could be enhanced due to enabled DNA interactions upon the PHD1 mutation. This model implies that the PHD1 binding surface is involved in intramolecular interactions beyond the recognition of the H3 tail. Through further PHD1 binding experiments interrogating ligand recognition, the PHD1 domain displays an indifference for a free N-terminus on its H3 tail ligand (**Figure S2.6A**). In addition, PHD1 binds other basic histone tails with reduced affinity (**Figure S2.6B**). Nonetheless, an arginine residue (H3R2) is needed for H3 tail binding by PHD1 (**Figure S2.2E**), and the D343A PHD1 mutation is in the predicted H3R2 binding pocket of PHD1. Our investigations into ligand recognition by PHD1 indicate that it is permissive for the recognition of an internal arginine residue within KDM5C.

DISCUSSION

Different reader and regulatory domains within chromatin binding proteins and modifying enzymes influence their activity and substrate specificity by recognizing distinct chromatin states through distinguishing histone modifications, features on the nucleosome, and surrounding DNA. Emerging structural studies of chromatin modifying enzymes in complex with nucleosomes have highlighted these multivalent interactions, with increasing observations of interactions with DNA contributing to nucleosome engagement by histone modifying enzymes^{50–62}. Despite the unique insertion of the ARID and PHD1 reader domains in the composite catalytic domain, the function of accessory domains within the KDM5 demethylase family has not been explored on nucleosomes. Here, we describe a hierarchy of regulation by these domains by investigating nucleosome recognition and demethylation in KDM5C, a unique member of the KDM5 family involved in regulation of neuronal gene transcription. We find that there are opposing roles of the ARID and PHD1 domains, with DNA recognition by ARID providing a beneficial interaction for nucleosome demethylation and regulation by PHD1 inhibiting nucleosome recognition and demethylation. We further demonstrate that DNA recognition is regulated by the PHD1 domain, allowing for sensing and specificity towards the H3K4me3 substrate. Our findings accentuate diverse regulatory mechanisms by accessory elements within KDM5C to control chromatin recognition and to modulate H3K4me3 demethylation.

Our findings of KDM5C nucleosome recognition and demethylation can be best explained by a regulatory model where PHD1 controls DNA recognition (**Figure 2.5**). Before catalysis, the H3K4me3 substrate is recognized and DNA binding is attenuated due to the restriction of the ARID-PHD1 linker by PHD1 (state I). Basal demethylation is achieved through transient interactions of ARID with nucleosomal DNA during catalysis (state II). Release of the

PHD1-imposed constraint on the ARID-PHD1 linker and ARID domain enables its improved interaction with DNA, leading to faster catalysis (state III). In our experiments, the D343A PHD1 mutation was revealed to be a mechanistic probe to release the PHD1-imposed restriction on DNA binding. In the context of chromatin, this release of inhibition could be achieved through binding of the H3 tail to PHD1, allowing for the regulation of demethylation by the surrounding chromatin environment. Formation of the demethylated H3 product, and its binding to PHD1, further reinforces an interaction of KDM5C with chromatin by enabling linker DNA recognition, most likely through the ARID-PHD1 linker region (state IV).

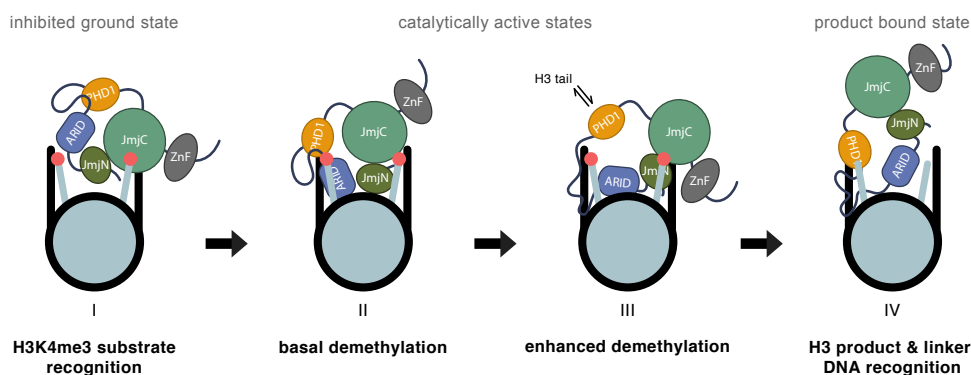


Figure 2.5. Model of KDM5C regulation by the ARID-linker-PHD1 region.

KDM5C recognizes H3K4me3 and binds to substrate nucleosomes through the catalytic domain (*pre-catalytic and inhibited ground state I*). DNA binding in the presence of H3K4me3 is attenuated due to restriction of the ARID-PHD1 linker by PHD1. During demethylation, ARID makes transient interactions with nucleosomal DNA to orient the catalytic domain towards the H3K4me3 tail for efficient demethylation (*catalytically active state II*). H3 tail binding to PHD1 releases the PHD1 interaction constraining the ARID-PHD1 linker and ARID domain, enabling ARID interactions with DNA to further enhance demethylation (*catalytically active state III*). After demethylation, binding of the product H3 tail to PHD1 enables linker DNA binding by the ARID-PHD1 linker region (*post-catalytic and product bound state IV*).

Unexpectedly, the k_{max} of demethylation by KDM5C is >100-fold lower on the substrate nucleosome than on the substrate peptide (**Figure 2.1C**, **Figure S2.1A**), whereas many histone modifying enzymes exhibit higher activity on corresponding nucleosome substrates versus peptides. However, lower activity on nucleosomes compared to peptide substrates has also

been observed in the unrelated H3K4me1/2 histone demethylases LSD1/KDM1A and LSD2/KDM1B^{58,63}. This lower activity could reflect possible nonproductive binding modes of KDM5C on the nucleosome or, more likely, intrinsic inaccessibility of the H3K4me3 substrate tail on the nucleosome due to histone tail-DNA interactions⁶⁴⁻⁶⁶. Furthermore, the presence of substrate inhibition under multiple turnover conditions of excess substrate peptide (>50 μ M) indicate that less productive states of KDM5C that are catalytically rate-limiting can form, and this appears to be driven by the ARID and PHD1 region (**Figure S2.1A**). Intriguingly, we observe cooperativity (Hill coefficients > 1) in nucleosome binding and demethylation (**Figure 2.1C, Figure S2.1B**). In addition, cooperativity occurs in peptide demethylation by wild type KDM5C¹⁻⁸³⁹ but not by KDM5C¹⁻⁸³⁹ Δ AP or KDM5C¹⁻⁸³⁹ Δ linker under single turnover conditions (**Figure S2.1A, Figure S2.5C**), suggesting that cooperativity might arise both from a multimeric state of KDM5C through its ARID-PHD1 linker region and from the nucleosome containing two H3 tails where binding and demethylation on one tail is promotive of the other tail.

Our finding of the beneficial role of the ARID domain towards KDM5C catalysis on nucleosomes can be rationalized by favorable transient interactions of the ARID domain with nucleosomal DNA to better orient the catalytic domains for demethylation and could make the substrate H3K4me3 more accessible through disrupting histone tail-DNA interactions⁶⁴⁻⁶⁷. This is supported by the previous observation that the ARID domain of KDM5C is required for its demethylase activity *in vivo* but not for its chromatin association¹⁵. This role of the ARID domain in productive nucleosome demethylation may be conserved within the KDM5 family, as the ARID domain is also required for *in vivo* demethylation by KDM5A/B and the *Drosophila* KDM5 homolog Lid^{8,14,16,17}. However, the sequence specificities of DNA binding by ARID domains in the KDM5 family might differ, as the ARID domains of KDM5A/B bind GC-rich DNA with different sequence preferences and we observe that ARID of KDM5C might possess some sequence specificity (**Figure S2.3A**) which requires further characterization¹⁷⁻¹⁹. Regardless of

DNA sequence preference, the ARID domain may be required for nucleosome demethylation in order to displace the H3K4me3 tail from interacting with DNA, making it accessible for engagement by the catalytic domain. This histone tail displacement function has been proposed for DNA binding reader domain modules and for the LSD1/CoREST complex, where the SANT2 domain interacts with nucleosomal DNA to displace the H3 tail for engagement by the LSD1 active site^{58,67–69}.

In contrast to the beneficial role of the ARID domain, we observe an unexpected inhibitory role of PHD1 towards KDM5C demethylation on nucleosomes. This finding suggests differential regulation by PHD1 in the KDM5 family, as PHD1 binding has a stimulatory role towards *in vitro* demethylation in KDM5A/B and PHD1 is required for demethylase activity *in vivo* for KDM5B and Lid^{8,14,29,30,32}. Our data suggests this inhibitory role is mediated by the ability of PHD1 to restrict the ARID-PHD1 linker and ARID domain from engaging DNA on the nucleosome (**Figure 2.5**). Alternatively, we also consider the possibility that the PHD1 domain could act directly on the catalytic domains to impair productive substrate nucleosome engagement. With weak affinity, indifference for a free N-terminus, non-specific histone tail binding, and a likely binding-induced conformational change, ligand recognition by PHD1 in KDM5C is strikingly different from that observed for the PHD1 domains in KDM5A and KDM5B. While further work is needed to identify how PHD1 inhibits DNA binding, we hypothesize that this could be achieved through an interaction between PHD1 and an arginine residue within the unstructured ARID-PHD1 linker region. This unique ARID-PHD1 linker (**Figure S2.4**) may contribute to distinct regulation by PHD1 in KDM5C. Although we are unable to directly test the effect of H3 tail binding to PHD1 on DNA recognition due to the low affinity regime, we hypothesize that the resulting binding releases inhibition, allowing for regulation of KDM5C activity by different chromatin environments. As a consequence, H3 tail binding by PHD1 might

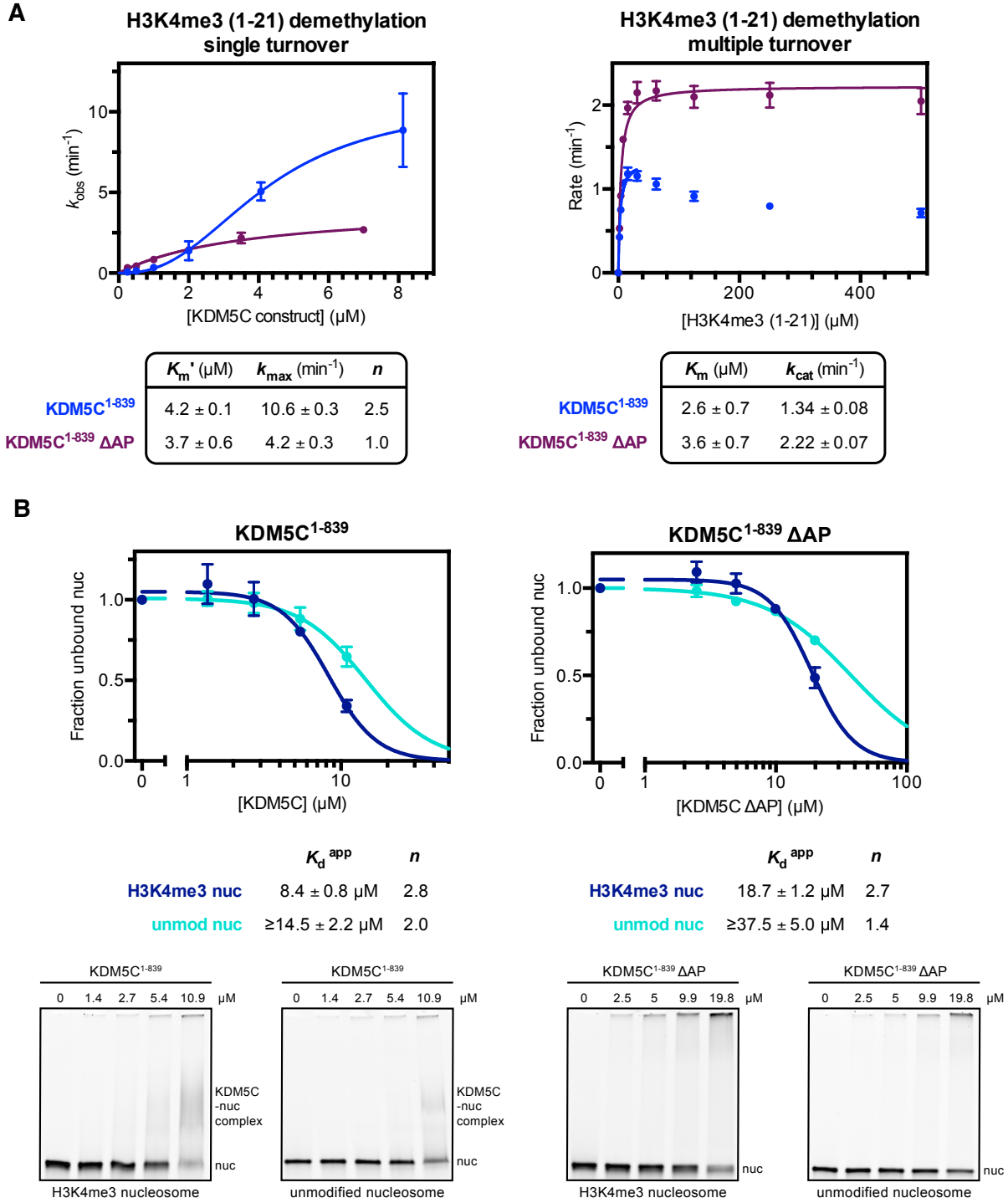
be stimulatory towards demethylation, as observed upon PHD1 binding in KDM5A/B, through a mechanistically distinct relief of negative regulation in KDM5C.

Unlike the ARID domain, whose DNA recognition is needed for nucleosome demethylation but not nucleosome binding, the ARID-PHD1 linker region drives nucleosome binding but does not appear to contribute to demethylation by KDM5C. Our data suggests nucleosome binding by the ARID-PHD1 linker is facilitated through DNA binding, where further investigation is needed to understand the basis and specificity of DNA recognition. Perplexingly, we observe diminished nucleosome binding upon deletion of the ARID-PHD1 linker as opposed to a 2-fold decrease in nucleosome binding upon deletion of the entire ARID and PHD1 region (**Figure 2.4A**, **Figure 2.1B**). Although the molecular basis for these effects requires further studies, this observed discrepancy could result from the ARID and PHD1 domains affecting nucleosome binding by the catalytic and zinc finger domains of KDM5C. While it remains unknown whether the linker region between ARID and PHD1 in other KDM5 members has a similar function or whether it is specific to KDM5C due to its different ARID-PHD1 linker, our findings add to the reports of intrinsically disordered regions as functional elements within chromatin binding proteins⁷⁰⁻⁷³.

Unexpectedly, KDM5C recognizes flanking DNA around the nucleosome in the presence of the unmodified H3 tail but not in the presence of the H3K4me3 substrate. While the function of this linker DNA recognition is unclear, it may serve to retain KDM5C at its target promoter and enhancer sites within open chromatin after demethylation. It may also enable processive demethylation of adjacent nucleosomes in euchromatin by KDM5C. Interestingly, the recognition of linker DNA has been observed in the mechanistically unrelated H3K4me1/2 histone demethylase LSD1/KDM1A, where demethylase activity is in contrast stimulated by linker DNA^{50,74}. The H3K36me1/2 demethylase KDM2A is also capable of recognizing linker DNA, where it is specifically recruited to unmethylated CpG islands at gene promoters through

its ZF-CxxC domain^{75,76}. These findings suggest that recognition of the chromatin state with accessible linker DNA may be utilized by histone modifying enzymes that function on euchromatin. While the sequence specificity of linker DNA recognition requires further investigation, it is evident that the sensing of the H3K4me3 substrate tail by KDM5C is preferred over recognition of linker DNA, a feature accessible in open chromatin. This observed hierarchy, coupled with KDM5C's overall weak affinity towards nucleosomes and dampened demethylase activity due to regulation by PHD1, suggests tunable demethylation by KDM5C. Thus, this multi-domain regulation might serve to establish H3K4me3 surveillance through KDM5C-catalyzed demethylation, which is well suited for the physiological role of this enzyme in fine tuning gene expression through H3K4me3 demethylation at enhancers and promoters of genes, as well as its role in genome surveillance by preventing activation of non-neuronal genes in adult neurons^{33,36}.

SUPPLEMENTAL FIGURES



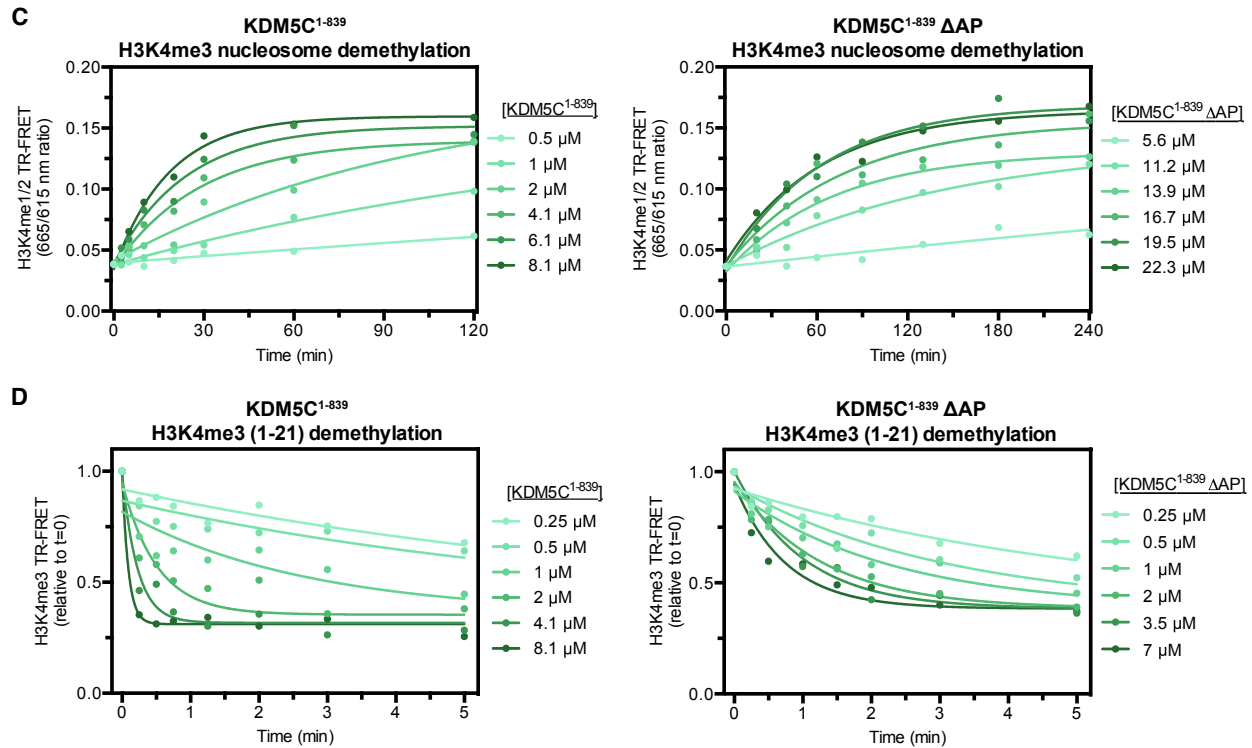
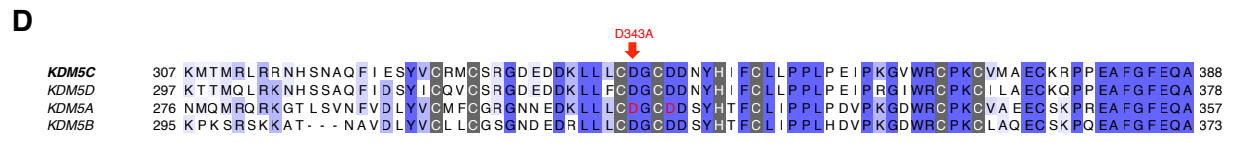
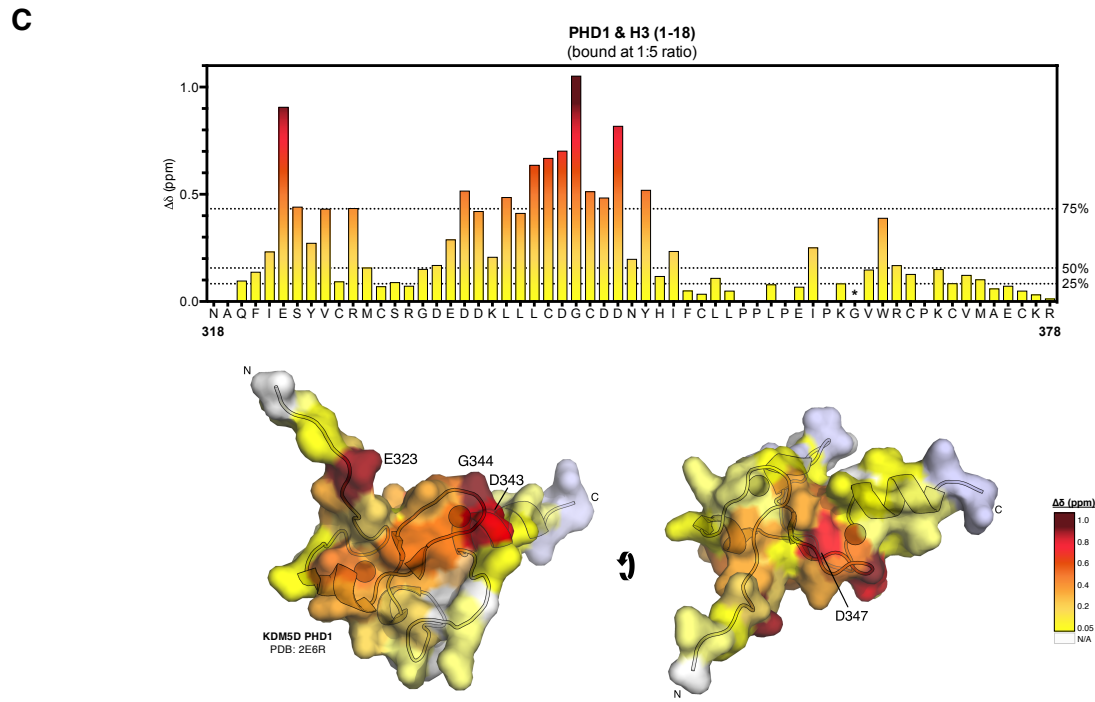
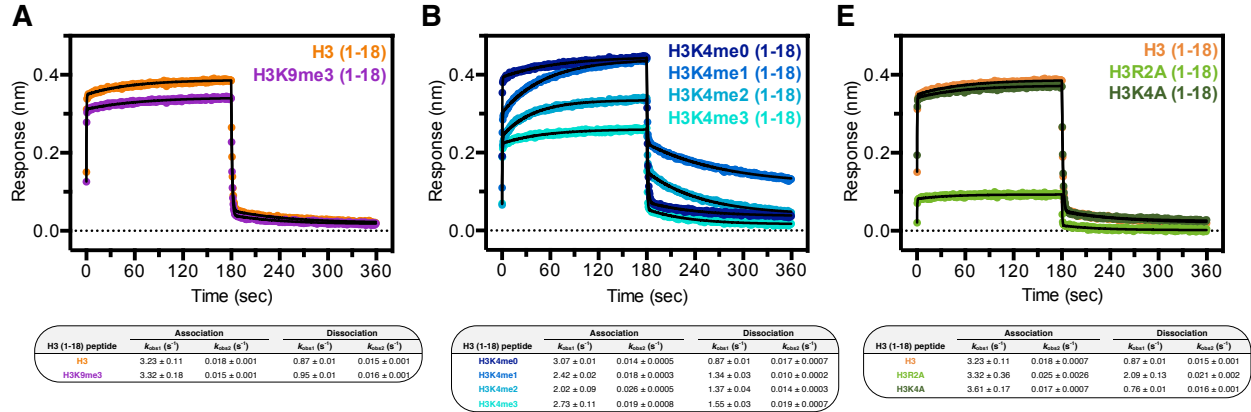


Figure S2.1. Substrate demethylation and nucleosome binding by KDM5C constructs.

(A) H3K4me3 substrate peptide demethylation by KDM5C constructs. *Left:* Demethylation kinetics of the H3K4me3 (1-21) substrate peptide by KDM5C constructs under single turnover conditions measured by a TR-FRET based kinetic assay. Observed rates are fit to a cooperative kinetic model, with n denoting the Hill coefficient. Representative kinetic traces used to determine observed demethylation rates are in Figure S2.1D. *Right:* Demethylation kinetics of the H3K4me3 (1-21) substrate peptide by KDM5C constructs under multiple turnover conditions measured by a formaldehyde release based kinetic assay. Deletion of the ARID and PHD1 region results in higher demethylase activity on the substrate peptide under multiple turnover conditions due to loss of substrate inhibition caused by this region. **(B)** Unmodified and substrate core nucleosome binding by KDM5C¹⁻⁸³⁹ and KDM5C¹⁻⁸³⁹ ΔAP. Nucleosome binding curves were measured by EMSA and fit to a cooperative binding model to determine apparent dissociation constants (K_d^{app}), with n denoting the Hill coefficient (*top*). Representative gel shifts of KDM5C binding to nucleosomes (*bottom*). Due to unattainable saturation of binding, a lower limit for the dissociation constant is presented for the unmodified nucleosome. **(C)** Representative demethylation kinetic traces of substrate nucleosome demethylation by KDM5C constructs (*left:* KDM5C¹⁻⁸³⁹, *right:* KDM5C¹⁻⁸³⁹ ΔAP) under single turnover conditions using TR-FRET based kinetic assay detecting formation of the H3K4me1/2 product nucleosome over time. Observed rates (k_{obs}) are obtained by fitting kinetic traces to an exponential function. **(D)** Representative demethylation kinetic traces of substrate peptide demethylation by KDM5C constructs (*left:* KDM5C¹⁻⁸³⁹, *right:* KDM5C¹⁻⁸³⁹ ΔAP) under single turnover conditions using TR-FRET based kinetic assay detecting loss of the H3K4me3 substrate peptide over time. Observed rates (k_{obs}) are obtained by fitting kinetic traces to an exponential function. All error bars represent SEM of at least two independent experiments ($n \geq 2$).



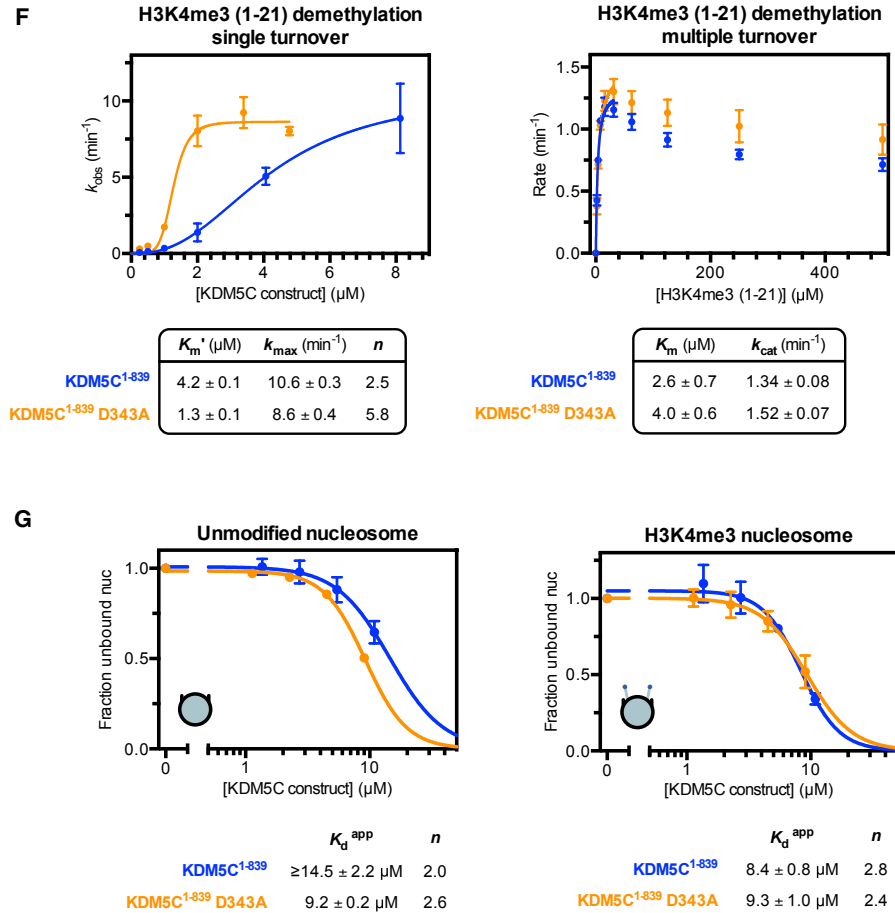


Figure S2.2. H3 ligand recognition by PHD1 and substrate demethylation and binding by PHD1 mutant KDM5C.

(A) Binding kinetic trace of immobilized Avitag-PHD1 binding to H3 (1-18) and H3K9me3 (1-18) tail peptides measured by bio-layer interferometry (BLI). Observed rates (k_{obs}) of association and dissociation are obtained by fitting kinetic traces to a two phase exponential function. (B) Binding kinetic trace of immobilized Avitag-PHD1 binding to H3K4me0/1/2/3 (1-18) tail peptides measured by bio-layer interferometry (BLI). Biphasic kinetic binding by PHD1 is modulated by the H3K4me state. (C) Chemical shift change of PHD1 residues upon binding of the H3 (1-18) tail peptide at 1:5 molar ratio (PHD:peptide) measured by NMR (*top*). The chemical shift change of G364 (* denoted by asterisk) could not be determined due to broadened chemical shift when bound. Dashed lines indicate 25th, 50th, and 75th percentile rankings, and residues are colored by a gradient from unperturbed (yellow) to significantly perturbed (maroon). Chemical shift perturbations colored by the gradient mapped to homologous residues in KDM5D PHD1 structure (PDB: 2E6R) (*bottom*). Significantly perturbed residues are labeled. (D) Binding kinetic trace of immobilized Avitag-PHD1 binding to H3 (1-18) and H3 mutant (1-18) tail peptides (H3R2A and H3K4A) measured by bio-layer interferometry (BLI). Recognition of the H3 tail by PHD1 depends on the R2 residue but not K4 residue in H3. (E) Sequence alignment of PHD1 domains in KDM5A-D. The H3R2 recognizing residues D312 and D315 of KDM5A are indicated in red, and the PHD1 mutation D343A from this study is denoted above KDM5C. Zinc coordinating residues are highlighted in gray. (F) H3K4me3 substrate peptide demethylation by PHD1 mutant KDM5C¹⁻⁸³⁹ relative to wild type. *Left*: Demethylation kinetics of the H3K4me3 (1-21) substrate peptide under single turnover conditions measured by a TR-FRET based kinetic assay. Observed rates are fit to a cooperative kinetic model, with n denoting the Hill coefficient. Unlike on the substrate nucleosome, the D343A PHD1 mutation does not increase catalytic rate on the substrate peptide but does increase overall catalytic efficiency. *Right*: Demethylation kinetics of the H3K4me3 (1-21) substrate peptide under multiple turnover conditions measured by a formaldehyde release based kinetic assay. The D343A PHD1 mutation does not affect catalysis on the substrate peptide under these conditions, nor does it significantly affect substrate inhibition. (G) Unmodified and substrate core nucleosome binding by PHD1 mutant KDM5C¹⁻⁸³⁹ relative to wild type. Nucleosome binding curves were measured by EMSA and fit to a cooperative binding model to determine apparent dissociation constants (K_d^{app}), with n denoting the Hill coefficient. Due to unattainable saturation of binding, a lower limit for the dissociation constant is presented for wild type KDM5C binding the unmodified nucleosome. All error bars represent SEM of at least two independent experiments ($n \geq 2$).

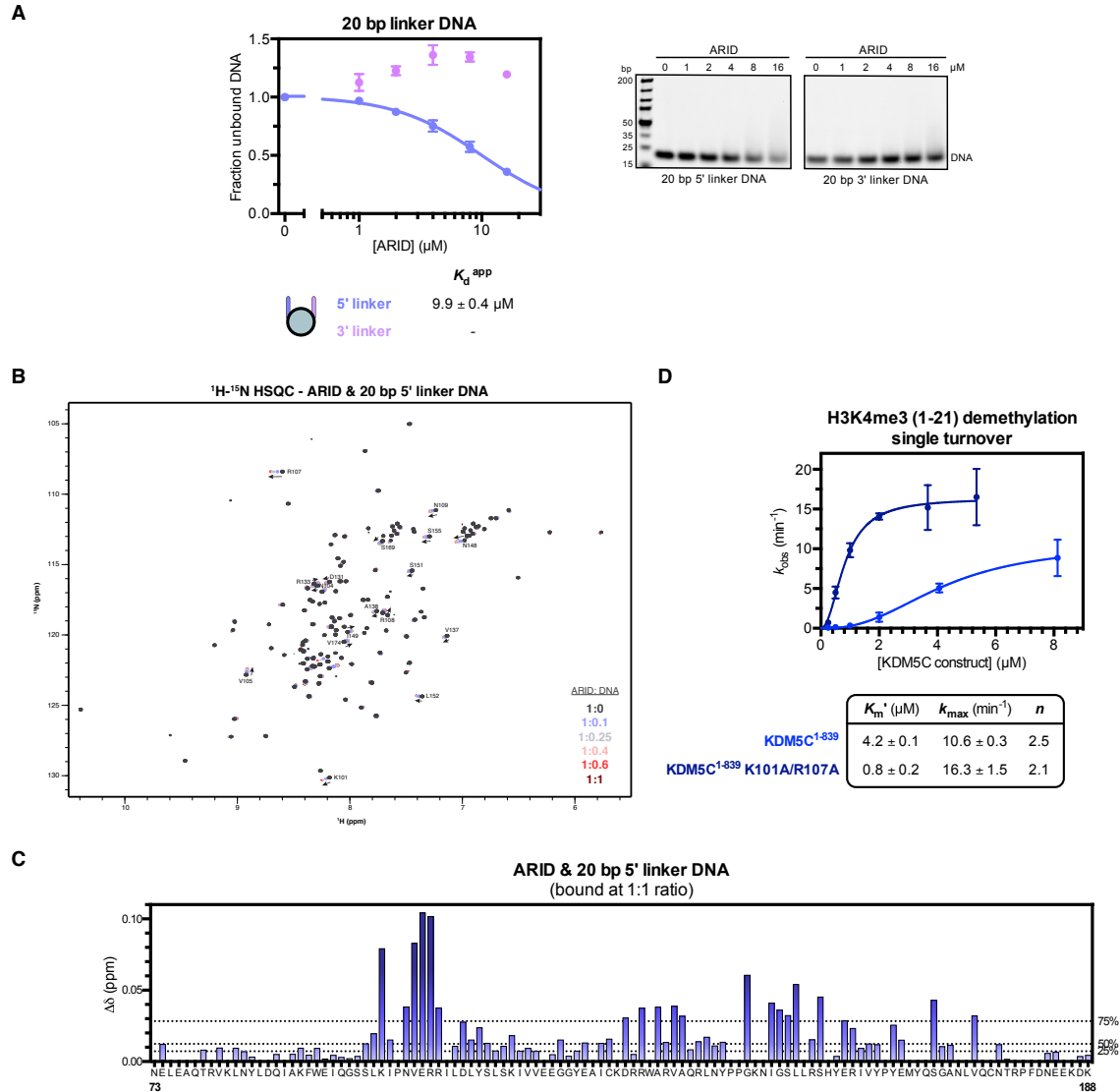


Figure S2.3. DNA recognition by ARID and substrate demethylation by ARID mutant KDM5C.

(A) 20 bp linker DNA fragment binding by the ARID domain. Fragments contain 5' and 3' flanking DNA sequences used in the 187 bp nucleosome. Binding curves were measured by EMSA and fit to a binding model to determine apparent dissociation constants (K_d^{app}) (left). Representative gel shifts of ARID binding to 20 bp flanking linker DNA fragments (right). (B) 2D ^1H - ^{15}N HSQC spectra of ARID titrated with increasing amounts of the 5' linker DNA 20 bp fragment with indicated molar ratios. Assignments of most perturbed residues in ARID are labeled. (C) Chemical shift change of ARID residue backbone assignments upon binding of the 5' linker DNA 20 bp fragment at 1:1 molar ratio measured by NMR. ARID backbone assignments could not be reliably transferred to a subset of residues and thus chemical shifts could not be determined (indicated by no values). Dashed lines indicate 25th, 50th, and 75th percentile rankings, and residues are colored by a gradient from unperturbed (light blue) to significantly perturbed (navy). (D) Demethylation kinetics of the H3K4me3 (1-21) substrate peptide by wild type and ARID mutant KDM5C¹⁻⁸³⁹ under single turnover conditions. Observed rates are fit to a cooperative kinetic model, with n denoting the Hill coefficient. Unlike on the substrate nucleosome, the K101A/R107A ARID double mutation does not decrease catalytic rate on the substrate peptide but does increase overall catalytic efficiency. All error bars represent SEM of at least two independent experiments ($n \geq 2$).

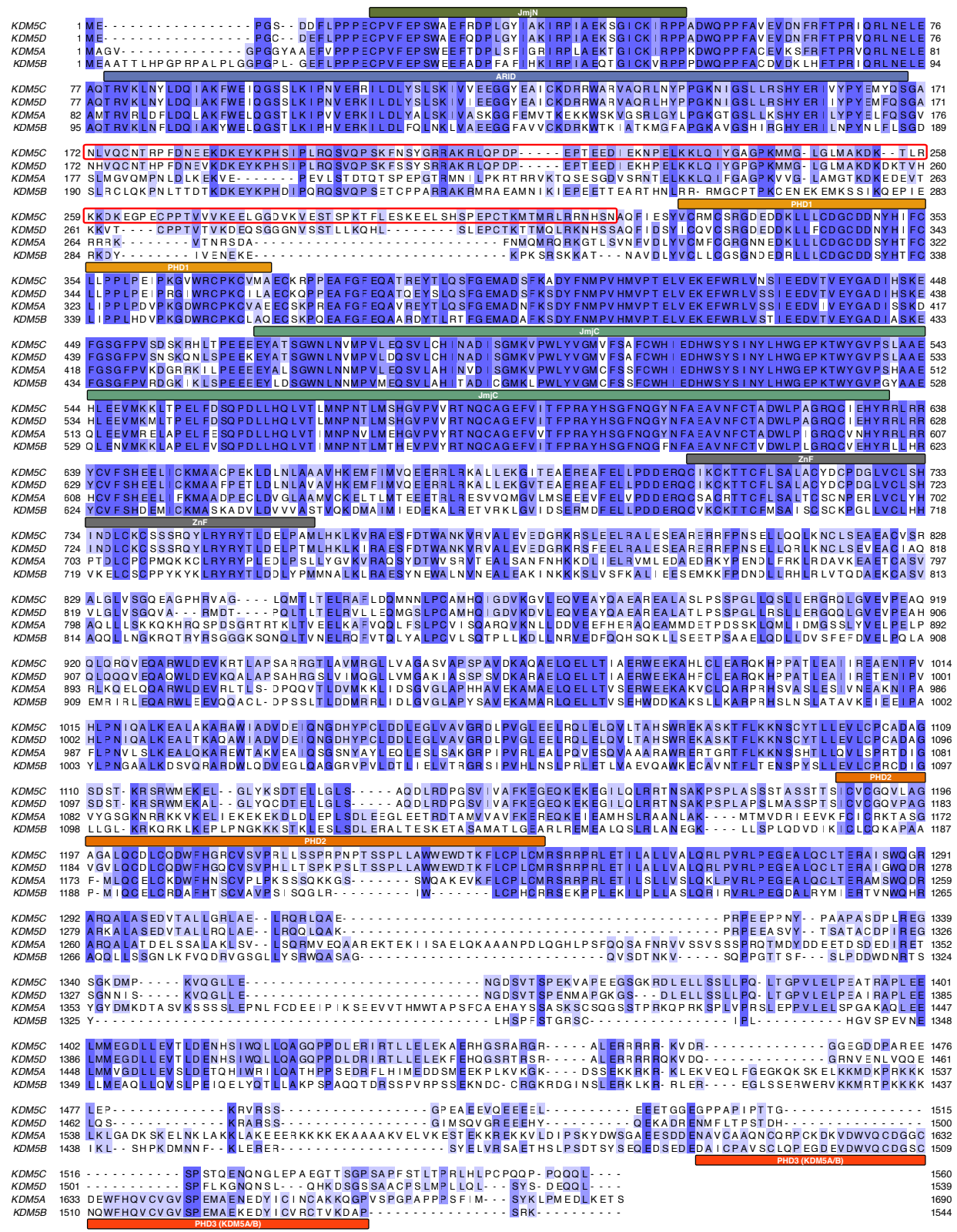
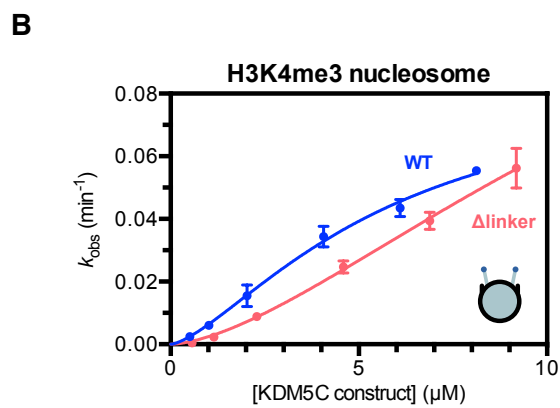
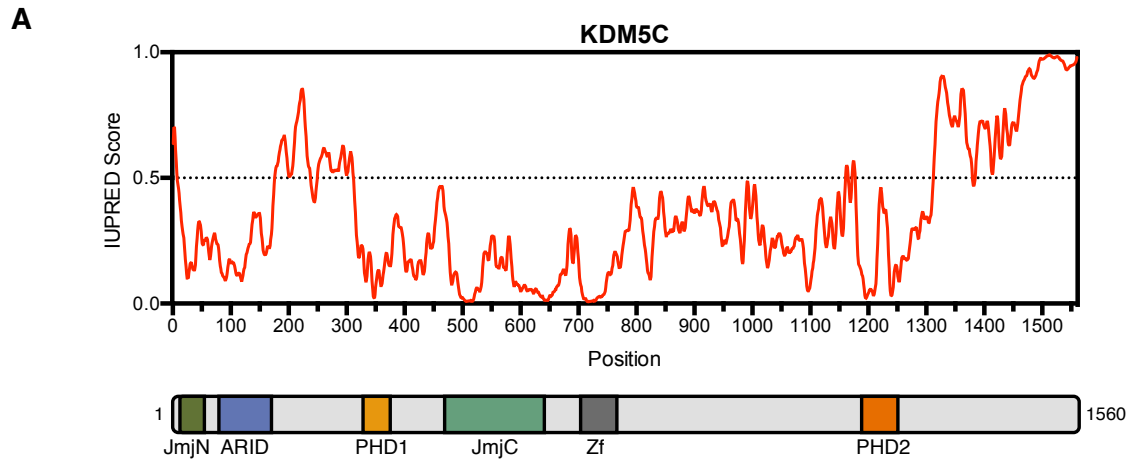
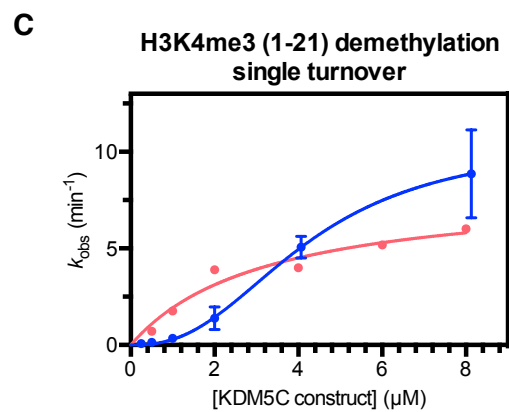


Figure S2.4. KDM5 family sequence alignment.

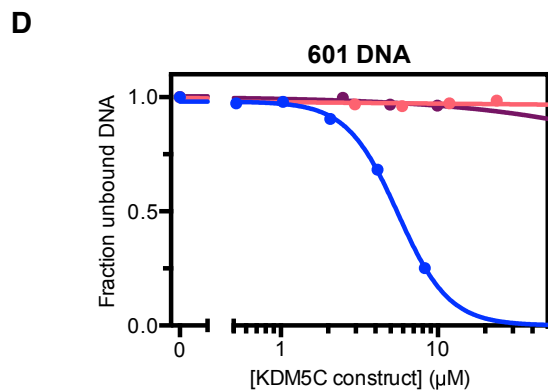
Sequence alignment of human KDM5A-D with annotated domains. KDM5C has a different and extended linker region between ARID and PHD1 (boxed in red).



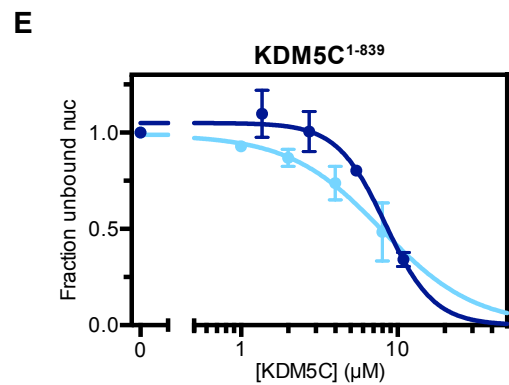
| | K_m^{app} (μM) | k_{max} (min^{-1}) | n |
|---|--------------------------------------|--|-----|
| KDM5C¹⁻⁸³⁹ | 5.7 ± 1.7 | 0.087 ± 0.018 | 1.5 |
| KDM5C¹⁻⁸³⁹ Δlinker | 14.2 ± 5.3 | 0.168 ± 0.061 | 1.6 |



| | K_m^{app} (μM) | k_{max} (min^{-1}) | n |
|---|--------------------------------------|--|-----|
| KDM5C¹⁻⁸³⁹ | 4.2 ± 0.1 | 10.6 ± 0.3 | 2.5 |
| KDM5C¹⁻⁸³⁹ Δlinker | 3.2 ± 1.3 | 8.2 ± 1.4 | 1.0 |



| | K_d^{app} | n |
|---|---------------------------|-----|
| KDM5C¹⁻⁸³⁹ | $5.6 \pm 0.1 \mu\text{M}$ | 2.7 |
| KDM5C¹⁻⁸³⁹ ΔAP | - | - |
| KDM5C¹⁻⁸³⁹ Δlinker | - | - |



| | K_d^{app} | n |
|---------------------------|---------------------------|-----|
| 147 bp H3K4me3 nuc | $8.4 \pm 0.8 \mu\text{M}$ | 2.8 |
| 187 bp H3K4me3 nuc | $7.9 \pm 1.6 \mu\text{M}$ | 1.5 |

F

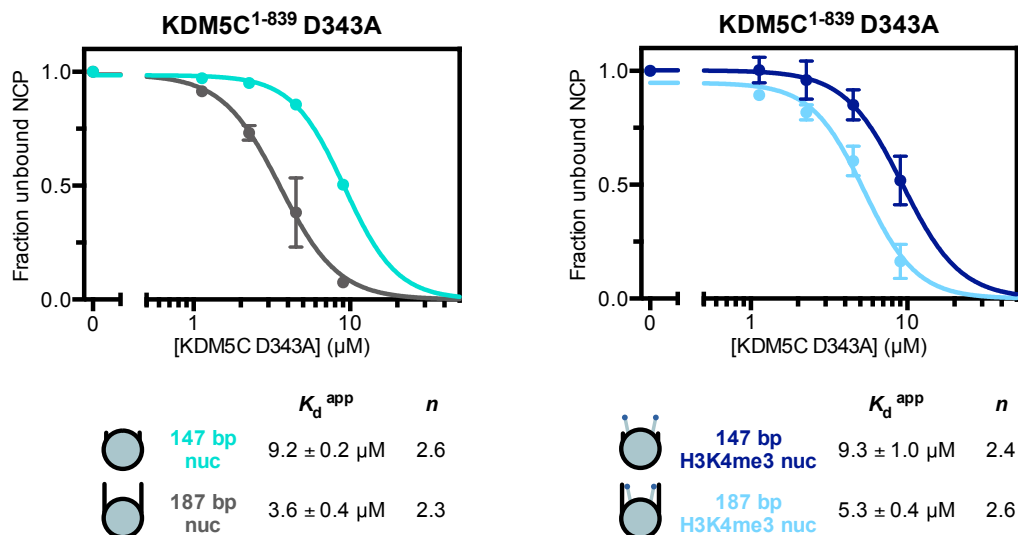
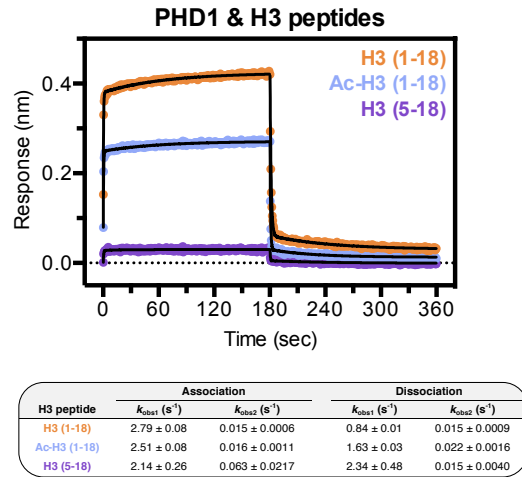


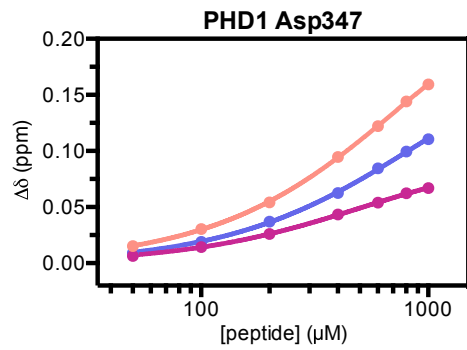
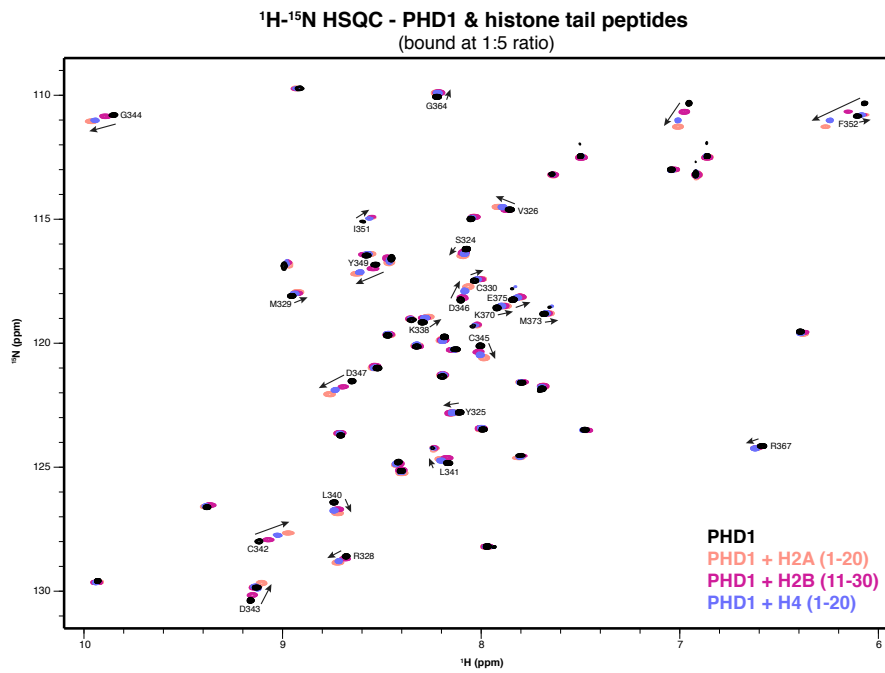
Figure S2.5. Characterization of ARID-PHD1 linker region contribution to substrate demethylation and linker DNA recognition by KDM5C constructs.

(A) IUPred profile⁷⁷ of predicted disorder in KDM5C (*top*) and annotated domain architecture of KDM5C (*bottom*). The linker between ARID and PHD1 is predicted to be disordered. (B) Demethylation kinetics of the H3K4me3 substrate nucleosome by wild type and KDM5C¹⁻⁸³⁹ Δlinker under single turnover conditions. Observed rates are fit to a cooperative kinetic model, with n denoting the Hill coefficient. Deletion of the ARID-PHD1 linker does not significantly affect the catalytic efficiency of substrate nucleosome demethylation. (C) Demethylation kinetics of the H3K4me3 (1-21) substrate peptide by wild type and KDM5C¹⁻⁸³⁹ Δlinker under single turnover conditions. Observed rates are fit to a cooperative kinetic model, with n denoting the Hill coefficient. Similarly to nucleosomes, deletion of the ARID-PHD1 linker does not significantly affect the catalytic efficiency of substrate peptide demethylation. (D) DNA (147 bp 601 core nucleosome positioning sequence) binding by KDM5C constructs. Binding curves were measured by EMSA and fit to a cooperative binding model to determine apparent dissociation constants (K_d^{app}). Deletion of the ARID-PHD1 linker diminishes DNA binding by KDM5C. (E) Nucleosome binding curves of KDM5C¹⁻⁸³⁹ binding to substrate nucleosomes with and without 20 bp flanking DNA. Nucleosome binding curves were measured by EMSA and fit to a cooperative binding model to determine apparent dissociation constants (K_d^{app}), with n denoting the Hill coefficient. (F) Binding curves of PHD1 mutant KDM5C¹⁻⁸³⁹ binding to unmodified and substrate nucleosomes with and without 20 bp flanking DNA. All error bars represent SEM of at least two independent experiments ($n \geq 2$).

A



B



| | K_d |
|-------------|--------------------|
| H2A (1-20) | $\geq 630 \mu M$ |
| H2B (11-30) | $393 \pm 27 \mu M$ |
| H4 (1-20) | $\geq 736 \mu M$ |

Figure S2.6. Features of ligand recognition and histone tail binding by PHD1.

(A) Binding kinetic trace of immobilized Avitag-PHD1 binding to H3 (1-18), N-terminally acetylated H3 (1-18), and H3 (5-18) tail peptides measured by bio-layer interferometry (BLI). Observed rates (k_{obs}) of association and dissociation are obtained by fitting kinetic traces to a two phase exponential function. Recognition of the H3 tail by PHD1 does not strongly depend on the H3 N-terminus but does depend on the first 4 residues of H3 (ARTK). **(B)** *Top*: 2D ^1H - ^{15}N HSQC spectra of PHD1 bound to histone tail peptides with 1:5 molar ratio. Backbone assignments of perturbed residues in PHD1 are labeled. *Bottom*: Binding of histone tail peptides by PHD1 measured by NMR titration HSQC experiments. The chemical shift change ($\Delta\delta$) of D347 in PHD1 was fit to obtain dissociation constants with standard error. Due to incomplete saturation of binding, a lower limit for dissociation constants is presented. Peptide sequences are H2A (1-20): SGRGKQGGKARAKAKTRSSR, H2B(11-30): KKGSKKAVTKAQKKGKRRK, and H4 (1-20): SGRGKGGKGLGKGGAKRHRK. PHD1 binds other histone tail peptides with a subset of H3 tail binding residues and with at least 3 to 6 fold lower affinity than H3 tail binding.

CHAPTER 3

Dysregulation of KDM5C by X-linked intellectual disability mutations

RESULTS

X-linked intellectual disability mutations enhance nucleosome recognition by KDM5C

Our proposed KDM5C regulatory model (**Figure 2.5**) provides a mechanistic framework for querying the effects of mutations in KDM5C that cause XLID (**Figure 3.1A**). Specifically, we sought to investigate the D87G and A388P mutations found at the beginning of ARID and immediately downstream of PHD1, respectively. The D87G mutation, associated with mild intellectual disability, has no effect on global H3K4me3 levels *in vivo*⁴⁶. The A388P mutation, associated with moderate intellectual disability, also has no effect on global H3K4me3 levels *in vivo* but also reduces demethylase activity *in vitro*^{6,78}. We initially interrogated nucleosome binding by KDM5C¹⁻⁸³⁹ D87G and A388P. Strikingly, relative to wild type KDM5C¹⁻⁸³⁹, we observe 4-9 fold enhanced binding of the XLID mutants to the unmodified core nucleosome (**Figure 3.1B**), suggesting that these mutations enable enhanced nucleosome engagement. The ARID and PHD1 region is required for this enhanced nucleosome binding, as there is no gain in nucleosome affinity due to the A388P mutation when the ARID and PHD1 region is removed (**Figure S3.1A**). Importantly, the gain in nucleosome affinity of the XLID mutants relative to wild type is more prominent on the unmodified core nucleosome than the substrate H3K4me3 core nucleosome, resulting in loss of binding specificity towards H3K4me3 by KDM5C due to the D87G and A388P mutations (**Figure 3.1C**).

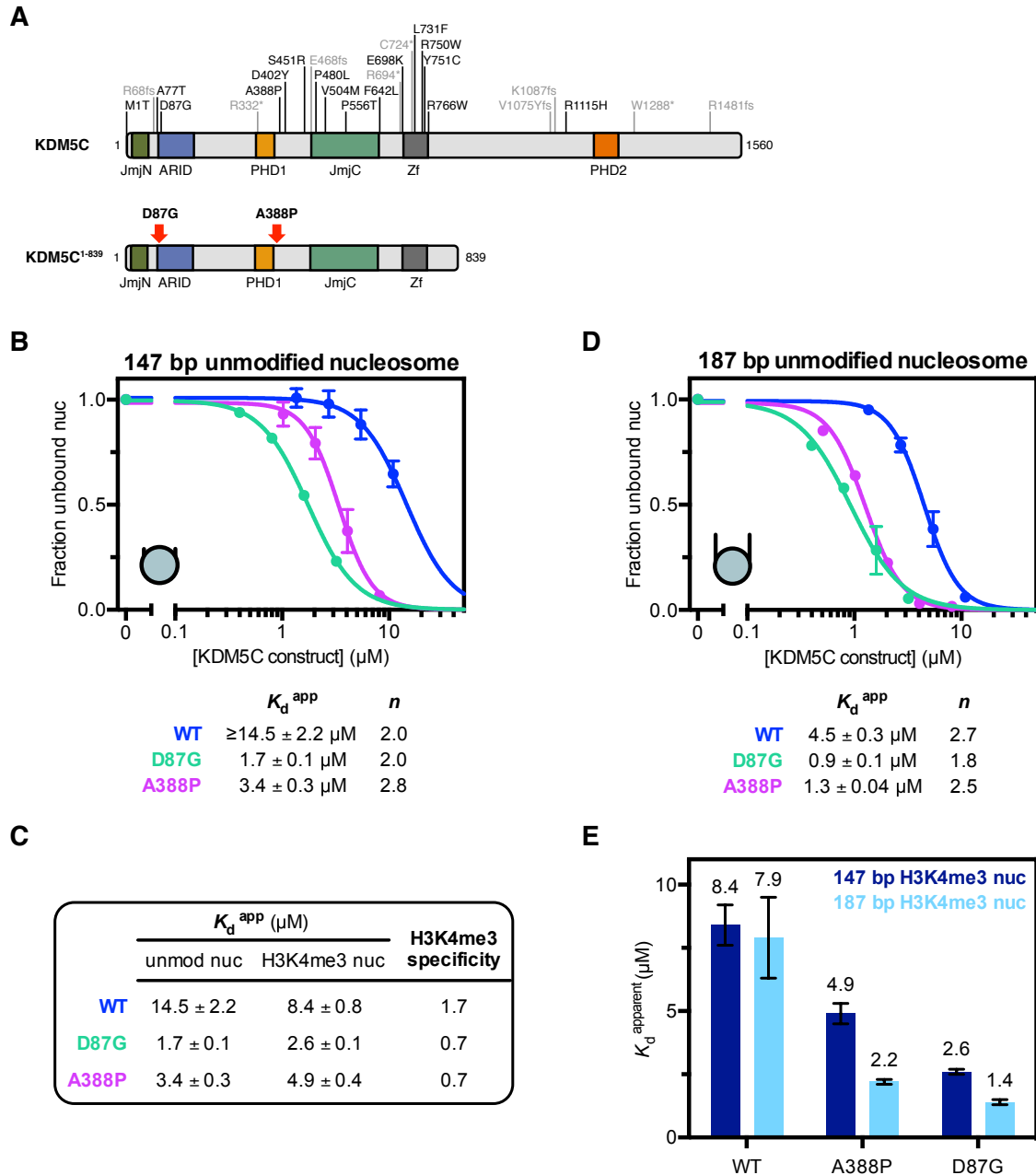


Figure 3.1. X-linked intellectual disability mutations enhance nucleosome binding by KDM5C.

(A) XLID mutations found in KDM5C (*top*) and the XLID mutations investigated in this study (*bottom*). **(B)** Unmodified core nucleosome binding by KDM5C¹⁻⁸³⁹ wild type (WT), D87G, and A388P. Nucleosome binding was measured by EMSA and curves fit to a cooperative binding model to determine apparent dissociation constants (K_d^{app}), with n denoting the Hill coefficient. Wild type binding curve replotted from Figure 2.3A for comparison. Due to unattainable saturation of binding, a lower limit for the dissociation constant is presented for WT KDM5C binding the unmodified nucleosome. **(C)** Apparent dissociation constants (K_d^{app}) of binding by KDM5C¹⁻⁸³⁹ WT, D87G, and A388P to unmodified and substrate core nucleosomes and resulting H3K4me3 fold binding specificity. Select dissociation constants are from Figure 2.1B and Figure 3.1B for comparison. **(D)** Binding curves of KDM5C¹⁻⁸³⁹ WT, D87G, and A388P binding to the unmodified 187 bp nucleosome with 20 bp flanking DNA. Wild type binding curve replotted from Figure 2.3A for comparison. **(E)** Binding of KDM5C¹⁻⁸³⁹ WT, D87G, and A388P to substrate nucleosomes with and without 20 bp flanking DNA with apparent dissociation constants (K_d^{app}) measured by EMSA (binding curves in Figure S3.1C). Select dissociation constants are replotted from Figure 2.4B and Figure 3.1C for comparison. All error bars represent SEM of at least two independent experiments ($n \geq 2$).

As the XLID mutations cause an overall affinity gain towards both unmodified and substrate nucleosomes, we reasoned that the recognition of the shared common epitope of DNA, rather than the H3 tail, is altered in the mutants. Indeed, relative to wild type KDM5C¹⁻⁸³⁹, we observe a similar 4-5 fold gain in affinity by the XLID mutants towards the 187 bp unmodified nucleosome with flanking DNA, with both D87G and A388P mutants converging to a high nucleosome affinity of $K_d^{app} \sim 1 \mu\text{M}$ (**Figure 3.1D**). As flanking DNA recognition by KDM5C appears to be regulated by PHD1, we further interrogated recognition of the 187 bp substrate nucleosome by the D87G and A388P mutants. Both KDM5C¹⁻⁸³⁹ D87G and A388P are capable of recognizing flanking DNA in the presence of H3K4me3, with a ~ 2 fold gain in affinity towards the 187 bp H3K4me3 nucleosome over the H3K4me3 core nucleosome (**Figure 3.1E**). These findings suggest that, similarly to the D343A PHD1 mutation (**Figure 2.4C**), the XLID mutations may disrupt the PHD1-mediated inhibition of DNA recognition by KDM5C. Our findings are consistent with the model that these XLID mutations are altering the ARID and PHD1 region to relieve the inhibition of DNA binding, enabling unregulated binding on the nucleosome.

X-linked intellectual disability mutations render KDM5C demethylation nonproductive in the presence of flanking DNA

We next measured the demethylase activity of KDM5C¹⁻⁸³⁹ D87G and A388P towards the H3K4me3 core nucleosome substrate. Despite these XLID mutants sharing similar enhanced nucleosome binding, their effects on nucleosome demethylation differ. The A388P mutation impairs KDM5C catalysis (k_{max}) by ~ 7 fold, while the D87G mutation increases catalytic efficiency (k_{max}/K_m^{app}) ~ 3 fold through an enhanced K_m^{app} , indicating both nonproductive and productive KDM5C states caused by these mutations (**Figure 3.2A**). The reduced demethylase activity caused by the A388P mutation is consistent with previous findings of reduced *in vitro* demethylation, with the 7-fold reduction on nucleosomes exceeding the previously reported 2-fold reduction on substrate peptide⁶. The reduced demethylase activity due to the A388P

mutation might be caused by impairment of the composite catalytic domain, as we observe reduced demethylase activity in A388P mutant KDM5C¹⁻⁸³⁹ ΔAP (**Figure S3.1B**). In contrast, the D87G mutation does not appear to affect the catalytic domain, and instead the improved catalytic efficiency reflects the enhancement in nucleosome binding.

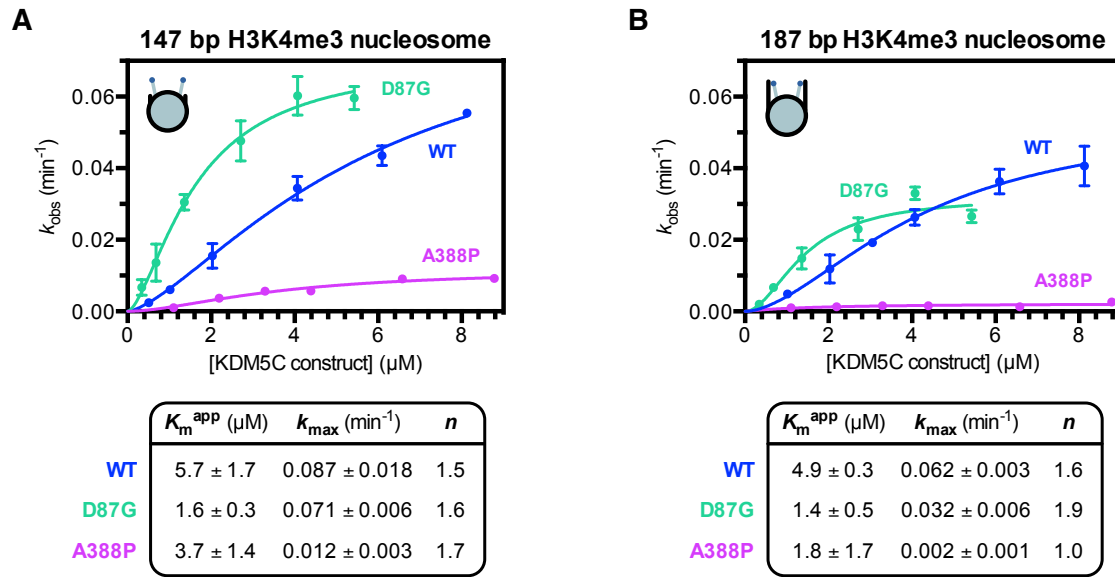


Figure 3.2. X-linked intellectual disability mutations reduce demethylase activity in the presence of flanking DNA.

(A) Demethylation kinetics of the core substrate nucleosome by KDM5C¹⁻⁸³⁹ wild type (WT), D87G, and A388P under single turnover conditions. Observed rates are fit to a cooperative kinetic model, with n denoting the Hill coefficient. Wild type kinetic curve replotted from Figure 2.1C for comparison. **(B)** Demethylation kinetics of the 187 bp substrate nucleosome by KDM5C¹⁻⁸³⁹ WT, D87G, and A388P under single turnover conditions. All error bars represent SEM of at least two independent experiments ($n \geq 2$).

Unlike wild type KDM5C, these XLID mutants recognize flanking DNA in the presence of H3K4me3, prompting us to measure demethylase activity on the 187 bp H3K4me3 nucleosome. Demethylation by wild type KDM5C¹⁻⁸³⁹ is only minimally reduced on the flanking DNA-containing substrate nucleosome compared to the core substrate nucleosome ($k_{max} \sim 0.06 \text{ min}^{-1}$ vs $k_{max} \sim 0.09 \text{ min}^{-1}$, respectively) (**Figure 3.2A, Figure 3.2B**). Interestingly, we find that addition

of flanking DNA to the substrate nucleosome results in strong inhibition of catalysis by KDM5C¹⁻⁸³⁹ A388P, with a 6-fold reduction in k_{max} relative to the core substrate nucleosome (**Figure 3.2B**). Addition of flanking DNA also reduces catalysis by KDM5C¹⁻⁸³⁹ D87G, although to a lesser degree of ~2-fold (**Figure 3.2B**). Despite maximal catalysis (k_{max}) by KDM5C¹⁻⁸³⁹ D87G being lower than wild type in the presence of flanking DNA, the D87G mutant is still ~2 fold more efficient (k_{max}/K_m^{app}) due to its enhanced nucleosome binding. Regardless, enhanced and unregulated linker DNA recognition caused by the XLID mutations results in a reduction in the catalytic rate of H3K4me3 nucleosome demethylation when flanking DNA is present.

A388P XLID mutation alters the state of the linker C-terminal to PHD1

The proximity of the A388P XLID mutation to PHD1 instigates whether PHD1 and its binding is affected by this mutation. The A388P mutation has been reported to reduce PHD1 binding to the H3K9me3 peptide by 2-fold through peptide pull down⁶. To examine the effect of the A388P mutation on PHD1, we utilized NMR spectroscopy using an extended construct of the PHD1 domain (PHD1^{ext}) to include residues surrounding A388 in the linker region between the PHD1 and JmjC domain. In titration experiments with the H3 tail peptide, the A388P mutation does not significantly affect the affinity of PHD1^{ext} towards the H3 tail (**Figure 3.3A**). In addition, the A388P mutation alters the ¹H-¹⁵N HSQC chemical shifts corresponding to residues in the linker region C-terminal to PHD1, but does not significantly affect chemical shifts assigned to residues found within PHD1 (**Figure 3.3B**). These results suggest that the A388P mutation does not impair PHD1 nor its ligand binding, but rather alters the state of the linker between the PHD1 and JmjC domains.

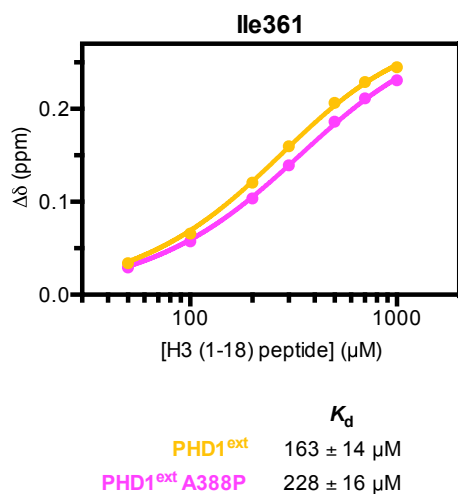
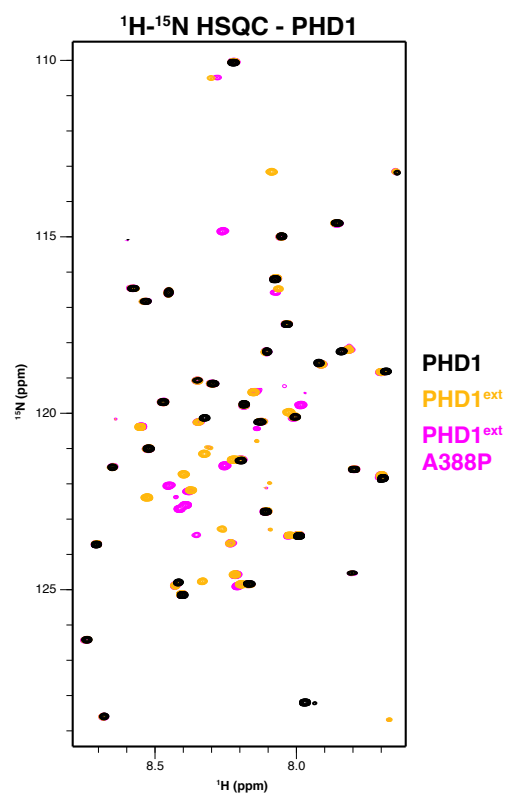
A**B**

Figure 3.3. The A388P XLID mutation does not reduce H3 tail binding by PHD1 but alters the state of the linker region C-terminal to PHD1.

(A) Binding of the H3 (1-18) tail peptide by PHD1^{ext} and PHD1^{ext} A388P mutant measured by NMR titration HSQC experiments. The chemical shift change ($\Delta\delta$) of I361 in PHD1 was fit to obtain dissociation constants with standard error. **(B)** 2D ¹H-¹⁵N HSQC spectra of PHD1, PHD1^{ext}, and PHD1^{ext} A388P mutant of random coil region containing chemical shifts of residues in the linker extension C-terminal to PHD1.

DISCUSSION

The mechanisms underlying disruption by the numerous XLID mutations found in KDM5C have remained elusive. Our findings, in addition to previous findings, suggest multiple mechanisms of disruption beyond only reducing demethylase activity^{6,15,43,45,46}. We previously described our KDM5C regulatory model, where DNA recognition is inhibited by the PHD1 domain such that the ARID-PHD1 linker and ARID domain are restricted in the absence of PHD1's H3 tail ligand. These regulatory interdomain interactions appear to be disrupted by the D87G and A388P XLID mutations adjacent to the ARID and PHD1 domains, resulting in enhanced nucleosome binding and loss of H3K4me3 specificity. As enhanced DNA recognition by XLID mutants is nonproductive with reduced demethylase activity in the presence of linker DNA, our findings suggest dysregulation of KDM5C demethylation at euchromatic loci, where this enzyme predominantly functions^{33,36}.

Our findings strongly support that the regulation of DNA recognition by KDM5C is disrupted by the D87G and A388P XLID mutations adjacent to the ARID and PHD1 domains, such that nucleosomal and linker DNA is constantly recognized. It is consistent with the model that these distinct XLID mutations are altering the conformational state of the ARID and PHD1 region, such that the inhibition on the DNA binding ARID domain and ARID-PHD1 linker is relieved through disrupted intramolecular interactions (**Figure 3.4**). The location of these mutations lend support to our model, where alterations in distal linker regions affect global conformations of functional elements within KDM5C such that ligand recognition is retained but the conformational coupling is broken. While it appears enigmatic what the effect of the D87G mutation is on intramolecular interactions or on the linking of the ARID domain, our findings suggest that the A388P mutation alters the PHD1-JmjC linker region to both disrupt the catalytic domain and promote relief of the PHD1-mediated inhibition of the ARID domain and ARID-

PHD1 linker. Beyond disruption of histone demethylase activity, our findings suggest an additional mechanism of dysregulation of KDM5C in XLID, that of enhanced nonproductive chromatin engagement and differential dysregulation of demethylation at different loci depending on the accessibility of linker DNA (**Figure 3.4**).

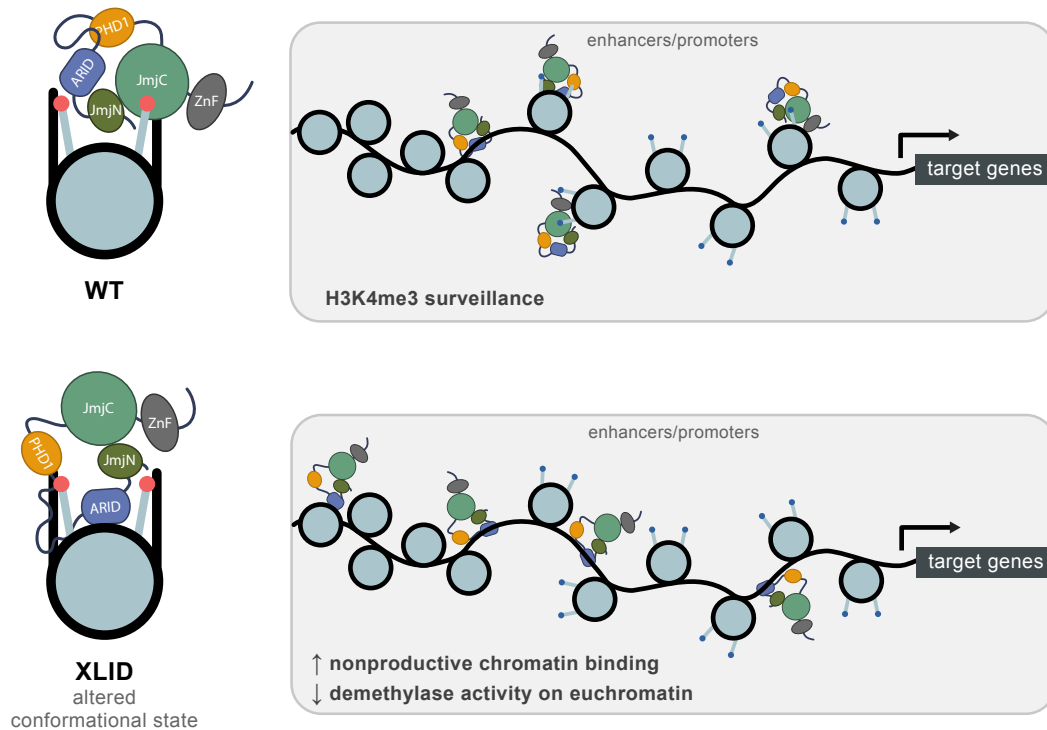


Figure 3.4. Model of H3K4me3 surveillance by KDM5C and dysregulation by XLID mutations on chromatin. Proposed function of H3K4me3 sensing and surveillance by KDM5C on its target chromatin regions at gene promoters and enhancers (*top*). Proposed altered conformational state of the ARID and PHD1 region in KDM5C due to XLID mutations in this region disrupting hypothesized intramolecular interactions, and predicted consequences on chromatin recognition and demethylation at KDM5C target sites (*bottom*).

Despite the reduced *in vitro* activity of KDM5C due to the A388P mutation, global H3K4me3 levels are unaffected with human KDM5C A388P *in vivo*⁷⁸. In contrast, increased global H3K4me3 levels are observed in a *Drosophila* intellectual disability model with A512P mutant Lid, signifying that further work is needed to profile H3K4me3 levels at genomic target

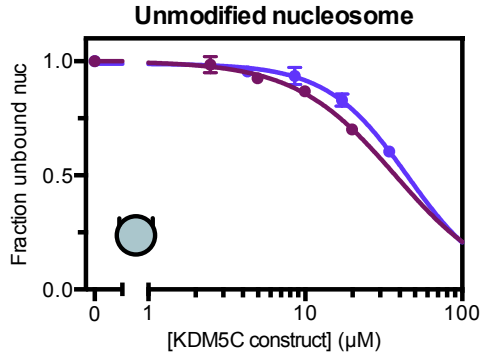
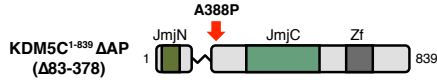
regions affected by XLID mutations in human KDM5C⁷⁹. Furthermore, we find that the demethylase activity of KDM5C D87G varies relative to wild type depending on the presence of linker DNA, which might account for the unaffected global H3K4me3 levels previously observed with this D87G mutation⁴⁶.

Interestingly, a gain of gene repressive function has been observed for the Y751C XLID mutation, where higher protein levels and lower H3K4me3 levels are found at the promoter of a down regulated gene unique to the Y751C mutant⁸⁰. This further insinuates locus specific consequences and possible enhanced chromatin binding, despite the reported lower *in vitro* peptide demethylation and unaffected global H3K4me3 levels by this mutant^{6,80}. Enhanced chromatin association has been recently reported as a mechanism of cancer mutations found in the acyl histone-binding YEATS reader domain of ENL, conferring a gain of function in recruitment towards active transcription⁸¹. Moreover, KDM5C occupies CpG island-containing promoters, and altered genomic DNA methylation patterns, with hypomethylated regions, have been reported due to KDM5C XLID mutations^{33,82–84}. It is tempting to speculate whether linker DNA recognition by KDM5C may directly protect DNA from methylation and if enhanced and unregulated linker DNA recognition by XLID mutants could cause further reinforcement to give rise to hypomethylation.

Our findings suggest that the chromatin environment, in particular the presence of accessible linker DNA, could govern altered demethylation and nonproductive chromatin recognition by KDM5C in XLID. Euchromatin-specific dysregulation of KDM5C demethylation might account for the hard-to-reconcile discrepancies between reported *in vitro* demethylase activities of KDM5C XLID mutants and their effect on global H3K4me3 levels. While additional XLID mutations elsewhere in KDM5C remain to be fully investigated, it is possible that these dispersed mutations share a common mechanism of disrupted conformational coupling between domains that regulate the sensing of chromatin and demethylation by KDM5C.

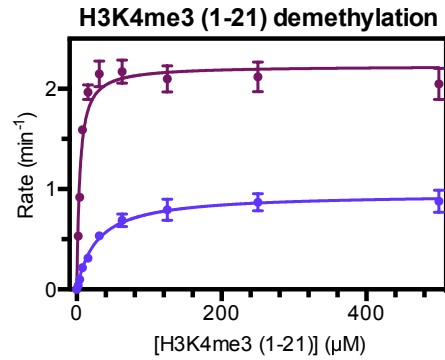
SUPPLEMENTAL FIGURES

A



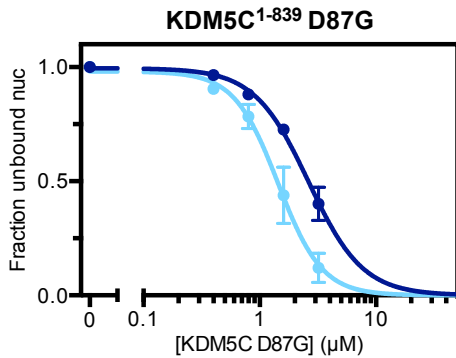
| | K_d^{app} | n |
|----------------------------------|---------------------------------|-----|
| KDM5C ¹⁻⁸³⁹ ΔAP | $\geq 37.5 \pm 5.0 \mu\text{M}$ | 1.4 |
| KDM5C ¹⁻⁸³⁹ ΔAP A388P | $\geq 45.1 \pm 3.3 \mu\text{M}$ | 1.7 |

B

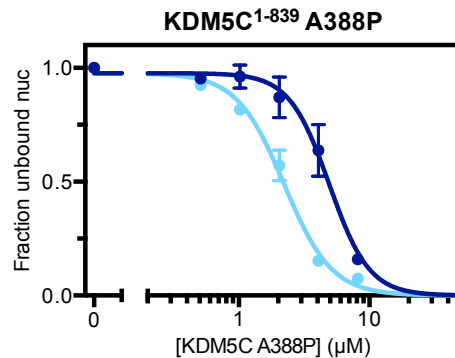


| | K_m (μM) | k_{cat} (min^{-1}) |
|----------------------------------|-------------------------|---------------------------------|
| KDM5C ¹⁻⁸³⁹ ΔAP | 3.6 ± 0.7 | 2.22 ± 0.07 |
| KDM5C ¹⁻⁸³⁹ ΔAP A388P | 26.6 ± 2.0 | 0.95 ± 0.02 |

C



| | K_d^{app} | n |
|-----------------------|---------------------------|-----|
| 147 bp H3K4me3 nuc | $2.6 \pm 0.1 \mu\text{M}$ | 1.9 |
| 187 bp H3K4me3 nuc | $1.4 \pm 0.1 \mu\text{M}$ | 2.3 |



| | K_d^{app} | n |
|-----------------------|---------------------------|-----|
| 147 bp H3K4me3 nuc | $4.9 \pm 0.4 \mu\text{M}$ | 2.8 |
| 187 bp H3K4me3 nuc | $2.2 \pm 0.1 \mu\text{M}$ | 2.4 |

Figure S3.1. Effect of A388P mutation on the catalytic domains and nucleosome binding by XLID mutants.

(A) Unmodified core nucleosome binding by KDM5C¹⁻⁸³⁹ ΔAP wild type and A388P. Nucleosome binding curves were measured by EMSA and fit to a cooperative binding model to determine apparent dissociation constants (K_d^{app}), with n denoting the Hill coefficient. The A388P mutation does not enhance nucleosome binding in the absence of the ARID and PHD1 region, indicating this region in KDM5C is altered by the A388P mutation to enable enhanced binding. (B) Demethylation kinetics of the H3K4me3 (1-21) substrate peptide by KDM5C¹⁻⁸³⁹ ΔAP wild type and A388P under multiple turnover conditions measured by a formaldehyde release based kinetic assay. The A388P mutation reduces demethylase activity of the catalytic domain alone, indicating distal structural disruption of the catalytic domain by this mutation. (C) Binding curves of KDM5C¹⁻⁸³⁹ D87G and A388P binding to substrate nucleosomes with and without 20 bp flanking DNA. All error bars represent SEM of at least two independent experiments ($n \geq 2$).

CHAPTER 4

Additional biochemical studies of KDM5C

Crosslinking studies of KDM5C and nucleosome bound KDM5C

The cooperativity that we observe in KDM5C nucleosome binding and demethylation (Chapter 2), in addition to substrate peptide demethylation, under single turnover conditions with excess enzyme suggests KDM5C might form a multimeric species. To investigate this, we used glutaraldehyde cross-linking to analyze states of KDM5C¹⁻⁸³⁹ and their molecular weights. Upon cross-linking of KDM5C¹⁻⁸³⁹ alone at micromolar concentrations, protein bands corresponding to the monomeric species and a higher molecular weight species are present (**Figure 4.1A**). This higher molecular weight band might correspond to a cross-linked trimer of KDM5C¹⁻⁸³⁹, in line with the observed Hill coefficients up to 2.8 (**Figure S2.1, Figure 2.3**). We then cross-linked KDM5C¹⁻⁸³⁹ to the 187 bp unmodified nucleosome, to which it has relatively the highest affinity and binds cooperatively (**Figure 2.3A**). As a large proportion of the nucleosome bound KDM5C complex did not fully form under the concentration conditions used (**Figure 4.1B**), protein bands corresponding to the cross-linked complex and their corresponding molecular weights were not observed (**Figure 4.1A**). However, the higher molecular weight band of cross-linked KDM5C¹⁻⁸³⁹ still forms in the presence of the nucleosome (**Figure 4.1A**). In addition, there are multiple species of the KDM5C-nucleosome complex present upon cross-linking (**Figure 4.1B**), suggesting that various binding stoichiometries of the nucleosome to KDM5C might be present in nucleosome binding. The multimeric species of KDM5C and the state of KDM5C when bound to nucleosomes requires further quantitative investigation.

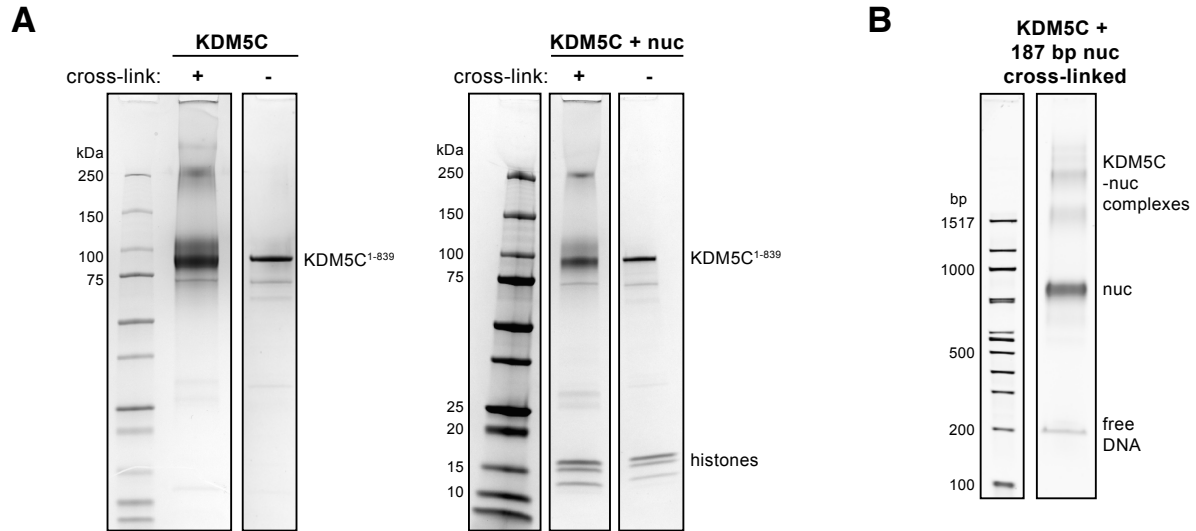


Figure 4.1. Glutaraldehyde cross-linking of KDM5C and nucleosome bound KDM5C.

(A) SDS-PAGE gels of uncross-linked and cross-linked KDM5C¹⁻⁸³⁹ (*left*) and KDM5C¹⁻⁸³⁹ when bound to the 187 bp unmodified nucleosome (*right*). KDM5C¹⁻⁸³⁹ was cross-linked at 7 μ M alone using glutaraldehyde and KDM5C¹⁻⁸³⁹ at 10 μ M with the 187 bp unmodified nucleosome at 3 μ M. **(B)** Native PAGE gel of glutaraldehyde cross-linked KDM5C¹⁻⁸³⁹ (5 μ M) to the 187 bp unmodified nucleosome (11 μ M).

Ligand recognition by PHD1

During initial investigations of the PHD1 domain of KDM5C to identify its ligands, we first tested binding to all histone tails found on the nucleosome through bio-layer interferometry (BLI), using peptides spanning 20 residues of each accessible histone tail. PHD1 surprisingly binds several histone tail peptides, in addition to the expected binding to the H3 tail (**Figure 4.2A**). These histone tail fragments bound by PHD1 were further investigated by NMR spectroscopy, where PHD1 binds non-H3 histone tail peptides with 3-6 fold reduced affinity and with fewer PHD1 residues relative to H3 tail binding (**Figure S2.6B**). This indicates that PHD1 is capable of less specific binding towards basic peptide ligands. However, the recognition of the H3 tail by PHD1 is specific, with recognition preferring the first 10 residues (**Figure 4.2A**) and dependent on the first 4 residues (**Figure S2.6A**). Despite these findings indicating that the first few H3 residues are recognized by PHD1, typical of most PHD domains, PHD1 prefers to bind longer peptide fragments of the H3 tail and shows little binding to the first 10 residues alone (**Figure 4.2B**). This might indicate that PHD1 has a secondary recognition site for other regions of the H3 tail beyond the immediate N-terminus. By NMR spectroscopy, PHD1 binding of the H3 (1-10) peptide is about 4-5 fold lower in affinity when compared to H3 (1-18) peptide binding and involves the same set of residues involved in binding the longer H3 (1-18) peptide (**Figure 2.2A**), obscuring the identification of residues involved in a secondary recognition site.

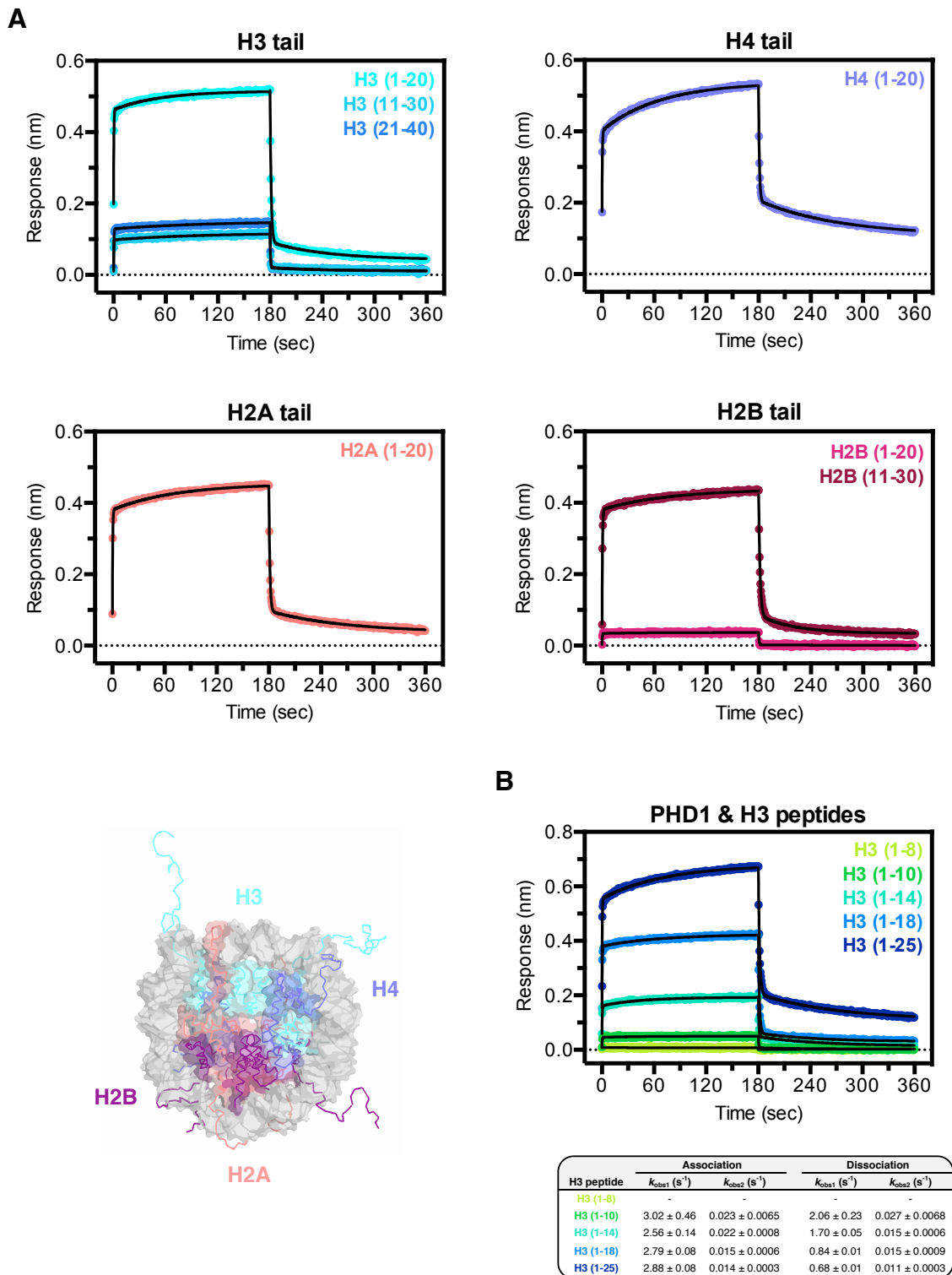


Figure 4.2. Binding kinetics of PHD1 domain and histone tail peptides.

(A) Binding kinetic traces of immobilized Avitag-PHD1 binding to H3, H4, H2A, and H2B histone tail peptides measured by bio-layer interferometry (*top*). Structure of the nucleosome with labeled histone tails (PDB:1KX5) (*bottom*). **(B)** Binding kinetic trace of immobilized Avitag-PHD1 binding to H3 tail peptides of varying length measured by bio-layer interferometry. Observed rates (k_{obs}) of association and dissociation are obtained by fitting kinetic traces to a two phase exponential function.

The biphasic binding kinetics observed in the binding of PHD1 to its ligands (**Figure S2.2, Figure 4.2**) is indicative of a two-step binding mechanism such as conformational selection or induced fit by the ligand. Several residues in PHD1 (D334, D337, L339, and H350) have broadened chemical shifts in the apo HSQC spectrum of PHD1 (**Figure 2.2A, Figure 4.3**). This may suggest that these PHD1 residues are dynamic and thus display exchange during the NMR timescale. Intriguingly, these residues localize near the predicted H3K4 binding pocket, and some are found within the PHD1 core, including the H350 residue which is a structurally conserved residue involved in zinc coordination by PHD domains (**Figure 4.3**). As the chemical shifts of these residues appear upon complete binding to the H3 tail, they may be stabilized in a certain conformation in the PHD1 bound state, which could either be selected for or induced by the H3 tail ligand. Dynamics within PHD1 could account for the low affinity of KDM5C PHD1 towards the H3 tail, which is at least 100-fold lower than the affinity of the homologous KDM5A PHD1, perhaps due to a higher entropic cost of ligand binding.

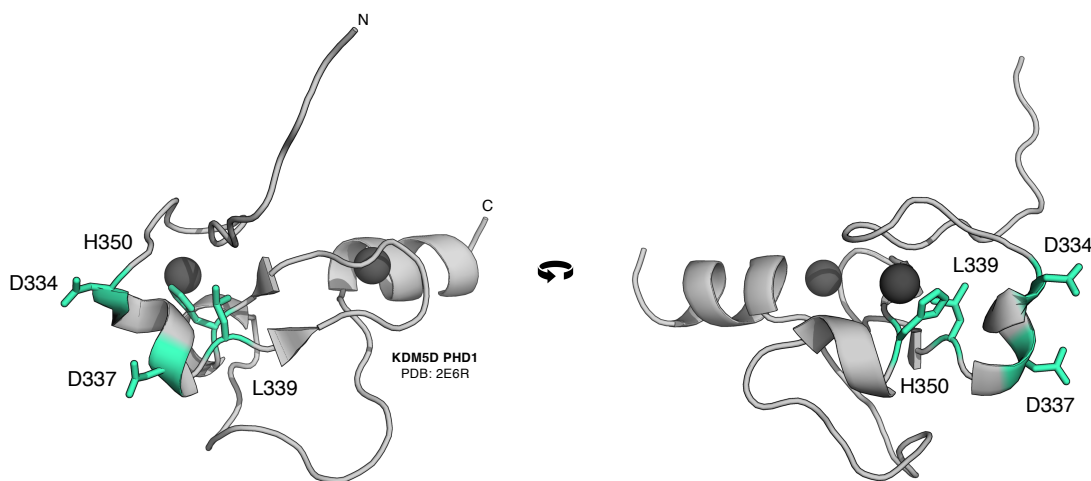


Figure 4.3. Dynamic residues in PHD1 with broadened chemical shifts in the apo PHD1 HSQC spectrum. KDM5C PHD1 residues (labeled, colored in cyan) with broadened chemical shifts in apo 2D ^1H - ^{15}N HSQC spectra mapped to homologous residues in the structure of KDM5D PHD1 (PDB: 2E6R).

One of the largest chemical shift changes that occurs upon binding of the H3 tail to PHD1 is of E323 (**Figure S2.2C**). This residue and its position N-terminal to PHD1 is homologous to acidic residues that form interactions with H3K4 by PHD domains with preference for the unmodified H3 tail⁸⁵. As E323 is predicted to contribute to the H3K4 binding pocket, we performed a closer analysis of chemical shift changes in PHD1 upon binding to H3 tail peptides with different H3K4 methylation states. Almost all chemical changes that occur upon H3 binding in PHD1 are reduced and diminished upon binding of methylated H3K4 tail peptides (**Figure 4.4A**). These reductions in perturbations are particularly prominent at certain residues and regions within PHD1 (**Figure 4.4B**) and localize to a face of PHD1 (**Figure 4.4C**). Binding to the H3K4me1 tail peptide primarily reduces the overall chemical shift change at E323, D337, and L339, suggesting these residues might be involved in unmodified H3K4 recognition and thus more drastically affected by the addition of monomethylation at H3K4 (**Figure 4.4C**). PHD1 binding to the H3K4me2 and K4me3 tail peptides results in a more global reduction in overall chemical shift changes, but more significant reductions are present at E323, C342, D343, G344, and D347 (**Figure 4.4B**). As these residues are further away from the predicted H3K4 binding pocket and more localized around the H3R2 pocket (**Figure 4.4C**), these H3K4me2/3-specific differences most likely reflect reduced engagement of the N-terminal residues of H3 due to the presence of bulkier K4me2/3. It may also reflect an inability of the H3K4me2/3 tail peptides to induce an overall conformational change in PHD1 due to a lack in engagement of the H3K4 binding pocket. Interestingly to note, the methylated H3K4 tail peptides are largely unable to affect the chemical shifts of the dynamic residues found near the H3K4 binding pocket, whose bound chemical shifts are only present and induced upon unmodified H3 tail binding (**Figure 4.5**). This may reflect a conformational coupling mechanism to discriminate against H3K4 methylation, as well as less specific basic ligands, by PHD1 for propagation of H3 tail binding to the rest of KDM5C, perhaps through the N-terminal linker with E323 engagement.

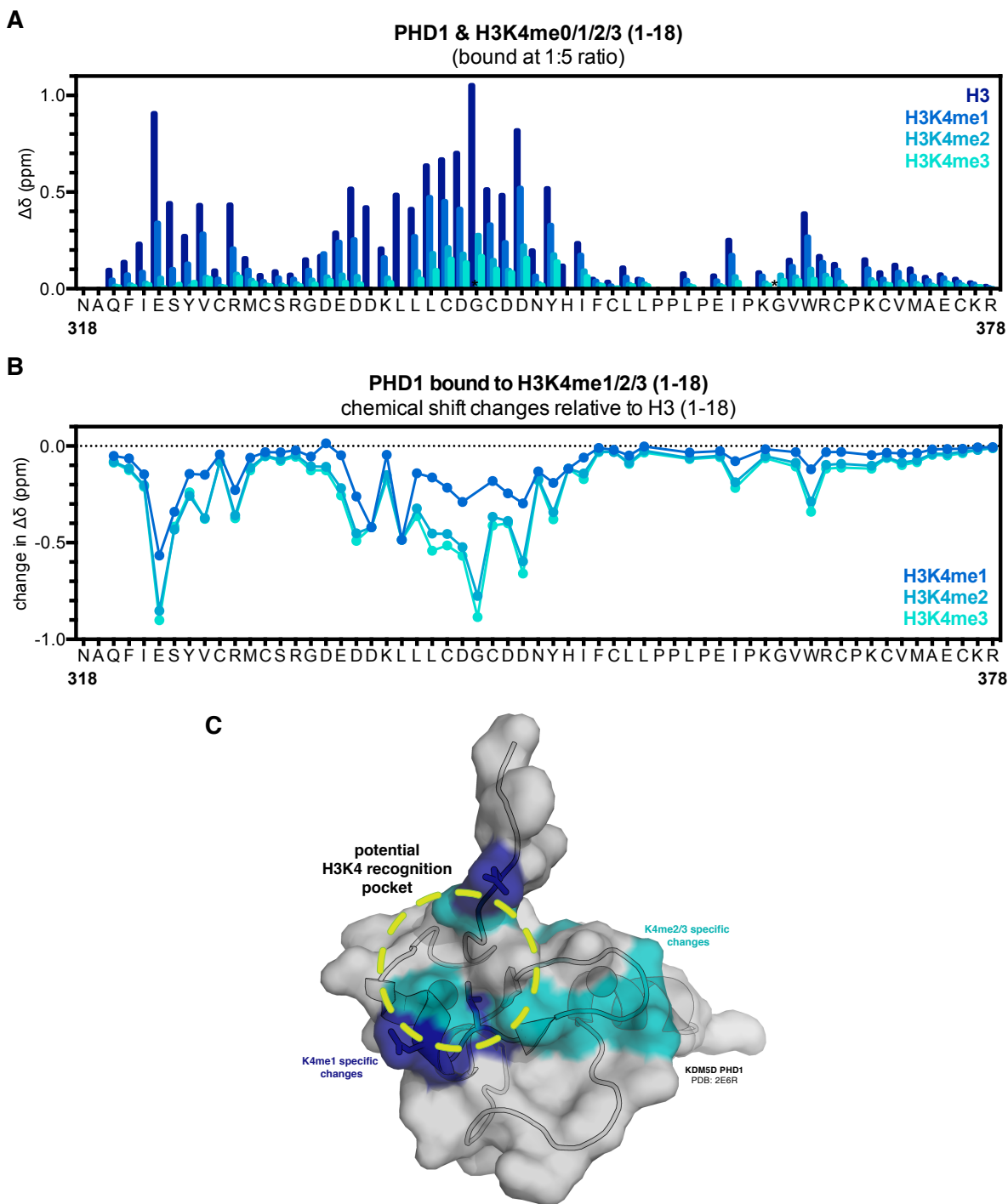
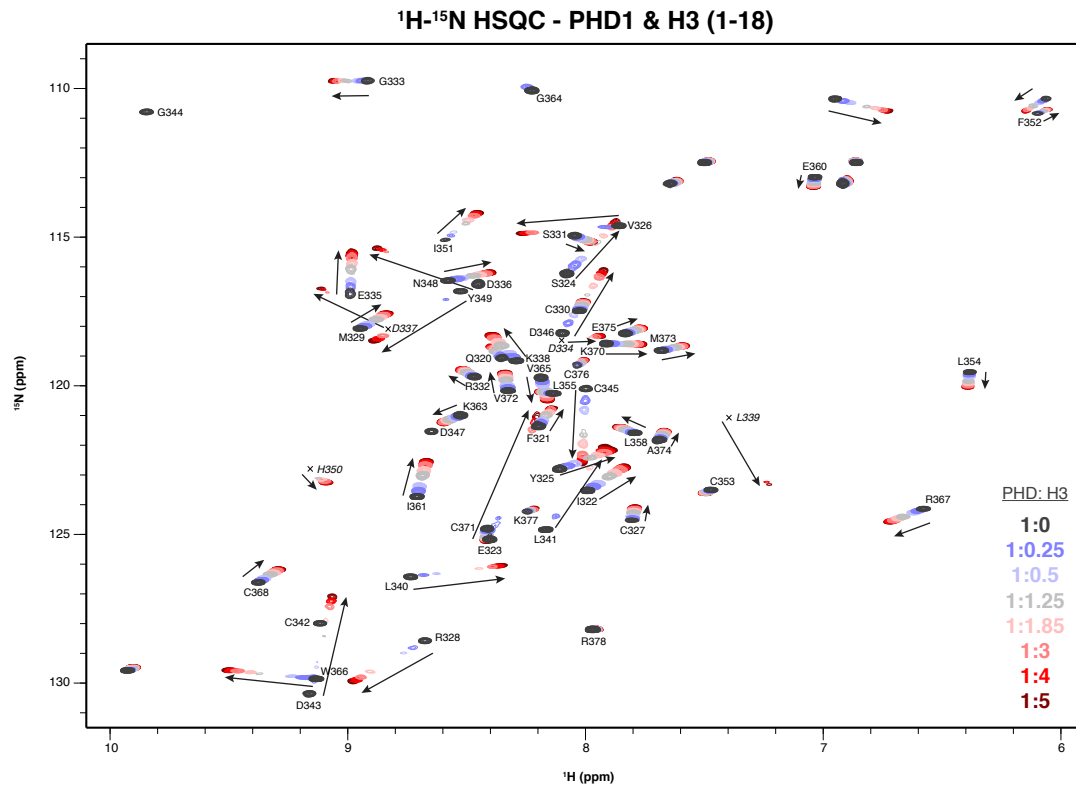
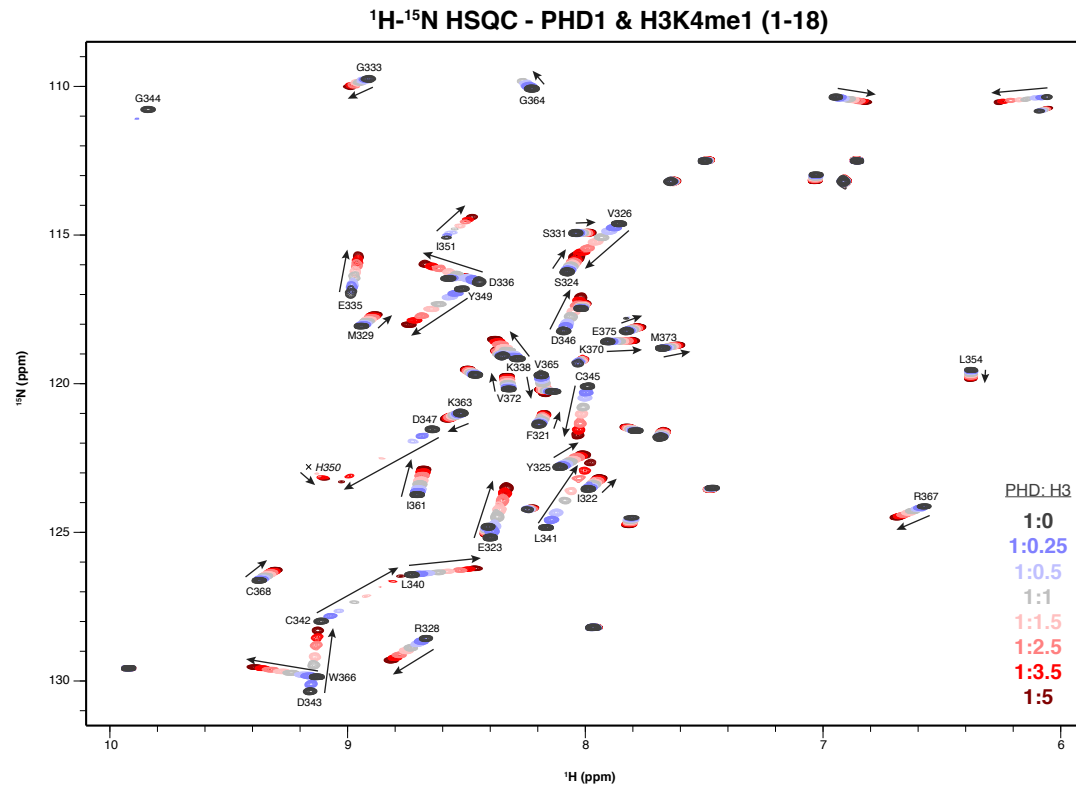


Figure 4.4. Chemical shift changes of PHD1 binding to H3K4me0/1/2/3 tail peptides and perturbation differences due to H3K4 methylation states.

(A) Chemical shift changes of PHD1 residues upon binding of H3K4me0/1/2/3 (1-18) tail peptides at 1:5 molar ratio (PHD:peptide) measured by HSQC NMR. The chemical shift changes of G344 and G364 (* denoted by asterisk) could not be determined due to broadened chemical shift when bound. **(B)** Difference in chemical shift changes of PHD1 residues upon binding to H3K4me1/2/3 (1-18) tail peptides relative to PHD1 binding to H3K4 (1-18) peptide at 1:5 molar ratio. **(C)** Largest differences in PHD1 residues' chemical shift changes upon binding to H3K4me1 and H3K4me2/3 tail peptides relative to binding the H3 tail peptide. Residues with K4me1 specific changes (dark blue) and K4me2/3 specific changes (teal) are colored and mapped to homologous residues in the KDM5D PHD1 structure (PDB: 2E6R).

A**B**

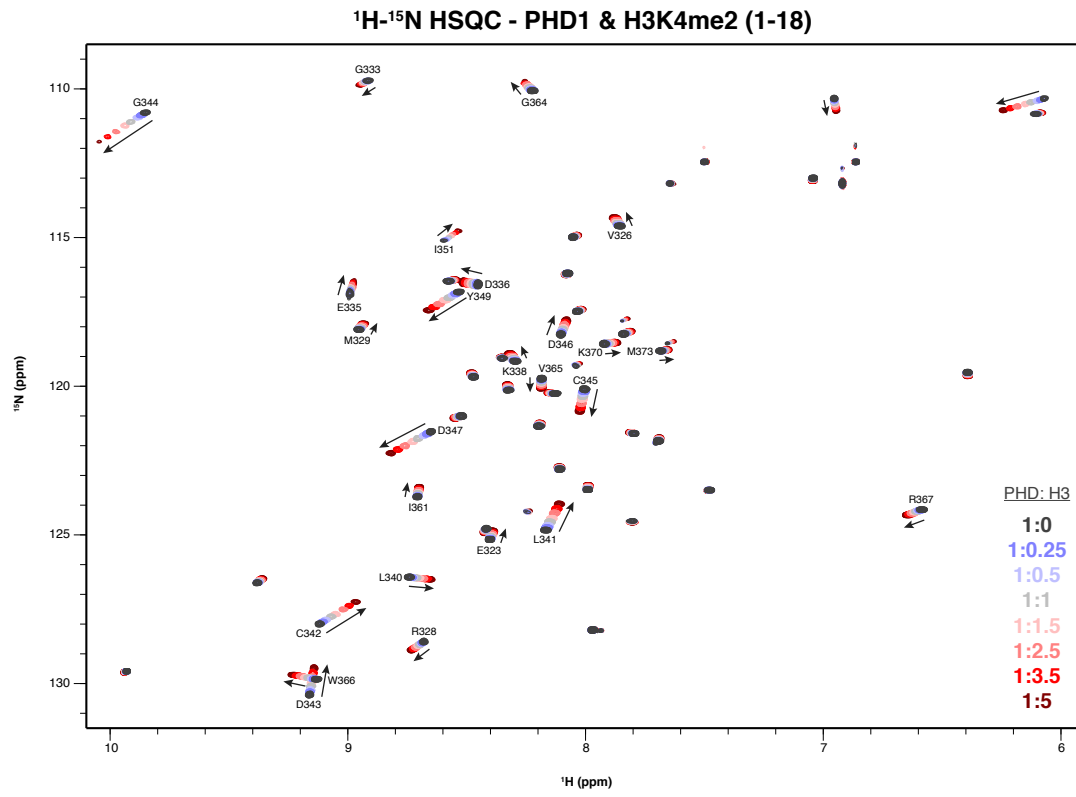
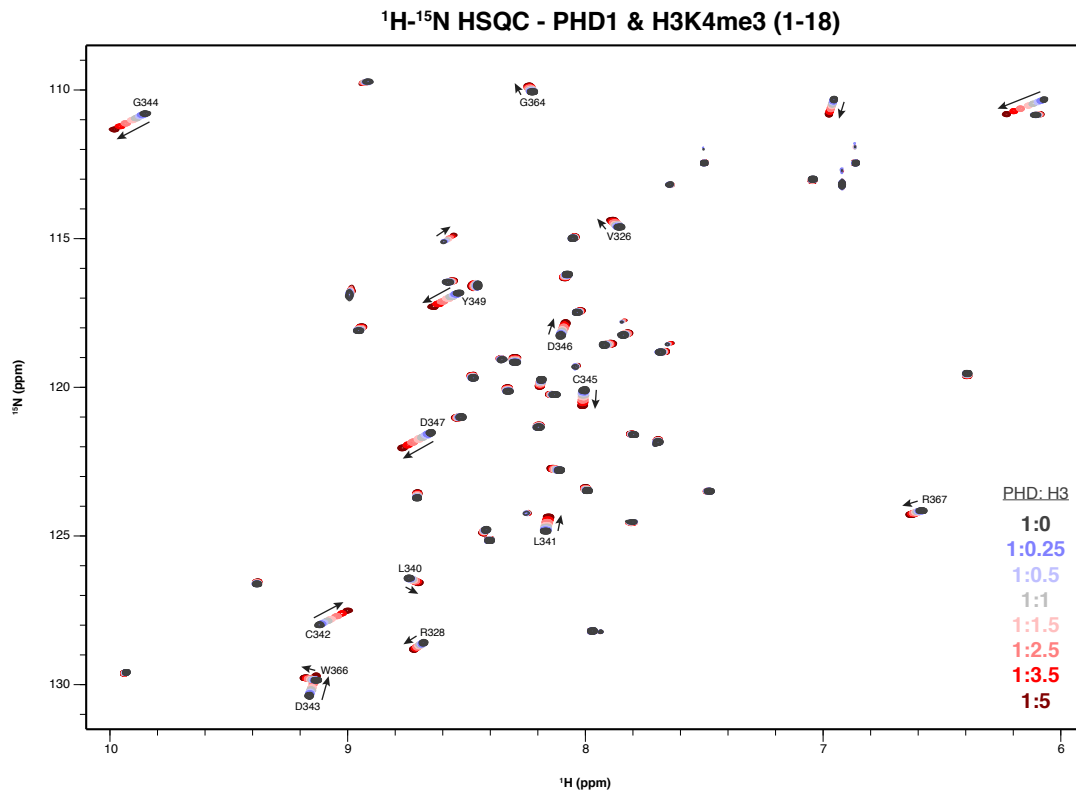
C**D**

Figure 4.5. HSQC spectra of PHD1 binding to H3K4me0/1/2/3 tail peptides.

(A) 2D ^1H - ^{15}N HSQC spectra of PHD1 titrated with increasing amounts of H3 (1-18) peptide with indicated molar ratios. Backbone assignments of residues in PHD1 are labeled. **(B)** 2D ^1H - ^{15}N HSQC spectra of PHD1 titrated with the H3K4me1 (1-18) peptide with indicated molar ratios. Perturbed residues in PHD1 upon binding are labeled. **(C)** 2D ^1H - ^{15}N HSQC spectra of PHD1 titrated with the H3K4me2 (1-18) peptide with indicated molar ratios. Perturbed residues in PHD1 upon binding are labeled. **(D)** 2D ^1H - ^{15}N HSQC spectra of PHD1 titrated with the H3K4me3 (1-18) peptide with indicated molar ratios. Perturbed residues in PHD1 upon binding are labeled.

Substrate preferences of KDM5C

H3K4me3 substrate peptide demethylation by KDM5C¹⁻⁸³⁹ exhibits substrate inhibition under multiple turnover conditions (**Figure S2.1A**), which is abolished by the deletion of the ARID and PHD1 domain region and only minimally reduced by the D343A PHD1 mutation (**Figure S2.2F**). This might indicate that a secondary H3K4me3 tail recognition site exists within the ARID and PHD1 region that contributes to a less productive state of KDM5C that is catalytically rate-limiting but not inactive. To probe if there are determining factors of the substrate peptide that causes substrate inhibition, we tested the demethylation of H3K4me3 substrate peptides of varying lengths by KDM5C¹⁻⁸³⁹ under multiple turnover conditions. The kinetics parameters of H3K4me3 demethylation are largely unaffected by substrate peptide length, with only a 2-3 fold reduction in the K_m upon shortening of the substrate peptide from 21 down to 10 residues of H3 (**Figure 4.6**). However, substrate inhibition is not present in the demethylation of the shorter H3K4me3 (1-10) peptide (**Figure 4.6**). This indicates that the catalytic domain does not strongly depend on the recognition of residues beyond the N-terminal H3K4me3, but that the secondary recognition site that causes substrate inhibition does depend on the recognition of H3 residues 11-17.

Perhaps this secondary recognition site is within PHD1 as PHD1 prefers to bind longer H3 tail peptides beyond the first 10 H3 residues (**Figure 4.2B**). The D343A PHD1 mutant KDM5C still displays substrate inhibition (**Figure S2.2F**), however, the D343 residue is only expected to be involved in H3R2 recognition and the D343A mutation may not affect the secondary H3 tail recognition site of PHD1. The D343A mutant PHD1 still retains chemical shift changes of several PHD1 residues upon H3 tail binding and has a similar binding affinity as PHD1 has towards the H3K4me3 tail peptide (**Figure 2.2**). This suggests that the D343A mutant may retain a low affinity recognition of H3 residues beyond the N-terminus and H3K4. A deeper investigation and mutational analysis of H3 recognition by PHD1 is needed to understand its

secondary H3 recognition site and to determine if it is responsible for substrate inhibition in KDM5C. Alternatively, non-specific binding of the H3K4me3 substrate tail by the ARID-PHD1 linker region, which also contains acidic residues, may contribute to the basis of substrate inhibition.

KDM5C¹⁻⁸³⁹ catalysis is about 8-fold lower under multiple turnover conditions than maximal catalysis achieved under single turnover conditions (**Figure S2.1A**). Modulation of the intrinsic activity of KDM5C due to relative concentrations of the H3K4me3 substrate might be physiologically relevant and contribute to differential KDM5C activities at various genomic loci depending on local concentrations of both KDM5C and H3K4me3 on chromatin.

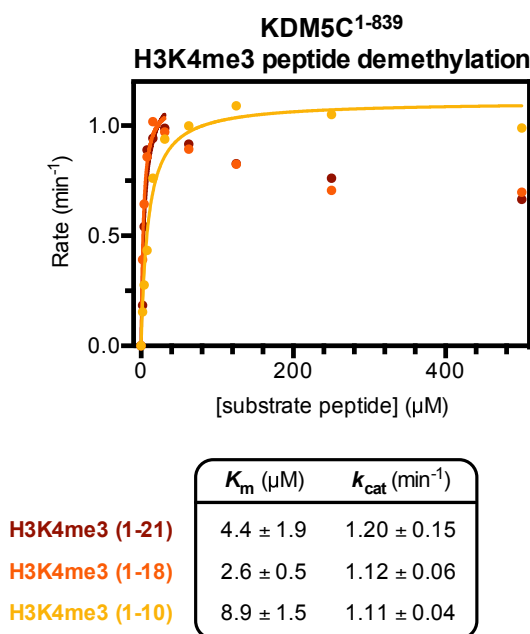


Figure 4.6. H3K4me3 substrate peptide demethylation by KDM5C.

Demethylation kinetics of different lengths of the H3K4me3 substrate peptide by KDM5C¹⁻⁸³⁹ under multiple turnover conditions measured by a formaldehyde release based kinetic assay. Observed initial rates are fit to a tight-binding kinetic model to determine Michaelis-Menten kinetic parameters.

CHAPTER 5

MATERIALS AND METHODS

Generation of KDM5C constructs

Human KDM5C gene was obtained from Harvard PlasmID (HsCD00337804) and Q175 was inserted to obtain the canonical isoform (NP_004178.2). KDM5C residues 1 to 839 were cloned into a pET28b His-Smt3 vector to produce 6xHis-SUMO-KDM5C and was mutated by site-directed mutagenesis for point mutants. The KDM5C¹⁻⁸³⁹ ΔAP construct was cloned by replacing residues 83-378 with a 4xGly linker. The KDM5C¹⁻⁸³⁹ Δlinker construct was cloned by replacing residues 176-317 with a (GGG)₅ linker.

Purification of KDM5C constructs

Recombinant His-tagged SUMO-KDM5C constructs were expressed in BL21(DE3) *E. coli* in LB media containing 50 μM ZnCl₂ and 100 μM FeCl₃ through induction at OD₆₀₀ ~0.6 using 100 μM IPTG followed by expression at 18 °C overnight. Collected cells were resuspended in 50 mM HEPES pH 8, 500 mM KCl, 1 mM BME, 5 mM imidazole, and 1 mM PMSF, supplemented with EDTA-free Pierce protease inhibitor tablets (Thermo Fisher Scientific) and benzonase, and lysed by microfluidizer. Lysate was clarified with ultracentrifugation and the recovered supernatant was then purified by TALON metal affinity resin (total contact time under 2 hrs) at 4 °C. The His-SUMO tag was then cleaved by SenP1 during overnight dialysis at 4 °C in 50 mM HEPES pH 7.5, 150 mM KCl, and 5 mM BME. KDM5C constructs were then purified by anion exchange (MonoQ, GE Healthcare) and subsequent size exclusion (Superdex 200, GE Healthcare) chromatography in 50 mM HEPES pH 7.5 and 150 mM KCl. Fractions were concentrated and aliquots snap frozen in liquid nitrogen for storage at -80 °C.

Nucleosomes and DNA

Recombinant human 5' biotinylated unmodified 147 bp mononucleosomes (16-0006), unmodified 187 bp mononucleosomes (16-2104), 5' biotinylated H3K4me3 147 bp mononucleosomes (16-0316), and 5' biotinylated H3K4me3 187 bp mononucleosomes (16-2316) were purchased from Epiccypher, Inc., in addition to biotinylated 147 bp 601 sequence DNA (18-005). 187 bp nucleosomes contain the 20 bp sequences 5' GGACCCTATACGCGGCCGCC and GCCGGTCGCGAACAGCGACC 3' flanking the core 601 positioning sequence. 20 bp flanking DNA duplex fragments were synthesized by Integrated DNA Technologies, Inc. For use in binding and kinetic assays, stock nucleosomes were buffer exchanged into corresponding assay buffer using a Zeba micro spin desalting column (Thermo Scientific).

Nucleosome and DNA binding assays

Nucleosome and DNA binding was assessed by EMSA. 100 nM nucleosomes (0.5 pmol) and various concentrations of KDM5C were incubated in binding buffer (50 mM HEPES pH 7.5, 50 mM KCl, 1mM BME, 0.01% Tween-20, 0.01% BSA, 5% sucrose) for 1 hr on ice prior to analysis by native 7.5% PAGE. For DNA binding, 100 nM 147 bp 601 sequence DNA or 500 nM 20 bp linker DNA fragments were incubated with various concentrations of ARID. Samples were separated using pre-run gels by electrophoresis in 1xTris-Glycine buffer at 100V for 2 hrs at 4 °C, stained using SYBR Gold for DNA visualization, and imaged using the ChemiDoc imaging system (Bio-Rad Laboratories). Bands were quantified using Bio-Rad Image Lab software to determine the fraction of unbound nucleosome to calculate apparent dissociation constants by fitting to the cooperative binding equation $Y = \frac{X^n}{K_d^n + X^n}$, where X is the concentration of KDM5C, n is the Hill coefficient, and K_d is the concentration of KDM5C at which nucleosomes are half bound.

Single turnover nucleosome demethylation kinetics

The demethylation of biotinylated H3K4me3 nucleosome was monitored under single turnover conditions (>10 fold excess of KDM5C over substrate) through the detection of H3K4me1/2 product nucleosome formation over time by TR-FRET of an anti-H3K4me1/2 donor with an anti-biotin acceptor reagent. Various concentrations of KDM5C were reacted with 25 nM 5' biotinylated H3K4me3 nucleosome in 50 mM HEPES pH 7.5, 50 mM KCl, 0.01% Tween-20, 0.01% BSA, 50 μ M alpha-ketoglutarate, 50 μ M ammonium iron(II) sulfate, and 500 μ M ascorbic acid at room temperature. 5 μ L time points were taken and quenched with 1.33 mM EDTA then brought to 20 μ L final volume for detection using 1 nM LANCE Ultra Europium anti-H3K4me1/2 antibody (TRF0402, PerkinElmer) and 50 nM LANCE Ultra Ulight-Streptavidin (TRF0102, PerkinElmer) in 0.5X LANCE detection buffer. Detection reagents were incubated with reaction time points for 2 hours at room temperature in 384 well white microplates (PerkinElmer OptiPlate-384) then TR-FRET emission at 665 nm and 615 nm by 320 nm excitation with 50 μ s delay and 100 μ s integration time was measured using a Molecular Devices SpectraMax M5e plate reader. TR-FRET was calculated as the 665/615 nm emission ratio and kinetic curves were fit to a single exponential function to determine k_{obs} of demethylation. k_{obs} parameters were then plotted as a function of KDM5C concentration and fit to the sigmoidal kinetic equation $Y = k_{max} * X^n / (K_{half}^n + X^n)$ using GraphPad Prism to determine k_{max} and K_m^{app} parameters of demethylation.

Purification of PHD1 for NMR

PHD1 (KDM5C residues 318-378) and PHD1^{ext} (KDM5C residues 318-396) was cloned into a pET28b His-Smt3 vector to express recombinant 6xHis-SUMO-PHD1 in BL21(DE3) *E. coli* in metal supplemented M9 minimal medium containing ¹⁵NH₄Cl (Cambridge Isotope Laboratories). ¹³C-glucose (Cambridge Isotope Laboratories) was used in medium for expression of ¹⁵N, ¹³C-labeled PHD1. Expression was induced at OD₆₀₀ ~0.6 using 1 mM IPTG for expression at 18 °C

overnight. Collected cells were resuspended in 50 mM HEPES pH 8, 500 mM KCl, 5 mM BME, 10 mM imidazole, and 1 mM PMSF, supplemented with benzonase, and lysed by sonication. Lysate was clarified with ultracentrifugation and the recovered supernatant was then purified by Ni-NTA affinity resin. The His-SUMO tag was then cleaved by SenP1 during overnight dialysis at 4 °C in 50 mM HEPES pH 7.5, 150 mM KCl, 50 μ M ZnCl₂ and 10 mM BME. Cleaved His-SUMO tag and SenP1 was captured by passing through Ni-NTA affinity resin and flow-through was then purified by anion exchange (MonoQ) chromatography in starting buffer of 50 mM HEPES pH 7.5, 150 mM KCl, 50 μ M ZnCl₂ and 10 mM BME. Flow-through MonoQ fractions containing PHD1 were concentrated and aliquots snap frozen in liquid nitrogen for storage at -80 °C.

PHD1 NMR and histone peptide NMR titrations

For backbone assignment of KDM5C PHD1, 400 μ M ¹⁵N, ¹³C-labeled PHD1 in 50 mM HEPES pH 7.5, 50 mM KCl, 5 mM BME, 50 μ M ZnCl₂, and 5% D₂O was used to perform 3D triple-resonance CBCA(CO)NH and CBCANH experiments at 298K using a 500 MHz Bruker spectrometer equipped with a cryoprobe. Triple-resonance experiments were also performed using 400 μ M ¹⁵N, ¹³C-labeled PHD1 bound to 2 mM H3 (1-18) peptide (1:5 ratio) to assign broadened backbone residues in apo spectra. 3D spectra were processed using NMRPipe then analyzed and assigned using CcpNMR Analysis. Out of 56 assignable residues, 54 in apo PHD1 and 53 residues in H3 bound PHD1 were assigned.

For 2D ¹H-¹⁵N HSQC spectra of KDM5C PHD1, 200 μ M ¹⁵N-labeled PHD1 in 50 mM HEPES pH 7.5, 50 mM KCl, 5 mM BME, 50 μ M ZnCl₂, and 5% D₂O was used to obtain 2D spectra at 298K using a 800 MHz Bruker spectrometer equipped with a cryoprobe. Chemical shift perturbation experiments were performed by obtaining HSQC spectra with increasing concentrations of histone tail peptides (GenScript) up to 1:5 molar ratio of PHD1:peptide. Data were processed

using Bruker TopSpin and analyzed using CcpNMR Analysis. Chemical shifts were scaled and calculated as $\Delta\delta = \sqrt{((\Delta\delta H)^2 + (\Delta\delta N/5)^2) / 2}$. Chemical shift values were then plotted as a function of histone peptide concentration and fit to the quadratic binding equation $Y = ((X + P_T + K_d) - \sqrt{(X + P_T + K_d)^2 - 4 * P_T * X}) * (Y_{max} - Y_{min}) / (2 * P_T)$, where X is the concentration of peptide and P_T is the concentration of PHD1, using GraphPad Prism to determine K_d values.

Purification of ARID for NMR

ARID (KDM5C residues 73-188) was cloned into a pET28b His-Smt3 vector to express recombinant 6xHis-SUMO-ARID in BL21(DE3) *E. coli* in metal supplemented M9 minimal medium containing $^{15}\text{NH}_4\text{Cl}$. Expression was induced at $\text{OD}_{600} \sim 0.6$ using 1 mM IPTG for expression at 18 °C overnight. Collected cells were resuspended in 50 mM HEPES pH 8, 500 mM KCl, 1 mM BME, 10 mM imidazole, and 1 mM PMSF, supplemented with EDTA-free Pierce protease inhibitor tablets and benzonase, and lysed by microfluidizer. Lysate was clarified with ultracentrifugation and the recovered supernatant was then purified by Ni-NTA affinity resin. The His-SUMO tag was then cleaved by SenP1 during overnight dialysis at 4 °C in 50 mM HEPES pH 7.5, 500 mM KCl, and 5 mM BME. Cleaved His-SUMO tag and SenP1 was captured by passing through Ni-NTA affinity resin and flow-through was then purified by size exclusion (Superdex 75, GE Healthcare) chromatography in 50 mM HEPES pH 7, 150 mM KCl, and 5 mM BME. Fractions were buffer exchanged into 50 mM HEPES pH 7, 50 mM KCl, and 5 mM BME then concentrated and aliquots snap frozen in liquid nitrogen for storage at -80 °C.

ARID and DNA NMR titration

For 2D ^1H - ^{15}N HSQC spectra of KDM5C ARID, 100 μM ^{15}N -labeled ARID in 50 mM HEPES pH 7, 50 mM KCl, 5 mM BME, and 5% D_2O was used to obtain 2D spectra at 298K using a 800 MHz Bruker spectrometer equipped with a cryoprobe. Chemical-shift perturbation experiments were performed by obtaining HSQC spectra with increasing concentrations of the 5' linker DNA

20 bp fragment up to 1:1 molar ratio of ARID:DNA. Data were processed using Bruker TopSpin and analyzed using CcpNMR Analysis. Chemical shifts were scaled and calculated as $\Delta\delta = \sqrt{((\Delta\delta_H)^2 + (\Delta\delta_N/5)^2) / 2}$. Previously determined assignments (BMRB: 15348) were transferred to a majority of resonances observed in the HSQC spectra of ARID⁴⁹.

Purification of ARID mutants

Recombinant His-tagged SUMO-ARID mutants were expressed in BL21(DE3) *E. coli* in 2xTY media through induction at OD₆₀₀ ~0.6 using 1 mM IPTG followed by expression at 18 °C overnight. Collected cells were resuspended in 50 mM HEPES pH 8, 500 mM KCl, 1 mM BME, 10 mM imidazole, and 1 mM PMSF, supplemented with benzonase, and lysed by sonication. Lysate was clarified with centrifugation and the recovered supernatant was then purified by Ni-NTA affinity resin. The His-SUMO tag was then cleaved by SenP1 for 2 hours at 4 °C in 50 mM HEPES pH 7, 500 mM KCl, and 5 mM BME. Cleaved His-SUMO tag and SenP1 was captured by passing through Ni-NTA affinity resin. The flow-through was buffer exchanged into 50 mM HEPES pH 7, 50 mM KCl, and 5 mM BME then concentrated and aliquots snap frozen in liquid nitrogen for storage at -80 °C.

Single turnover peptide demethylation kinetics

The demethylation of biotinylated H3K4me3 peptide was monitored under single turnover conditions (>10 fold excess of KDM5C over substrate) through the detection of H3K4me3 substrate loss over time by TR-FRET of an anti-rabbit IgG donor, recognizing an anti-H3K4me3 rabbit antibody, with an anti-biotin acceptor reagent. Various concentrations of KDM5C were reacted with 25 nM H3K4me3 (1-21)-biotin peptide (AS-64357, AnaSpec) in 50 mM HEPES pH 7.5, 50 mM KCl, 0.01% Tween-20, 0.01% BSA, 50 μM alpha-ketoglutarate, 50 μM ammonium iron(II) sulfate, and 500 μM ascorbic acid at room temperature. 2.5 μL time points were taken and quenched with 2 mM EDTA then brought to 20 μL final volume for detection using 1:500

dilution anti-H3K4me3 antibody (05-745R, EMD Millipore), 1 nM LANCE Ultra Europium anti-rabbit IgG antibody (PerkinElmer AD0082), and 50 nM LANCE Ultra Ulight-Streptavidin (PerkinElmer TRF0102) in 0.5X LANCE detection buffer. Detection reagents were added stepwise with 30 min incubation of anti-H3K4me3 antibody and Ulight-Streptavidin with reaction time points followed by 1 hr incubation with Europium anti-rabbit antibody in 384 well white microplates (PerkinElmer OptiPlate-384). TR-FRET emission at 665 nm and at 615 nm by 320 nm excitation with 50 μ s delay and 100 μ s integration time was measured using a Molecular Devices SpectraMax M5e plate reader. TR-FRET was calculated as the 665/615 nm emission ratio then subject to normalization to H3K4me3 substrate signal before demethylation. Kinetic curves were fit to a single exponential function, with the plateau set to nonspecific background of H3K4me2 product detection, to determine k_{obs} of the H3K4me3 demethylation step. k_{obs} parameters were then plotted as a function of KDM5C concentration and fit to the sigmoidal kinetic equation $Y = k_{max} * X^n / (K_{half}^n + X^n)$ using GraphPad Prism to determine k_{max} and K_m parameters of demethylation.

Multiple turnover peptide demethylation kinetics

A fluorescence-based enzyme coupled assay was used to detect the formaldehyde product of demethylation of H3K4me3 peptide under multiple turnover conditions (excess of substrate peptide over KDM5C). Various concentrations of H3K4me3 (1-21) substrate peptide (GenScript) were added with 1mM alpha-ketoglutarate to initiate demethylation by $\sim 1 \mu$ M KDM5C in 50 mM HEPES pH 7.5, 50 mM KCl, 50 μ M ammonium iron(II) sulfate, 2 mM ascorbic acid, 2 mM NAD⁺, and 0.05 U formaldehyde dehydrogenase (Sigma-Aldrich) at room temperature. Upon initiation, fluorescence (350 nm excitation, 460 nm emission) was measured in 20 sec intervals over 30 min using a Molecular Devices SpectraMax M5e plate reader. NADH standards were used to convert fluorescence to the rate of product concentration formed. Initial rates of the first 3 min of demethylation were plotted as a function of substrate concentration and fit to the tight-

binding quadratic velocity equation $Y = V_{\max} * ((X + E_T + K_m) - \sqrt{(X + E_T + K_m)^2 - 4 * E_T * X}) / (2 * E_T)$ using GraphPad Prism to determine Michaelis-Menten kinetic parameters of demethylation.

Histone peptide binding kinetics

Bio-layer interferometry was used to measure binding kinetics of histone peptides to biotinylated Avitag-PHD1. Avitag followed by a linker was inserted into pET28b His-Smt3-PHD1³¹⁸⁻³⁷⁸ to generate recombinant endogenously biotinylated 6xHis-SUMO-Avitag-(GS)₂-PHD1 through coexpression with BirA in BL21(DE3) *E. coli* in 2xTY media containing 50 μ M ZnCl₂ and 50 μ M biotin. Expression was induced at OD₆₀₀ ~0.7 using 0.4 mM IPTG for expression at 18 °C overnight. Collected cells were resuspended in 50 mM HEPES pH 8, 500 mM KCl, 5 mM BME, 10 mM imidazole, 50 μ M biotin, and 1 mM PMSF, supplemented with benzonase, and lysed by sonication. Lysate was clarified with ultracentrifugation and the recovered supernatant was then purified by Ni-NTA affinity resin. The His-SUMO tag was then cleaved by SenP1 during overnight dialysis at 4 °C in 50 mM HEPES pH 8, 150 mM KCl, 50 μ M ZnCl₂ and 10 mM BME. Cleaved His-SUMO tag and SenP1 was captured by passing through Ni-NTA affinity resin and flow-through was then purified by anion exchange (MonoQ) chromatography in starting buffer of 50 mM HEPES pH 8, 150 mM KCl, 50 μ M ZnCl₂ and 10 mM BME. Flow-through MonoQ fractions containing Avitag-PHD1 were analyzed by western blotting to identify biotinylated fractions, which were then concentrated and aliquots snap frozen in liquid nitrogen for storage at -80 °C. Using the Octet Red384 system (ForteBio) at 1000 rpm and 25 °C, 100 nM Avitag-PHD1 was loaded onto streptavidin biosensors (ForteBio) for 10 min in assay buffer (50 mM HEPES pH 8, 50 mM KCl, 50 μ M ZnCl₂, 5 mM BME, and 0.05% Tween-20) followed by 120 sec baseline then association and dissociation of 100 μ M peptide (GenScript) in assay buffer. Data were processed by subtracting a single reference experiment of loaded Avitag-PHD1 without peptide. A two phase exponential function was used to fit the biphasic kinetic data using Origin software.

Glutaraldehyde crosslinking

KDM5C and nucleosome-bound KDM5C were cross-linked using 0.05% glutaraldehyde on ice for 30-60 min. KDM5C was incubated with the 187 bp nucleosome on ice for 1 hr in 50 mM HEPES pH 7.5, 50 mM KCl, 1mM BME prior to cross-linking at 2-3 mg/mL. KDM5C alone was cross-linked at 1 mg/mL in 50 mM HEPES pH 7.5, 50 mM KCl. Cross-linking was quenched using 100 mM Tris pH 7.5 followed by 4-20% SDS-PAGE analysis. Cross-linked nucleosome-bound KDM5C was further analyzed by native 7.5% PAGE, separated using pre-run gels by electrophoresis in 1xTris-Glycine buffer at 100V for 2 hrs at 4 °C, stained using SYBR Gold for DNA visualization, and imaged using the ChemiDoc imaging system.

REFERENCES

1. Kouzarides, T. Chromatin Modifications and Their Function. *Cell* **128**, 693–705 (2007).
2. Musselman, C. A., Lalonde, M.-E., Côté, J. & Kutateladze, T. G. Perceiving the epigenetic landscape through histone readers. *Nat. Struct. Mol. Biol.* **19**, 1218–1227 (2012).
3. Villaseñor, R. & Baubec, T. Regulatory mechanisms governing chromatin organization and function. *Curr. Opin. Cell Biol.* **70**, 10–17 (2021).
4. Li, B., Carey, M. & Workman, J. L. The Role of Chromatin during Transcription. *Cell* **128**, 707–719 (2007).
5. Kimura, H. Histone modifications for human epigenome analysis. *Journal of Human Genetics* **58**, 439–445 (2013).
6. Iwase, S., Lan, F., Bayliss, P., de la Torre-Ubieta, L., Huarte, M., Qi, H. H., Whetstine, J. R., Bonni, A., Roberts, T. M. & Shi, Y. The X-linked mental retardation gene SMCX/JARID1C defines a family of histone H3 lysine 4 demethylases. *Cell* **128**, 1077–1088 (2007).
7. Klose, R. J., Yan, Q., Tothova, Z., Yamane, K., Erdjument-Bromage, H., Tempst, P., Gilliland, D. G., Zhang, Y. & Kaelin, W. G., Jr. The retinoblastoma binding protein RBP2 is an H3K4 demethylase. *Cell* **128**, 889–900 (2007).
8. Yamane, K., Tateishi, K., Klose, R. J., Fang, J., Fabrizio, L. A., Erdjument-Bromage, H., Taylor-Papadimitriou, J., Tempst, P. & Zhang, Y. PLU-1 is an H3K4 demethylase involved in transcriptional repression and breast cancer cell proliferation. *Mol. Cell* **25**, 801–812 (2007).
9. Lee, M. G., Norman, J., Shilatifard, A. & Shiekhattar, R. Physical and functional association of a trimethyl H3K4 demethylase and Ring6a/MBLR, a polycomb-like protein. *Cell* **128**, 877–887 (2007).
10. Shi, Y., Lan, F., Matson, C., Mulligan, P., Whetstine, J. R., Cole, P. A., Casero, R. A. & Shi,

- Y. Histone demethylation mediated by the nuclear amine oxidase homolog LSD1. *Cell* **119**, 941–953 (2004).
11. Christensen, J., Agger, K., Cloos, P. A. C., Pasini, D., Rose, S., Sennels, L., Rappsilber, J., Hansen, K. H., Salcini, A. E. & Helin, K. RBP2 belongs to a family of demethylases, specific for tri- and dimethylated lysine 4 on histone 3. *Cell* **128**, 1063–1076 (2007).
 12. Horton, J. R., Engstrom, A., Zoeller, E. L., Liu, X., Shanks, J. R., Zhang, X., Johns, M. A., Vertino, P. M., Fu, H. & Cheng, X. Characterization of a Linked Jumonji Domain of the KDM5/JARID1 Family of Histone H3 Lysine 4 Demethylases. *J. Biol. Chem.* **291**, 2631–2646 (2016).
 13. Johansson, C., Velupillai, S., Tumber, A., Szykowska, A., Hookway, E. S., Nowak, R. P., Strain-Damerell, C., Gileadi, C., Philpott, M., Burgess-Brown, N., Wu, N., Kopec, J., Nuzzi, A., Steuber, H., Egner, U., Badock, V., Munro, S., LaThangue, N. B., Westaway, S., Brown, J., Athanasou, N., Prinjha, R., Brennan, P. E. & Oppermann, U. Structural analysis of human KDM5B guides histone demethylase inhibitor development. *Nat. Chem. Biol.* **12**, 539–545 (2016).
 14. Li, L., Greer, C., Eisenman, R. N. & Secombe, J. Essential functions of the histone demethylase lid. *PLoS Genet.* **6**, e1001221 (2010).
 15. Brookes, E., Laurent, B., Öunap, K., Carroll, R., Moeschler, J. B., Field, M., Schwartz, C. E., Gecz, J. & Shi, Y. Mutations in the intellectual disability gene KDM5C reduce protein stability and demethylase activity. *Hum. Mol. Genet.* **24**, 2861–2872 (2015).
 16. Xiang, Y., Zhu, Z., Han, G., Ye, X., Xu, B., Peng, Z., Ma, Y., Yu, Y., Lin, H., Chen, A. P. & Chen, C. D. JARID1B is a histone H3 lysine 4 demethylase up-regulated in prostate cancer. *Proc. Natl. Acad. Sci. U. S. A.* **104**, 19226–19231 (2007).
 17. Tu, S., Teng, Y.-C., Yuan, C., Wu, Y.-T., Chan, M.-Y., Cheng, A.-N., Lin, P.-H., Juan, L.-J. & Tsai, M.-D. The ARID domain of the H3K4 demethylase RBP2 binds to a DNA CCGCCC motif. *Nat. Struct. Mol. Biol.* **15**, 419–421 (2008).

18. Scibetta, A. G., Santangelo, S., Coleman, J., Hall, D., Chaplin, T., Copier, J., Catchpole, S., Burchell, J. & Taylor-Papadimitriou, J. Functional analysis of the transcription repressor PLU-1/JARID1B. *Mol. Cell. Biol.* **27**, 7220–7235 (2007).
19. Yao, W., Peng, Y. & Lin, D. The flexible loop L1 of the H3K4 demethylase JARID1B ARID domain has a crucial role in DNA-binding activity. *Biochem. Biophys. Res. Commun.* **396**, 323–328 (2010).
20. Lan, F., Collins, R. E., De Cegli, R., Alpatov, R., Horton, J. R., Shi, X., Gozani, O., Cheng, X. & Shi, Y. Recognition of unmethylated histone H3 lysine 4 links BHC80 to LSD1-mediated gene repression. *Nature* **448**, 718–722 (2007).
21. Klein, B. J., Wang, X., Cui, G., Yuan, C., Botuyan, M. V., Lin, K., Lu, Y., Wang, X., Zhao, Y., Bruns, C. J., Mer, G., Shi, X. & Kutateladze, T. G. PHF20 Readers Link Methylation of Histone H3K4 and p53 with H4K16 Acetylation. *Cell Rep.* **17**, 1158–1170 (2016).
22. Shi, X., Hong, T., Walter, K. L., Ewalt, M., Michishita, E., Hung, T., Carney, D., Peña, P., Lan, F., Kaadige, M. R., Lacoste, N., Cayrou, C., Davrazou, F., Saha, A., Cairns, B. R., Ayer, D. E., Kutateladze, T. G., Shi, Y., Côté, J., Chua, K. F. & Gozani, O. ING2 PHD domain links histone H3 lysine 4 methylation to active gene repression. *Nature* **442**, 96–99 (2006).
23. Li, H., Ilin, S., Wang, W., Duncan, E. M., Wysocka, J., Allis, C. D. & Patel, D. J. Molecular basis for site-specific read-out of histone H3K4me3 by the BPTF PHD finger of NURF. *Nature* **442**, 91–95 (2006).
24. Peña, P. V., Davrazou, F., Shi, X., Walter, K. L., Verkhusha, V. V., Gozani, O., Zhao, R. & Kutateladze, T. G. Molecular mechanism of histone H3K4me3 recognition by plant homeodomain of ING2. *Nature* **442**, 100–103 (2006).
25. Wysocka, J., Swigut, T., Xiao, H., Milne, T. A., Kwon, S. Y., Landry, J., Kauer, M., Tackett, A. J., Chait, B. T., Badenhorst, P., Wu, C. & Allis, C. D. A PHD finger of NURF couples histone H3 lysine 4 trimethylation with chromatin remodelling. *Nature* **442**, 86–90 (2006).

26. Sanchez, R. & Zhou, M.-M. The PHD finger: a versatile epigenome reader. *Trends Biochem. Sci.* **36**, 364–372 (2011).
27. Klein, B. J., Piao, L., Xi, Y., Rincon-Arano, H., Rothbart, S. B., Peng, D., Wen, H., Larson, C., Zhang, X., Zheng, X., Cortazar, M. A., Peña, P. V., Mangan, A., Bentley, D. L., Strahl, B. D., Groudine, M., Li, W., Shi, X. & Kutateladze, T. G. The histone-H3K4-specific demethylase KDM5B binds to its substrate and product through distinct PHD fingers. *Cell Rep.* **6**, 325–335 (2014).
28. Zhang, Y., Yang, H., Guo, X., Rong, N., Song, Y., Xu, Y., Lan, W., Zhang, X., Liu, M., Xu, Y. & Cao, C. The PHD1 finger of KDM5B recognizes unmodified H3K4 during the demethylation of histone H3K4me_{2/3} by KDM5B. *Protein Cell* **5**, 837–850 (2014).
29. Torres, I. O., Kuchenbecker, K. M., Nnadi, C. I., Fletterick, R. J., Kelly, M. J. S. & Fujimori, D. G. Histone demethylase KDM5A is regulated by its reader domain through a positive-feedback mechanism. *Nat. Commun.* **6**, 6204 (2015).
30. Zhao, S., Chuh, K. N., Zhang, B., Dul, B. E., Thompson, R. E., Farrelly, L. A., Liu, X., Xu, N., Xue, Y., Roeder, R. G., Maze, I., Muir, T. W. & Li, H. Histone H3Q5 seronylation stabilizes H3K4 methylation and potentiates its readout. *Proc. Natl. Acad. Sci. U. S. A.* **118**, (2021).
31. Wang, G. G., Song, J., Wang, Z., Dormann, H. L., Casadio, F., Li, H., Luo, J.-L., Patel, D. J. & Allis, C. D. Haematopoietic malignancies caused by dysregulation of a chromatin-binding PHD finger. *Nature* **459**, 847–851 (2009).
32. Longbotham, J. E., Chio, C. M., Dharmarajan, V., Trnka, M. J., Torres, I. O., Goswami, D., Ruiz, K., Burlingame, A. L., Griffin, P. R. & Fujimori, D. G. Histone H3 binding to the PHD1 domain of histone demethylase KDM5A enables active site remodeling. *Nat. Commun.* **10**, 94 (2019).
33. Iwase, S., Brookes, E., Agarwal, S., Badeaux, A. I., Ito, H., Vallianatos, C. N., Tomassy, G. S., Kasza, T., Lin, G., Thompson, A., Gu, L., Kwan, K. Y., Chen, C., Sartor, M. A., Egan, B.,

- Xu, J. & Shi, Y. A Mouse Model of X-linked Intellectual Disability Associated with Impaired Removal of Histone Methylation. *Cell Rep.* **14**, 1000–1009 (2016).
34. Jensen, L. R., Bartenschlager, H., Rujirabanjerd, S., Tzschach, A., Nümann, A., Janecke, A. R., Spörle, R., Stricker, S., Raynaud, M., Nelson, J., Hackett, A., Fryns, J.-P., Chelly, J., de Brouwer, A. P., Hamel, B., Gecz, J., Ropers, H.-H. & Kuss, A. W. A distinctive gene expression fingerprint in mentally retarded male patients reflects disease-causing defects in the histone demethylase KDM5C. *Pathogenetics* **3**, 2 (2010).
35. Jensen, L. R., Amende, M., Gurok, U., Moser, B., Gimmel, V., Tzschach, A., Janecke, A. R., Tariverdian, G., Chelly, J., Fryns, J.-P., Van Esch, H., Kleefstra, T., Hamel, B., Moraine, C., Gecz, J., Turner, G., Reinhardt, R., Kalscheuer, V. M., Ropers, H.-H. & Lenzner, S. Mutations in the JARID1C gene, which is involved in transcriptional regulation and chromatin remodeling, cause X-linked mental retardation. *Am. J. Hum. Genet.* **76**, 227–236 (2005).
36. Scandaglia, M., Lopez-Atalaya, J. P., Medrano-Fernandez, A., Lopez-Cascales, M. T., Del Blanco, B., Lipinski, M., Benito, E., Olivares, R., Iwase, S., Shi, Y. & Barco, A. Loss of Kdm5c Causes Spurious Transcription and Prevents the Fine-Tuning of Activity-Regulated Enhancers in Neurons. *Cell Rep.* **21**, 47–59 (2017).
37. Outchkourov, N. S., Muiño, J. M., Kaufmann, K., van Ijcken, W. F. J., Groot Koerkamp, M. J., van Leenen, D., de Graaf, P., Holstege, F. C. P., Grosveld, F. G. & Timmers, H. T. M. Balancing of histone H3K4 methylation states by the Kdm5c/SMCX histone demethylase modulates promoter and enhancer function. *Cell Rep.* **3**, 1071–1079 (2013).
38. Shen, H., Xu, W., Guo, R., Rong, B., Gu, L., Wang, Z., He, C., Zheng, L., Hu, X., Hu, Z., Shao, Z.-M., Yang, P., Wu, F., Shi, Y. G., Shi, Y. & Lan, F. Suppression of Enhancer Overactivation by a RACK7-Histone Demethylase Complex. *Cell* **165**, 331–342 (2016).
39. Gonçalves, T. F., Gonçalves, A. P., Fintelman Rodrigues, N., dos Santos, J. M., Pimentel, M. M. G. & Santos-Rebouças, C. B. KDM5C mutational screening among males with

- intellectual disability suggestive of X-Linked inheritance and review of the literature. *Eur. J. Med. Genet.* **57**, 138–144 (2014).
40. Tzschach, A., Lenzner, S., Moser, B., Reinhardt, R., Chelly, J., Fryns, J.-P., Kleefstra, T., Raynaud, M., Turner, G., Ropers, H.-H., Kuss, A. & Jensen, L. R. Novel JARID1C/SMCX mutations in patients with X-linked mental retardation. *Hum. Mutat.* **27**, 389 (2006).
 41. Santos, C., Rodriguez-Revena, L., Madrigal, I., Badenas, C., Pineda, M. & Milà, M. A novel mutation in JARID1C gene associated with mental retardation. *Eur. J. Hum. Genet.* **14**, 583–586 (2006).
 42. Abidi, F. E., Holloway, L., Moore, C. A., Weaver, D. D., Simensen, R. J., Stevenson, R. E., Rogers, R. C. & Schwartz, C. E. Mutations in JARID1C are associated with X-linked mental retardation, short stature and hyperreflexia. *J. Med. Genet.* **45**, 787–793 (2008).
 43. Rujirabanjerd, S., Nelson, J., Tarpey, P. S., Hackett, A., Edkins, S., Lucy Raymond, F., Schwartz, C. E., Turner, G., Iwase, S., Shi, Y., Andrew Futreal, P., Stratton, M. R. & Gecz, J. Identification and characterization of two novel JARID1C mutations: suggestion of an emerging genotype–phenotype correlation. *European Journal of Human Genetics* **18**, 330–335 (2010).
 44. Xu, J., Burgoyne, P. S. & Arnold, A. P. Sex differences in sex chromosome gene expression in mouse brain. *Human Molecular Genetics* **11**, 1409–1419 (2002).
 45. Vallianatos, C. N., Farrehi, C., Friez, M. J., Burmeister, M., Keegan, C. E. & Iwase, S. Altered Gene-Regulatory Function of KDM5C by a Novel Mutation Associated With Autism and Intellectual Disability. *Front. Mol. Neurosci.* **11**, 104 (2018).
 46. Tahiliani, M., Mei, P., Fang, R., Leonor, T., Rutenberg, M., Shimizu, F., Li, J., Rao, A. & Shi, Y. The histone H3K4 demethylase SMCX links REST target genes to X-linked mental retardation. *Nature* **447**, 601–605 (2007).
 47. Jones, B. N., Quang-Dang, D.-U., Oku, Y. & Gross, J. D. A kinetic assay to monitor RNA decapping under single- turnover conditions. *Methods Enzymol.* **448**, 23–40 (2008).

48. Longbotham, J. E., Kelly, M. J. S. & Fujimori, D. G. Recognition of Histone H3 Methylation States by the PHD1 Domain of Histone Demethylase KDM5A. *ACS Chem. Biol.* (2021). doi:10.1021/acscchembio.0c00976
49. Koehler, C., Bishop, S., Dowler, E. F., Schmieder, P., Diehl, A., Oschkinat, H. & Ball, L. J. Backbone and sidechain ¹H, ¹³C and ¹⁵N resonance assignments of the Bright/ARID domain from the human JARID1C (SMCX) protein. *Biomol. NMR Assign.* **2**, 9–11 (2008).
50. Kim, S.-A., Zhu, J., Yennawar, N., Eek, P. & Tan, S. Crystal Structure of the LSD1/CoREST Histone Demethylase Bound to Its Nucleosome Substrate. *Mol. Cell* **78**, 903–914.e4 (2020).
51. Kasinath, V., Beck, C., Sauer, P., Poepsel, S., Kosmatka, J., Faini, M., Toso, D., Aebersold, R. & Nogales, E. JARID2 and AEBP2 regulate PRC2 in the presence of H2AK119ub1 and other histone modifications. *Science* **371**, (2021).
52. Finogenova, K., Bonnet, J., Poepsel, S., Schäfer, I. B., Finkl, K., Schmid, K., Litz, C., Strauss, M., Benda, C. & Müller, J. Structural basis for PRC2 decoding of active histone methylation marks H3K36me_{2/3}. *Elife* **9**, (2020).
53. Worden, E. J., Zhang, X. & Wolberger, C. Structural basis for COMPASS recognition of an H2B-ubiquitinated nucleosome. *Elife* **9**, (2020).
54. Li, W., Tian, W., Yuan, G., Deng, P., Sengupta, D., Cheng, Z., Cao, Y., Ren, J., Qin, Y., Zhou, Y., Jia, Y., Gozani, O., Patel, D. J. & Wang, Z. Molecular basis of nucleosomal H3K36 methylation by NSD methyltransferases. *Nature* **590**, 498–503 (2021).
55. Bilokapic, S., Suskiewicz, M. J., Ahel, I. & Halic, M. Bridging of DNA breaks activates PARP2–HPF1 to modify chromatin. *Nature* **585**, 609–613 (2020).
56. Bilokapic, S. & Halic, M. Nucleosome and ubiquitin position Set2 to methylate H3K36. *Nat. Commun.* **10**, 3795 (2019).
57. Hsu, P. L., Shi, H., Leonen, C., Kang, J., Chatterjee, C. & Zheng, N. Structural Basis of H2B Ubiquitination-Dependent H3K4 Methylation by COMPASS. *Mol. Cell* **76**, 712–723.e4

- (2019).
58. Marabelli, C., Marrocco, B., Pilotto, S., Chittori, S., Picaud, S., Marchese, S., Ciossani, G., Forneris, F., Filippakopoulos, P., Schoehn, G., Rhodes, D., Subramaniam, S. & Mattevi, A. A Tail-Based Mechanism Drives Nucleosome Demethylation by the LSD2/NPAC Multimeric Complex. *Cell Rep.* **27**, 387–399.e7 (2019).
 59. Poepsel, S., Kasinath, V. & Nogales, E. Cryo-EM structures of PRC2 simultaneously engaged with two functionally distinct nucleosomes. *Nat. Struct. Mol. Biol.* **25**, 154–162 (2018).
 60. Park, S. H., Ayoub, A., Lee, Y.-T., Xu, J., Kim, H., Zheng, W., Zhang, B., Sha, L., An, S., Zhang, Y., Cianfrocco, M. A., Su, M., Dou, Y. & Cho, U.-S. Cryo-EM structure of the human MLL1 core complex bound to the nucleosome. *Nat. Commun.* **10**, 1–13 (2019).
 61. Xue, H., Yao, T., Cao, M., Zhu, G., Li, Y., Yuan, G., Chen, Y., Lei, M. & Huang, J. Structural basis of nucleosome recognition and modification by MLL methyltransferases. *Nature* **573**, 445–449 (2019).
 62. Hatazawa, S., Liu, J., Takizawa, Y., Zandian, M., Negishi, L., Kutateladze, T. G. & Kurumizaka, H. Structural basis for binding diversity of acetyltransferase p300 to the nucleosome. *iScience* **25**, 104563 (2022).
 63. Dhall, A., Shelton, P. M. M., Delachat, A. M.-F., Leonen, C. J. A., Fierz, B. & Chatterjee, C. Nucleosome Binding by the Lysine Specific Demethylase 1 (LSD1) Enzyme Enables Histone H3 Demethylation. *Biochemistry* **59**, 2479–2483 (2020).
 64. Gatchalian, J., Wang, X., Ikebe, J., Cox, K. L., Tencer, A. H., Zhang, Y., Burge, N. L., Di, L., Gibson, M. D., Musselman, C. A., Poirier, M. G., Kono, H., Hayes, J. J. & Kutateladze, T. G. Accessibility of the histone H3 tail in the nucleosome for binding of paired readers. *Nat. Commun.* **8**, 1489 (2017).
 65. Morrison, E. A., Bowerman, S., Sylvers, K. L., Wereszczynski, J. & Musselman, C. A. The conformation of the histone H3 tail inhibits association of the BPTF PHD finger with the

- nucleosome. *Elife* **7**, (2018).
66. Stützer, A., Liokatis, S., Kiesel, A., Schwarzer, D., Sprangers, R., Söding, J., Selenko, P. & Fischle, W. Modulations of DNA Contacts by Linker Histones and Post-translational Modifications Determine the Mobility and Modifiability of Nucleosomal H3 Tails. *Mol. Cell* **61**, 247–259 (2016).
 67. Peng, Y., Li, S., Onufriev, A., Landsman, D. & Panchenko, A. R. Binding of regulatory proteins to nucleosomes is modulated by dynamic histone tails. *Nat. Commun.* **12**, 5280 (2021).
 68. Weaver, T. M., Morrison, E. A. & Musselman, C. A. Reading More than Histones: The Prevalence of Nucleic Acid Binding among Reader Domains. *Molecules* **23**, (2018).
 69. Pilotto, S., Speranzini, V., Tortorici, M., Durand, D., Fish, A., Valente, S., Forneris, F., Mai, A., Sixma, T. K., Vachette, P. & Mattevi, A. Interplay among nucleosomal DNA, histone tails, and corepressor CoREST underlies LSD1-mediated H3 demethylation. *Proc. Natl. Acad. Sci. U. S. A.* **112**, 2752–2757 (2015).
 70. Musselman, C. A. & Kutateladze, T. G. Characterization of functional disordered regions within chromatin-associated proteins. *iScience* **24**, 102070 (2021).
 71. Contreras-Martos, S., Piai, A., Kosol, S., Varadi, M., Bekesi, A., Lebrun, P., Volkov, A. N., Gevaert, K., Pierattelli, R., Felli, I. C. & Tompa, P. Linking functions: an additional role for an intrinsically disordered linker domain in the transcriptional coactivator CBP. *Sci. Rep.* **7**, 4676 (2017).
 72. Jiao, L., Shubbar, M., Yang, X., Zhang, Q., Chen, S., Wu, Q., Chen, Z., Rizo, J. & Liu, X. A partially disordered region connects gene repression and activation functions of EZH2. *Proc. Natl. Acad. Sci. U. S. A.* **117**, 16992–17002 (2020).
 73. Keenen, M. M., Brown, D., Brennan, L. D., Renger, R., Khoo, H., Carlson, C. R., Huang, B., Grill, S. W., Narlikar, G. J. & Redding, S. HP1 proteins compact DNA into mechanically and positionally stable phase separated domains. *Elife* **10**, (2021).

74. Kim, S.-A., Chatterjee, N., Jennings, M. J., Bartholomew, B. & Tan, S. Extranucleosomal DNA enhances the activity of the LSD1/CoREST histone demethylase complex. *Nucleic Acids Res.* **43**, 4868–4880 (2015).
75. Zhou, J. C., Blackledge, N. P., Farcas, A. M. & Klose, R. J. Recognition of CpG island chromatin by KDM2A requires direct and specific interaction with linker DNA. *Mol. Cell Biol.* **32**, 479–489 (2012).
76. Blackledge, N. P., Zhou, J. C., Tolstorukov, M. Y., Farcas, A. M., Park, P. J. & Klose, R. J. CpG islands recruit a histone H3 lysine 36 demethylase. *Mol. Cell* **38**, 179–190 (2010).
77. Erdős, G., Pajkos, M. & Dosztányi, Z. IUPred3: prediction of protein disorder enhanced with unambiguous experimental annotation and visualization of evolutionary conservation. *Nucleic Acids Res.* **49**, W297–W303 (2021).
78. Poeta, L., Padula, A., Lioi, M. B., van Bokhoven, H. & Miano, M. G. Analysis of a Set of KDM5C Regulatory Genes Mutated in Neurodevelopmental Disorders Identifies Temporal Coexpression Brain Signatures. *Genes* **12**, (2021).
79. Zamurrad, S., Hatch, H. A. M., Drelon, C., Belalcazar, H. M. & Secombe, J. A Drosophila Model of Intellectual Disability Caused by Mutations in the Histone Demethylase KDM5. *Cell Rep.* **22**, 2359–2369 (2018).
80. Wei, G., Deng, X., Agarwal, S., Iwase, S., Disteché, C. & Xu, J. Patient Mutations of the Intellectual Disability Gene KDM5C Downregulate Netrin G2 and Suppress Neurite Growth in Neuro2a Cells. *Journal of Molecular Neuroscience* **60**, 33–45 (2016).
81. Wan, L., Chong, S., Xuan, F., Liang, A., Cui, X., Gates, L., Carroll, T. S., Li, Y., Feng, L., Chen, G., Wang, S.-P., Ortiz, M. V., Daley, S. K., Wang, X., Xuan, H., Kentsis, A., Muir, T. W., Roeder, R. G., Li, H., Li, W., Tjian, R., Wen, H. & David Allis, C. Impaired cell fate through gain-of-function mutations in a chromatin reader. *Nature* **577**, 121–126 (2020).
82. Schenkel, L. C., Aref-Eshghi, E., Skinner, C., Ainsworth, P., Lin, H., Paré, G., Rodenhiser, D. I., Schwartz, C. & Sadikovic, B. Peripheral blood epi-signature of Claes-Jensen

syndrome enables sensitive and specific identification of patients and healthy carriers with pathogenic mutations in KDM5C. *Clinical Epigenetics* **10**, (2018).

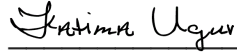
83. Coursimault, J., Goldenberg, A., Nicolas, G., Saugier-Veber, P., Coutant, S., Vincent, A., Pouliquen, D., Feltin, C., Aref-Eshghi, E., Sadikovic, B. & Lecoquierre, F. Contribution of DNA methylation profiling to the reclassification of a variant of uncertain significance in the KDM5C gene. *European Journal of Medical Genetics* **65**, 104556 (2022).
84. Grafodatskaya, D., Chung, B. H. Y., Butcher, D. T., Turinsky, A. L., Goodman, S. J., Choufani, S., Chen, Y.-A., Lou, Y., Zhao, C., Rajendram, R., Abidi, F. E., Skinner, C., Stavropoulos, J., Bondy, C. A., Hamilton, J., Wodak, S., Scherer, S. W., Schwartz, C. E. & Weksberg, R. Multilocus loss of DNA methylation in individuals with mutations in the histone H3 lysine 4 demethylase KDM5C. *BMC Med. Genomics* **6**, 1 (2013).
85. Li, Y. & Li, H. Many keys to push: diversifying the 'readership' of plant homeodomain fingers. *Acta Biochimica et Biophysica Sinica* **44**, 28–39 (2012).

Publishing Agreement

It is the policy of the University to encourage open access and broad distribution of all theses, dissertations, and manuscripts. The Graduate Division will facilitate the distribution of UCSF theses, dissertations, and manuscripts to the UCSF Library for open access and distribution. UCSF will make such theses, dissertations, and manuscripts accessible to the public and will take reasonable steps to preserve these works in perpetuity.

I hereby grant the non-exclusive, perpetual right to The Regents of the University of California to reproduce, publicly display, distribute, preserve, and publish copies of my thesis, dissertation, or manuscript in any form or media, now existing or later derived, including access online for teaching, research, and public service purposes.

DocuSigned by:



92ADD4F67391466...

Author Signature

8/24/2022

Date